Development of a Miniaturized Chemiresistive Gas Sensor Based on Carbon Nanomaterials for the Detection of Nitrogen Dioxide in Air

Dissertation

zur Erlangung des

Doktorgrades der Naturwissenschaften

(Dr. rer. nat.)

an der Fakultät Chemie und Pharmazie

der Universität Regensburg

Deutschland

vorgelegt von

Fabian Johannes Raphael Aumer

aus Regensburg

Juli 2021

Die vorliegende Dissertation enstand in der Zeit zwischen Juni 2018 und Juli 2021 am Institut für Analytische Chemie, Chemo- und Biosensorik der Universtität Regensburg sowie bei der Infineon Technologies AG in Neubiberg.

Die Arbeit wurde angeleitet von **Prof. Dr. Antje Bäumner** und **Dr. Thomas Hirsch.**

Promotionsgesuch eingereicht am:	22.07.2021
Kolloquiumstermin:	15.09.2021

Prüfungsausschuss

Vorsitzender:	Prof. Dr. Oliver Tepner
Erstgutachterin:	Prof. Dr. Antje Bäumner
Zweitgutachter:	Prof. Dr. Rudolf Bierl
Drittprüfer:	Dr. Rainer Müller

‚Nanos gigantum humeris insidentes.‘

Danksagung

Ich möchte mich zuerst bei **Prof. Dr. Antje Bäumner** sowie **Dr. Thomas Hirsch** bedanken, dass sie mir die Möglichkeit gegeben haben meine Promotion zu diesem spannenden und aktuellen Thema anzufertigen. Weiterhin gilt mein Dank auch **Dr. Wolfgang Dettmann** der mir die Möglichkeit gegeben hat diese Arbeit in seinem Team zu verwirklichen.

Vielen Dank an **Prof. Dr. Rudolf Bierl** für die Übernahme des Zweitgutachtens, sowie **Dr. Rainer Müller** für die Übernahme des Drittgutachtens und **Prof. Dr. Oliver Tepner** für die Ausübung der Funktion des Prüfungsvorsitzenden.

Weiterhin vielen Dank an **Dr. Alexander Zöpfl**, **Dr. Alexandra Roth**, **Dr. Werner** Breuer, **Dr. Patrick Hanekamp**, **Dr. Cecilia Carbonelli**, **Torsten Hinz**, **Sebastian Schober**, **Fabian Hecht**, **Birgit Griesberger**, **Fabiola Bermudez-Elsinger** sowie **Derek Debié**.

Beim Team des ‚4. Stocks' möchte ich mich bedanken bei **Patrick Recum**, **Lukas Wunderlich** sowie **Dr. Eva-Maria Kirchner** die mich immer tatkräftig unterstützt haben.

Beim Team der Abteilung möchte ich mich bedanken, vor allem bei **Simon Gassner**, **Moritz Schlagmann**, **Thomas Stadelmayer**, **Borja Mingorance Saez** und **Fabian Merbeler** für den regen fachlichen Austausch und das gute Arbeitsklima.

Desweiteren möchte ich mich für die immerwährende Unterstüzung und Geduld bei meiner Freundin **Mia Elisabeth Randlev Johansen** und meinen Eltern **Elisabeth** und **Johann Aumer** bedanken.

Table of Contents

Scientific Original Publications and Peer Reviewed Review Articles

4. 'Perspectives on Chemiresistive Gas Sensors Based on Nanomaterials, *prepared to be submitted to MDPI Chemosensors upon invitation to the Special Issue 'High-Sensitivity and - Selectivity Gas Sensors with Nanoparticles, Nanostructures, and Thin Films'.*

3. **Fabian Aumer**, Eva-Maria Kirchner, Sebastian A. Schober, Thomas Hirsch 'Impedimetric Sensing of NO_2 with Carbon Nanomaterials at Ambient Temperatures and in Presence of Humidity', *in Revision for ACS Applied Nanomaterials* **July 2021.**

2. **Fabian Aumer**, Torsten Hinz, 'Electrical Impedance Spectroscopy on 8-channel PSoC-Based Miniaturized Board to Enable Data-Rich Environmental Sensing', *submitted to Smart Systems Integration, January 30th 2021. Publication* **July 2021.**

1. **Fabian Aumer**, Fabian Hecht, Anton Kroener, Patrick Recum, Dr. Thomas Hirsch, 'Carbon Nanomaterials for Miniaturized Gas Sensors', *published at Mikrosystemtechnikkongress,* **October 30th 2019**.

Declaration of Collaborations

Most of the experimental and theoretical work presented in this thesis was carried out solely by the author. However, some of the results were obtained together with other researchers. In accordance with § 8 Abs. 1 Satz 2 Punkt 7 of the "Ordnung zum Erwerb des akademischen Grades eines Doktors der Naturwissenschaften (Dr. rer. nat.) an der Universität Regensburg vom 18. Juni 2009", this section gives information about these collaborations. Thomas Hirsch (TH) and Antje Bäumner supervised the research, TH and the author (FA) conceived and designed this work.

Chapter 1: Perspectives on Chemiresistive Gas Sensors Based on Nanomaterials

This chapter is published as a review article. The literature survey was performed by the FA. The concept and structure of the manuscript was planned together with TH. FA wrote the manuscript. TH revised the manuscript and is the corresponding author.

Chapter 2: Carbon Nanomaterials for Miniaturized Gas Sensors

Patrick Recum synthesized the materials. Fabian Hecht deposited the materials onto the sensor devices supervised by FA. FA performed the flake size characterization and the gas measurements. Patrick Recum performed Raman spectroscopy of the sensor surfaces. The manuscript was written by FA and revised by TH. FA is the corresponding author.

Chapter 3: Electrical Impedance Spectroscopy on 8-channel PSoC-Based Miniaturized Board to Enable Data-Rich Environmental Sensing

FA designed the system in cooperation with Torsten Hinz. FA built the system and validated it in cooperation with Torsten Hinz. FA wrote the script and is the corresponding author.

Chapter 4: Carbon Nanomaterial-based Impedimetric Sensor for NO_2 monitoring at Ambient Temperatures and in Presence of Humidity

Eva-Maria Kirchner fabricated the nanomaterials and performed Raman Spectroscopy on the final samples. FA deposited the nanomaterials and performed electrical characterization under gas influence on the sensor surface. Sebastian Schober helped process the data under supervision of FA. Further data analysis including PCA was done by FA. FA and TH wrote the manuscript and TH revised it. TH is the corresponding author.

1 Perspectives on Chemiresistive Gas Sensors Based on Nanomaterials

1.1 Abstract

Nanomaterials are in the focus of research due to their extraordinary electrical, physical and optical properties compared to their bulk counterparts. Recently the fabrication as well as the applicability of nanomaterials to the bigger scale of CMOS compatible processes are under investigation. Society is growing more aware of pollution in general and the impact of air is more connected to health issues. Therefore, the need for gas sensors for sickness prevention and health preservation in homes and offices is rising. Compared to other sensing principles chemiresistive sensors are well suited for these applications due to a variety of reasons like many target gases, their cheap price and high sensitivity. This critical review is focused on recent advances in research towards chemiresistive gas sensors based on nanomaterials. The first topic are the various gas sensing principles and their advantages and disadvantages. Second is the discussion of the basic sensing mechanism of metal oxide (MOX) sensors and the interaction between nanomaterial and gas molecules. Next, the different gas sensing properties of selected materials are discussed and the sensors targeting toxic gases are evaluated. This is followed by an assessment of sensors for environmental monitoring and multigas sensor elements. Lastly, the perspectives of gas sensing towards the before mentioned specifications and an outlook towards future research in nanomaterial-based gas sensing is given.

This chapter was prepared to be submitted to MDPI Chemosensors upon invitation to the Special Issue 'High-Sensitivity and -Selectivity Gas Sensors with Nanoparticles, Nanostructures, and Thin Films' and will be submitted shortly.

Author contributions: This review article was prepared to be submitted to MDPI Chemosensors upon invitation to the Special Issue 'High-Sensitivity and -Selectivity Gas Sensors with Nanoparticles, Nanostructures, and Thin Films'. The literature survey was performed by FA. The concept and structure of the manuscript was planned together with TH. FA wrote the manuscript. TH revised the manuscript and is the corresponding author.

1.2 Introduction

Sensor development for the detection of environmentally relevant gases is an important field of research with a huge impact on society. Gas sensors are mainly based on materials that change one or more of their physical properties when exposed to target gases. Up to now there are many techniques and principles for the identification and determination of gases, such as infrared spectroscopy (IR), or photoacoustic spectroscopy (PAS). These techniques enable to detect gases with high selectivity at even extreme low concentrations and offer high accuracy and long lifetime at a high cost and difficulties at miniaturization. While catalytic sensors have a simple setup, they are limited to flammable gases. MOX sensors are easily miniaturized and have sensitivity down to sub ppm level, but also require energy for heating which usually prevents their use in portable devices. As shown, the methods to detect gases are manifold and differ in sensitivity, selectivity, availability, price and many more factors. The market for gas sensors is steadily growing. The first reason is its importance for many areas. These include, but are not limited to, industrial process and production control, quality control in food, guarantee of functionality as in the lambda probe, safety aspects such as warning against poisonous gases or in the event of a gas leak. The second aspect is that gases are usually colorless and mostly odorless, and, according to recent findings, health risks are associated with long-term exposure. Especially in the environmental and healthcare sector, it is desirable to improve the sensors usability by miniaturizing them, manufacturing, and using them in large

numbers. This will lead to a denser information network especially when internet of things we become more popular. This is especially useful if it is therefore necessary to track the entry of industrial exhaust gases into the environment or exhaust gases from road traffic with high spatio-temporal resolution and to study their influence on climate and health.

In cities, the state of the art to measure air pollution is to set up bulky and expensive measurement stations for various gases and fine particles. In all of Germany, currently there are 260 measurement stations whereas five of them are located in the city of Munich, Bavaria [1,2]. Therefore, their use is limited and there is no dense mesh to allow air pollution sensing for a single person. For the aforementioned scenarios miniaturized, selective, sensitive, reversible and long-term stable sensors are required in order to broaden the mesh. Electrochemical sensors combined with nanomaterials fill exactly this niche. Their ultra-high surface to volume ratio leads to outstanding sensitivity. Selectivity can be easily achieved by functionalizing materials or combining multiple nanomaterials in one sensor element. Through the inherent low size and easy setup, miniaturization is possible.

1.3 Sensing Mechanisms in Chemiresistive Sensors

Chemiresistive sensors interact with the analyte gases by adsorption that can be read-out by monitoring the electrical resistance of the sensor. There are different principles leading to a signal change for MOX and nanomaterials based sensors. The material that is affected by the gas in MOX sensors is a polycrystalline semiconductor metal oxide. By heating the surface (typically >100 °C) chemisorption of oxygen ions takes place. These ionized oxygen adsorbates in turn then react with target gases. Electron-accepting gases can receive electrons from the material, whereas electron-donating gases can add electrons to the

material. In Figure 1.1a) a schematic drawing of a MOX sensor is shown, while the electron transfer in presence of two gases is shown in b).

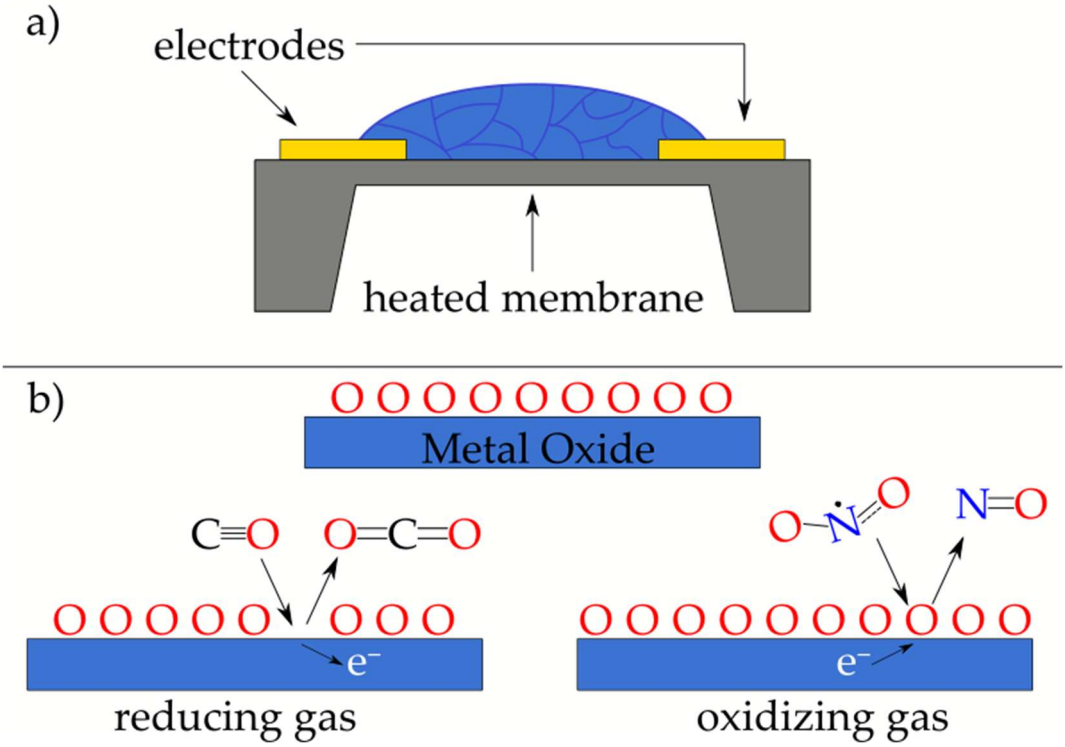

Figure 1.1. a) Schematic of a MOX sensor with a heated membrane, electrodes for resistance measurement and metal oxide layer on top. b) Metal oxide layer with adsorbed surface oxygen atoms; bottom left: addition of electrons to the system and removal of surface oxygen through reducing gas; bottom right: removal of electron from the system and addition of surface oxygen in presence of an oxidizing gas.

This respectively leads to resistance increase through the reduction of electrons in the valence band and to a resistance decrease in n-type MOX sensors by adding more electrons that can participate in the charge transport. For p-type MOX sensors the resistances decrease and increase inversely. Additional electrons decrease the amount of available charge carriers through the reaction with so-called holes. Removing electrons increases the amount of positive charge carriers, therefore lowering the resistance. Operating temperatures in these types of sensors can reach up to 850 °C to achieve sensitivity. NO_2, O_3 and O_2 are typical oxidizing (electron accepting) gases, while H_2, CO and volatile organic compounds (VOCs) are generally reducing (electron donating) gases.

For semiconductor-based sensors, the charge transfer works slightly different. Unlike the MOX principle, no ionized oxygen is present at the surface to react with the target gases see figure 1.2. Through theoretical modelling it is suspected that the target gases physically adsorb on the surface and the charge transfer reaction occurs directly to the nanomaterials [3].

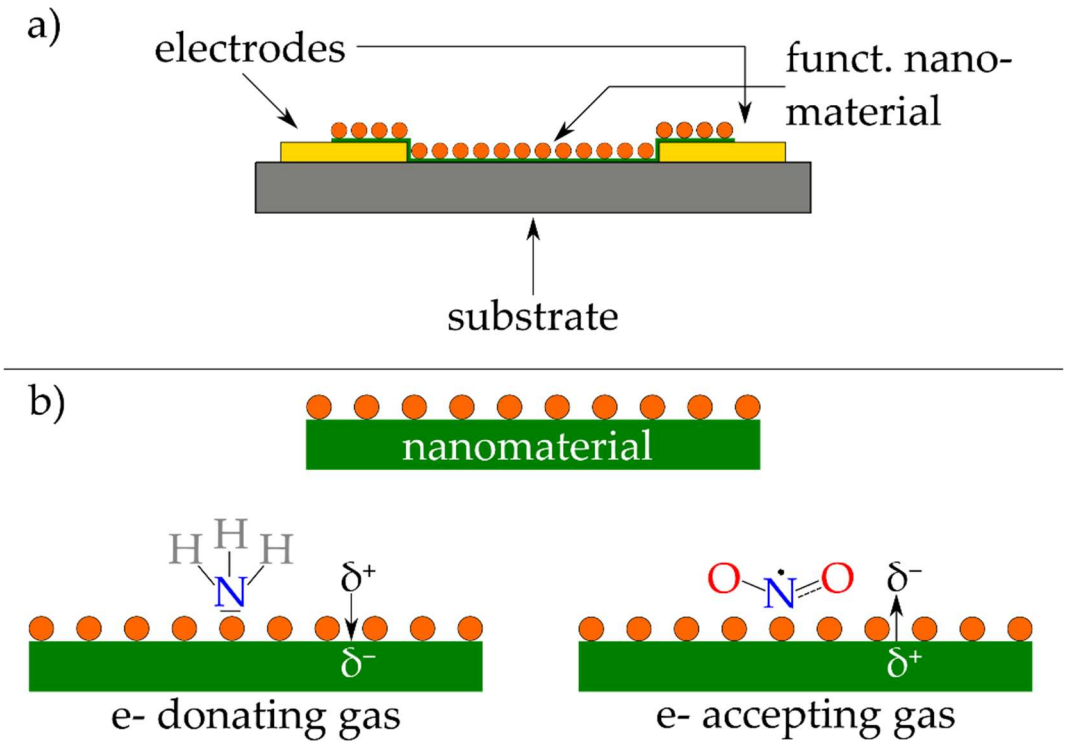

Figure 1.2. Nanomaterial-based gas sensor: a) shows a functionalized nanomaterial on top of a substrate and gold electrodes. The substrate can optionally be heated. b) shows the surface in close-up. On the bottom left an electron donating gas is interacting with the nanomaterial and induces a negative partial charge. On the right bottom side an electron accepting gas interacts and induces a positive charge.

In practice, the surfaces often suffer from reactive defect sites that are introduced by synthesis, processing, or handling, which can deal as preferable adsorption sites [4]. This in turn leads to a charge transfer whose quantity and direction depend on the target gas and the sensing substrate. NO_x and other oxidizing gases behave like electron acceptors, while most VOCs or NH_3 act as electron donators. N-type materials show a decrease in resistance after exposure to electron donating gases and an increase in resistance for electron accepting gases and vice versa for p-type materials. A second possible influence is the modulation

in the Schottky barrier by analyte exposure through the adsorption of gas molecules on the built-in potential as well as the Schottky barrier change. As illustrated in Figure 1.3 for n-type sensing material and NO_2 exposure this means the Fermi level (E_F) shifts towards the valence band, therefore increasing the resistance, the Schottky barrier and decreasing the built-in potential. By exposing the n-type surface to NH_3, the Fermi level is shifted towards the conductance band (E_C), thus decreasing the resistance, the Schottky barrier and increasing the built-in potential. Generally, if the sensing surface is more affine to a certain gas species, higher selectivity over other gases is expected. In turn, this lowers the desorption rate of the affine gas molecules from the surface and leads to longer response times.

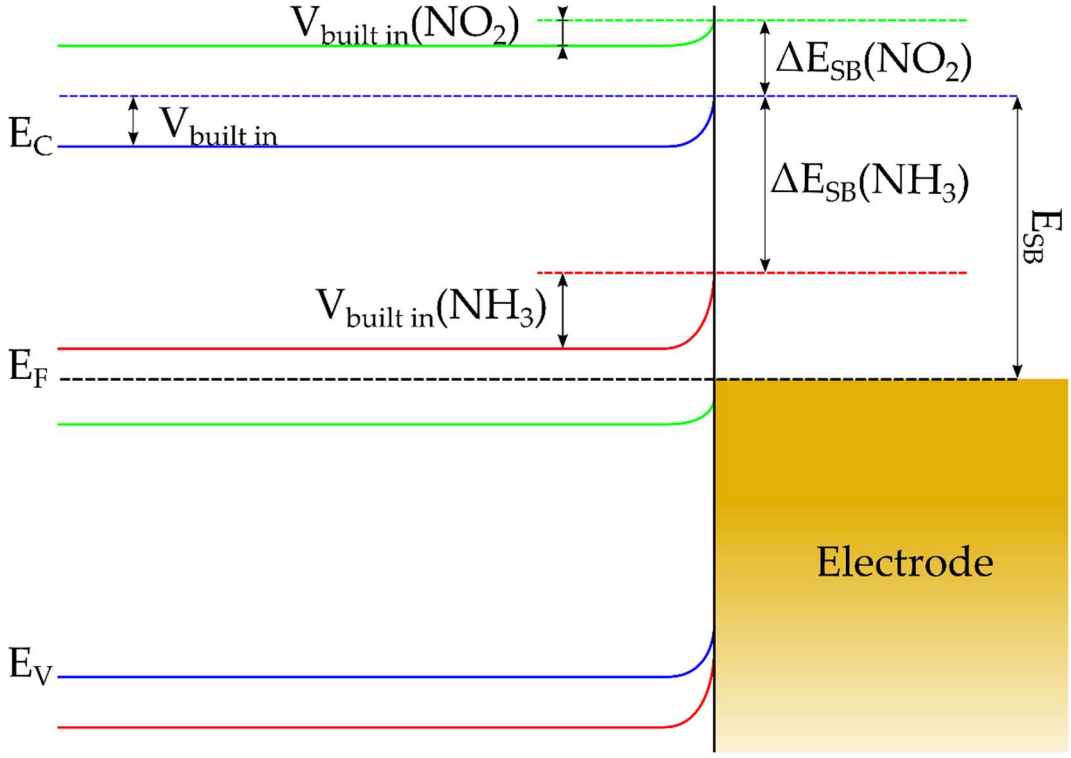

Figure 1.2. Influence of different gas molecules adsorbing on the sensor and their influence on the Schottky barrier (SB) as well as the built-in potential $V_{built\ in}$. Illustration adapted from [5].

Due to the rise in different synthesis methods for all kinds of nanomaterials research towards their use as sensing materials is increasing. Their low spatial dimensions make them interesting for gas sensing applications. In this work we

will discuss carbon-based materials and graphene derivatives, transition metal chalcogenides as well as different material composites.

1.4 Sensors for Harmful Gases

For environmental monitoring the quantification of harmful gases like NO_2 and CO_2 is of high interest. In terms of NO_2 sensing according to the Occupational Safety and Health Administration in the United States, an NO_2 sensor should be able to detect less than 5 ppm of NO_2 [6]. For CO_2 sensing an LOD of 400 ppm is sufficient as the CO_2 concentration in air is at that level.

1.4.1 Sensors for NO_2

An overview of recently reported NO_2 sensors based on carbon nanomaterials and composites is listed in Table 1.1. Zhang *et al.* used graphene in combination with octahedral SnO_2 to achieve high sensitivity of 12.5% at the threshold level of 5 ppm analyte gas [7], while Fei *et al.* were able to reach an ultralow detection limit of only 45 ppb when combining graphene with polystyrene (PS) beads [8]. Both these sensors work at room temperature and in a dry testing ambient. For reduced graphene oxide (rGO) different materials like WO_3, MoS_2 and Fe_3O_4 were applied to form nanocomposites with promising properties. A sensor based on rGO fibers and WO_3 nanorods shows a sensitivity of 9.2 % after 8 min of exposure to 5 ppm [9]. While rGO in combination with drop casted MoS_2 nanoparticles exhibits an ultra-high response of 2483% towards 10 ppm NO_2 at 80 °C, the response and recovery time are comparatively high with approximately 12 min and 30 min respectively [10]. Tung *et al.* showed that by adding Fe_3O_4 particles of different sizes to rGO the sensitivity towards NO_2 alters [11]. The initial sensitivity of 2.5% at 2.5 ppm NO_2 for pure rGO went up to 4% after adding Fe_3O_4 particles with 20 nm diameter. Addition of Fe_3O_4 NPs with smaller diameters decreased the sensitivity. This is proposed to the different distribution behavior of the NPs, which can change the surface interaction between rGO and gas, the

improved electron transfer as well as the enlarged specific surface area (Figure 1.4).

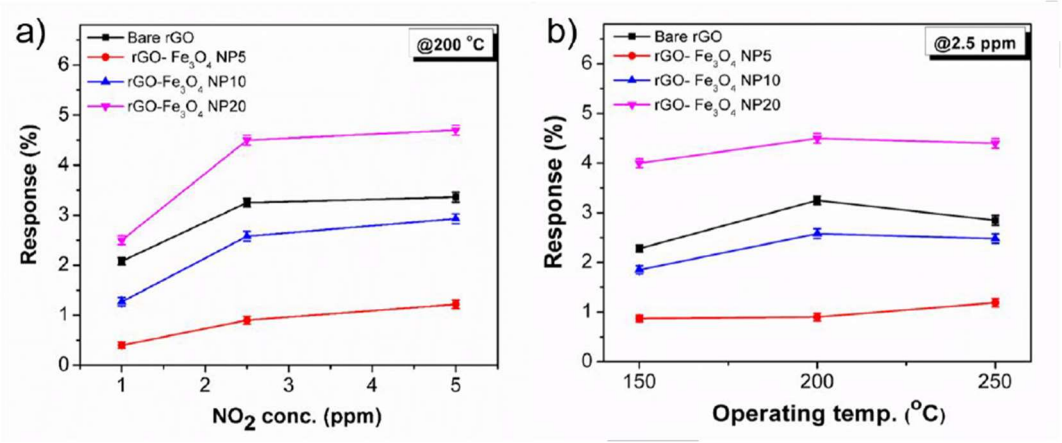

Figure 1.4. Comparison of a) sensitivity towards NO_2 for the different material composites at 200 °C and b) at 2.5 ppm at varying temperatures. rGO-Fe_3O_4 NPs of 20 nm diameter show the highest sensitivity. NP5, NP10, NP20 refers to particles of 5, 10, and 20 nm in diameter. Reprinted from [11], with permission from Elsevier.

For multiwalled carbon nanotubes (MWCNTs) Liu *et al.* verified, that nitrogen-doped polypyrrole/MWCNT composites sensitivity towards NO_2 can be tuned by annealing them. Different annealing temperatures between 200 °C and 400 °C showed that the optimum for that system was at 350 °C [12]. By annealing, the sensitivity was increased from 0.56% up to 24.82% at 5 ppm NO_2. Due to annealing, the polypyrrole spread more and therefore more chemisorption sites for gases are created, leading to higher sensitivity as shown in Figure 1.5.

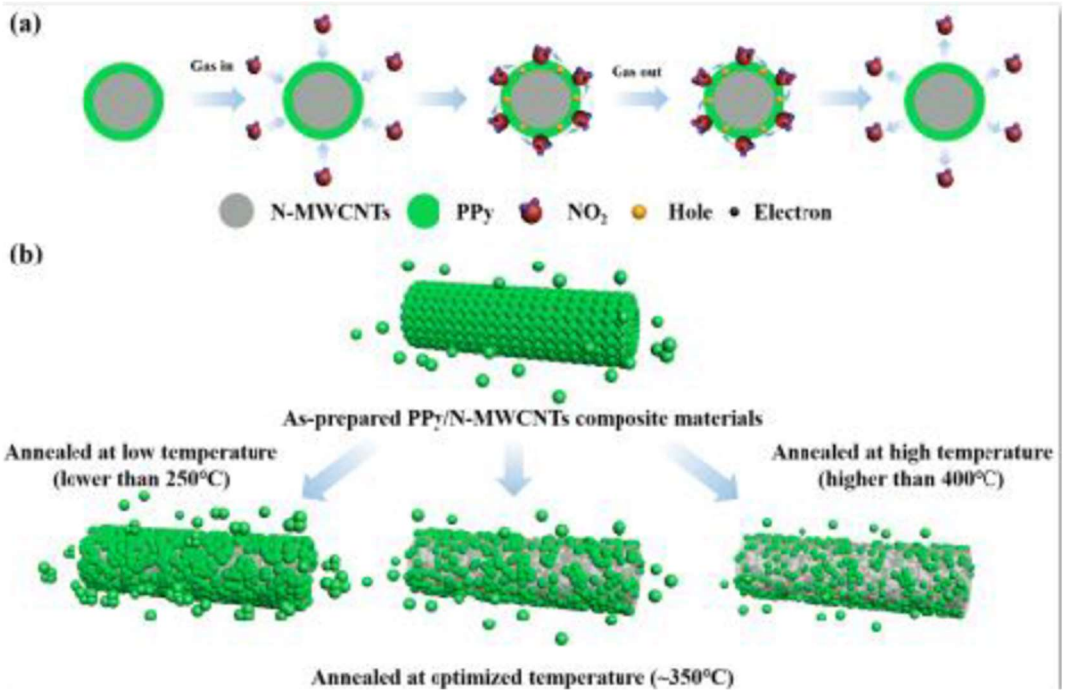

Figure 1.5. Sensing mechanism and electron transfer in MWCNTs coated with polypyrrole a) and surface composition after different annealing steps b). Reprinted from [12], with permission from Elsevier.

Another example of nanocomposites improving sensing properties are iridium oxide (IrO_x) decorated MWCNT sensors [13]. Compared to bare MWCNTs the IrOx loaded MWCNTs sensors exhibited higher stability and sensitivity. Improving the sensitivity towards 250 ppb NO_2 in 50%r.h. from 0.25 to 3.9 while operated at 150 °C. The iridium oxide nanoparticles improve the charge transfer between gas molecules and the sensor layer, therefore allowing for higher sensitivity. In the presented samples the nanoparticles exist in two states, IrO_2 and Ir_2O_3. The high sensitivity seems to originate from a redox reaction between Ir(III) and NO_2 in the form of:

$$NO_2(g) + Ir^{2+} \rightarrow NO_2^-(ad) + Ir^{3+} \quad (1)$$

Even though the sub-ppm sensitivity is outstanding, the moderate response time of 30 min and the high recovery time in the range of hours make this material combination only suitable if no fast read-out is necessary.

For nanocomposites not including graphene, CNTs or derivatives, similar findings have been published. Kulkarni *et al.* demonstrated that composites of

polyaniline and WO_3 showed a higher response towards toxic gases like NO_2 and NH_3 than their individual counterparts did [14]. Fort *et al.* mixed p-type Co_3O_4 and Al-doped ZnO (n-type) metallic nanoparticles in ratios from 0% to 100% and found that even small amounts of another material can have a rather large influence on the overall behavior of the sensor system [15]. Through the formation of pn-junctions the electrical behavior is modified. The optimum working temperature, the magnitude of the response as well as the sensor behavior cannot be derived from superimposing the single materials behavior. Through the presence of homo-, and heterojunctions the sensitivity is improved and stabilized (Figure 1.6).

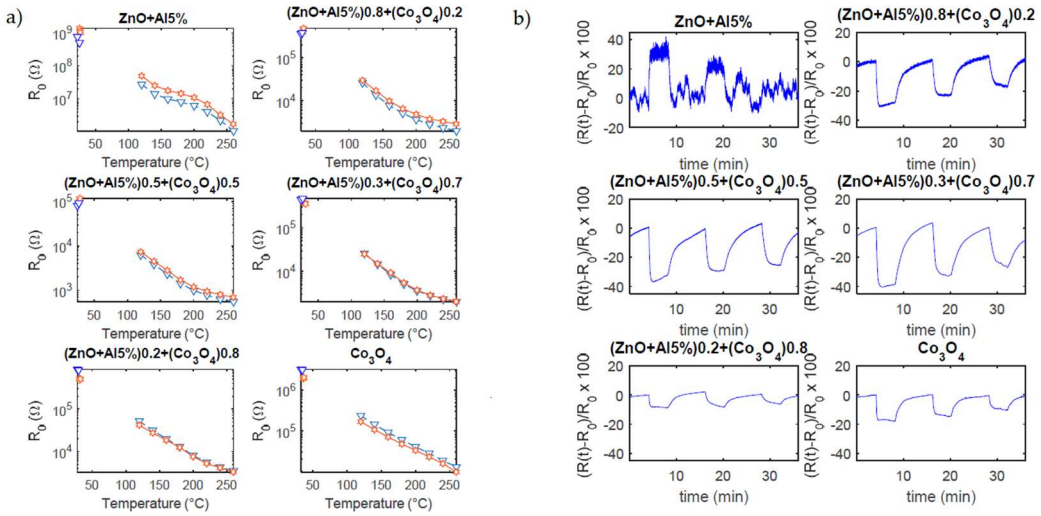

Figure 1.6. Resistance of Co_3O_4, Al-doped ZnO, and their mixtures (a). The mixtures resistances are lower than the initial resistances of the pure oxides. Sensitivities towards NO_2 of pure oxides and composites. The mixtures sensitivities also differ from the ones of pure oxides in b). Reprinted from [15].

A different approach apart from heating the surface to achieve sensitivity is presented by Yan *et al.* who used UV light to aid in detection of NO_2 [16]. This increased the response sevenfold up to 26% at 100 ppm and allows for responses to sub-ppm level concentrations. The UV irradiation cleans the surface from contaminants and provides more active adsorption sites. It also increases the desorption rate of analyte molecules from the surface and, in turn, decreases the recovery time of the sensor (Figure 1.7).

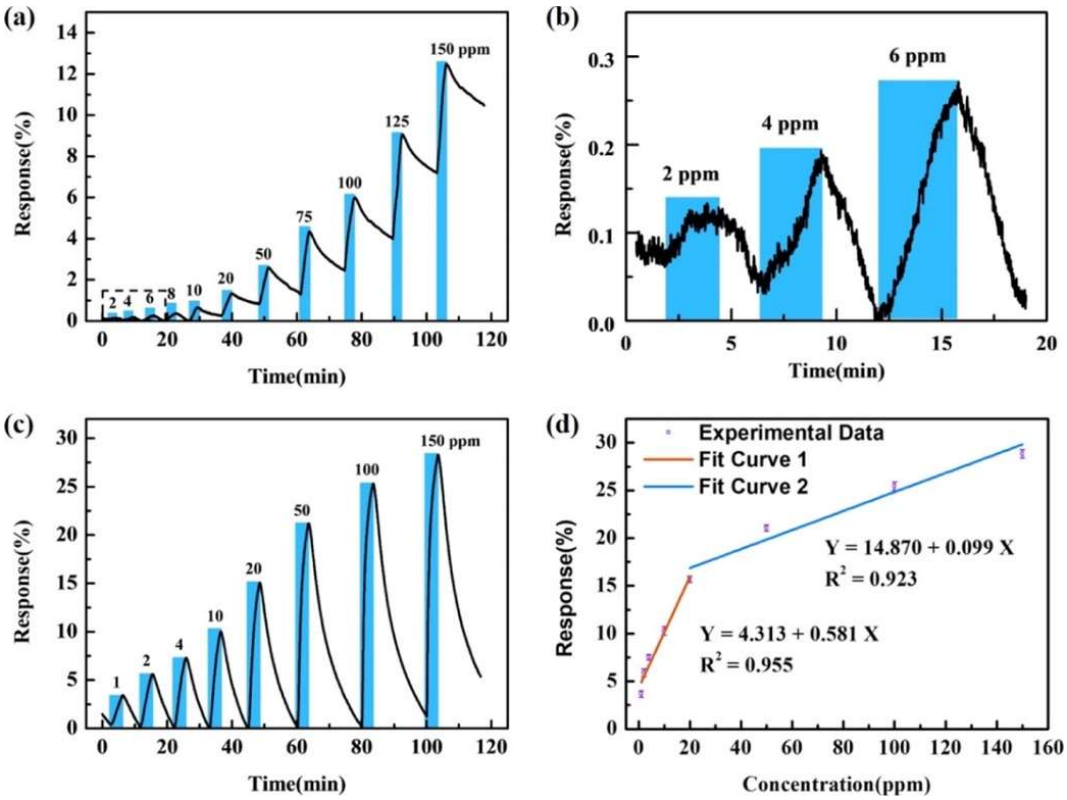

Figure 1.7. Response to NO_2 of varying concentrations and recovery of sensor without a) and b), with UV irradiation c). Fit curves of response values to NO_2 at RT with UV light. Reprinted with permission from [16] American Chemical Society.

1.4.2 Sensors for CO_2

Whereas for NO_2 many chemiresistive type sensors exist, the amount of chemiresistive CO_2 sensors is comparably low. Due to the low chemical reactivity of the CO_2 molecules, it is difficult to incite a chemical reaction at the surface of a sensor. Even though most conventional CO_2 sensors use infrared spectroscopy to avoid that issue, a few chemiresistive devices that overcome the problems are listed in Table 1.1. Bhadra *et al*. used electrospun PS as substrate and polymerized polyaniline containing graphene on top of the PS core [17]. The sensor response of pure PS/polyaniline material increased by adding graphene to the system from 0.59 up to 0.79. This result is owed to graphene's high electron transfer rate. The response and recovery time stay unaltered at 65 s with and without graphene. Unfortunately, the reasons for the same reaction time are not discussed. The work of Kanaparthi *et al.* shows, that it's possible to build a chemiresistor for CO_2 solely based on MOX nanomaterials (Figure 1.8) [18].

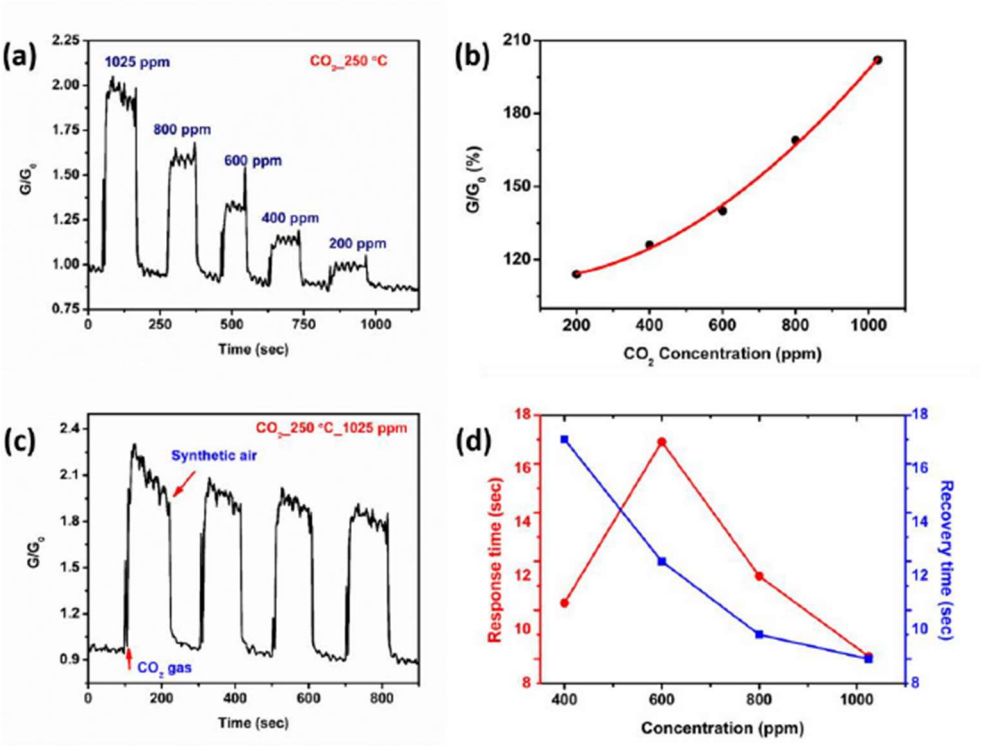

Figure 1.8. a) Sensor response towards different CO_2 concentrations c) repeatability towards the same concentration steps b) exponential sensitivity of sensor towards increasing analyte concentrations and d) response and recovery times are decreasing with increasing CO_2 content in the measurement chamber. Reprinted with permission from [18] Copyright 2019 American Chemical Society).

The high surface to volume ratio of the ZnO sensing layer allows for high sensitivity of 0.1125 at 600 ppm of analyte. The system also shows a short sub 20 s response and recovery time. ZnO and its oxygen deficiency leads to an n-type semiconducting behavior donating electrons. Through a series of reactions, the charge carrier concentration and therefore conductivity can be increased. For the maximum response at 50%r.h., the explanation is that towards this concentration the oxygen species and hydroxyl groups on the sensing layer increase and therefore the reactivity does. Beyond 50%r.h. the high amount of hydroxyl groups inhibits the reaction with oxygen groups and subsequently lowers the response. George *et al.* used a combination MOX nanomaterial and highly structured carbon nanotubes, whereas NiO nanoflakes acting as a p-type semiconductor [19]. The low selectivity of NiO as a room temperature gas sensor can be counteracted by the high sensitivity of the MWCNTs. Through a series of

interactions between CO_2 and hydrogen and hydroxyl ions carbonate ions form at the surface of the sensor. The CO_2 molecules consume electrons at the surface with each interaction, therefore lowering the resistance in the p-type material as shown in Figure 1.9.

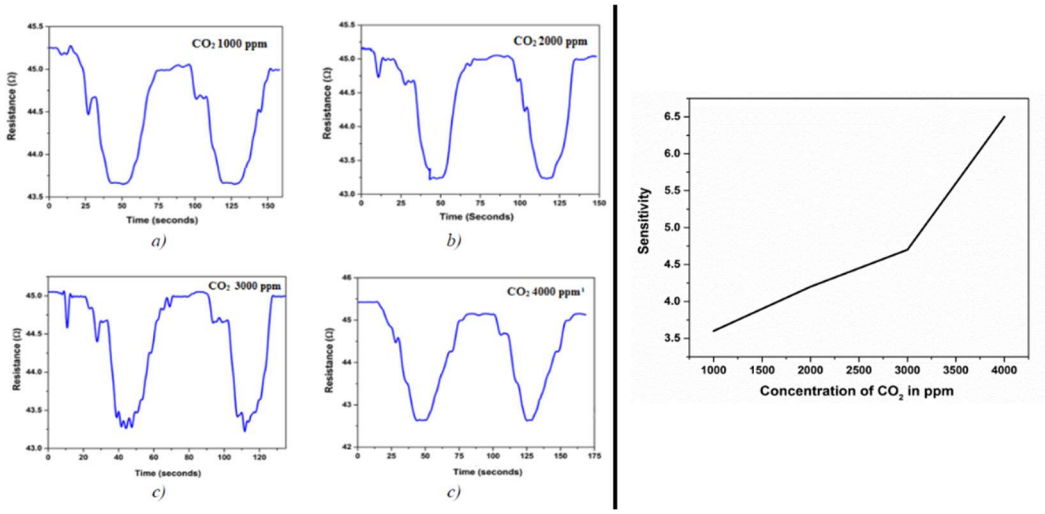

Figure 1.9. Left hand side: Sensitivity of the NiO-MWCNT nanocomposites towards a) 1000 ppm, b) 2000 ppm, c) 3000 ppm and d) 4000 ppm of CO_2. On the right hand the linear increase in sensitivity is shown. Reprinted from [19].

Table 1.1. Summary of sensor properties as NO_2 and CO_2 sensors of different material combinations.

Material	Response Definition	Sensitivity	Detection Limit	Operation Gases	Response/ Recovery Time	Operation Temperature	Identifier
graphene / SnO_2	$\frac{R_g-R_{air}}{R_{air}}*100$	5 ppm: 12.5%	-	NO_2 pure	180 s / 1500 s	R.T.	[7]
graphene / polystyrene beads	$\frac{R-R_0}{R_0}$	1 ppm: 2%	45 ppb	dry air	- / -	R.T.	[8]
rGO fiber / WO_3 nanorods	$\frac{R_g-R_{air}}{R_{air}}*100$	5 ppm: 9.2%	1 ppm	(2.6% r.h.)	480 s / 528 s	100 °C	[9]
rGO / MoS_2 NPs	$\frac{I_g-I_0}{I_0}*100\%$	10 ppm: 2483%	27.9 ppb (theoretical)	dry N_2 + diluted gas	12 min / 30 min	80 °C	[10]
rGO / Fe_3O_4	$\frac{R_{air}-R_{gas}}{R_{gas}}*100$	5 ppm: 1.7%	1 ppm	pure gases	300 s / 350 s	200 °C	[11]
CNTs / polypyrrole	$\frac{R_g-R_a}{R_a}*100\%$	5 ppm: 24.82%	250 ppb	25°C, dry air + dry N_2	65 s / 668 s	R.T.	[12]
MWCNTs / IrO_x NPs	$\frac{R_0-R_{gas}}{R_0}$	250 ppb: 3.9%	1 ppb, LOQ 3.2 ppb (theoretical)	dry	30 min / hours	25 – 150 °C	[13]
polyaniline / WO_3	$\frac{R_a-R_g}{R_a}*100\%$	100 ppm: 35%	1 ppm	40% r.h. + air	- / -	R.T.	[14]

Co_3O_4 / Al/ZnO	$\frac{R-R_0}{R_0}$	50 ppm: -40%	-	dry synthetic air + gas	1 min / 5 min	120 – 260 °C	[15]

Material	**Response Definition**	**Sensitivity**	**Detection Limit**	**Testing ambient**	**Response/ Recovery Time**	**Operating Temperature**	**Identifier**
polyaniline / graphene on polystyrol	$\frac{R_g-R_0}{R_0}$	60 ppm: 0.78	20 ppm	diluted in N_2	65 s / 65 s	R.T.	[17]
ZnO nanoflakes	$\frac{G}{G_0}$	600 ppm: 0.1125	200 ppm	pure gas	9 s / 9 s	250 °C	[18]
NiO / CNT	$\frac{R_a-R_g}{R_g}$	4000 ppm:6.5	1000 ppm	pure gas	15 s / 15 s	R.T.	[19]

1.4.3 Sensors for other Toxic Gases

To ensure human safety it is of utmost importance to detect harmful gases with sensors. The lowest limit of detection possible is desirable for these types of sensors. While for ammonia (NH_3) the maximum intake over an 8 h workday is set to 50 ppm by the Occupational Safety and Health Administration [20], the WHO recommends a limit of 81 ppb for 30 min of exposure for formaldehyde [21].

In terms of graphene-based sensors different approaches were used. Kodu et al. compared V_2O_5 layers on top of a graphene, deposited via pulsed laser deposition technique with epitaxial graphene (EG) on SiC [22]. The V_2O_5 functionalization enhanced the sensitivity towards NO_2, O_3, SO_2, CO and NH_3. The selectivity towards NH_3 over the other gases is also improved. Both graphene samples showed similar adsorption sites. This indicates that NH_3 binding takes mostly place at the functionalization. They also showed that by irradiating the sensing layer with UV light (365 nm) the sensitivity as well as the response and recovery times change. For EG the effect from irradiation is outstandingly strong. The typical p-type sensor response changes to an n-type response after shining UV-light on the surface. The light exposure leads to desorption of gas atoms from the surface, therefore cleaning it and opening up free binding sites. Adsorbates that act as p-type dopants like O_2 and H_2O are removed from this step and lead to the change of behavior Figure 1.10.

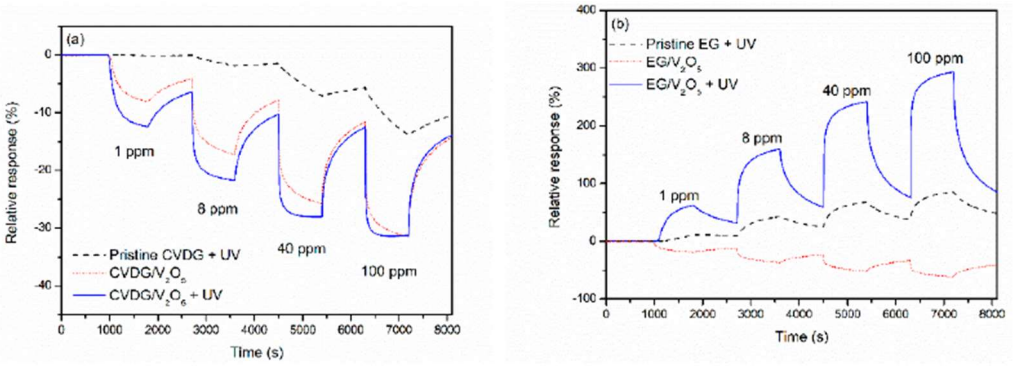

Figure 1.10. Sensor responses towards different NH_3 concentrations of a) pure CVDG and functionalized CVDG under UV (365 nm) irradiation. Red dotted line shows the reference without UV irradiation. b) Response of epitaxial graphene with and without functionalization and UV irradiation. Reprinted from [21].

The functionalization of graphene with MOX NPs has also been reported [23, 24]. Rodner *et al.* used Fe_3O_4 NPs to functionalize graphene and achieved responses of 0.04% and 0.02% for 1 ppb of formaldehyde and benzene respectively. The response and recovery times are approximately 50 s and 70 s, which is suitable for fast harmful gas detection. An alternative way for composite material is created from graphene foam (GF) by growing graphene on nickel foam by chemical vapor deposition (CVD) followed by etching the nickel with $FeCl_3$. Lastly graphene oxide (GO) was added by dipping the GF in GO solution. The GF/GO compound showed approx. 1.55 higher response towards 1500 ppm isopropanol as well as good selectivity against ethanol and methanol [25]. The lowest step of 100 ppm with a response of approx. 7% is acceptable for ethanol, where the threshold limit value (TLV) is 1000 ppm according to the National Institute for Occupational Safety and Health (NIOSH).

Research based-on CNTs is reported by Muangrat *et al.* who combined graphene nanosheets (GNS) with CNTs through a facile two-step CVD method [26]. Through the addition of GNS the response to approx. 1000 ppm ethanol increased from 0.22 to 0.69 and the limit of detection (LOD) decreased from 257 ppm to 13 ppm. Using a composite increased the recovery time significantly by almost a factor 4, while the response time remained unchanged. Janfaza *et al.*

used polymer NPs with CNTs to detect VOCs [27]. When exposed to the same gas concentrations, the sensor is most responsive to hexanal, and least responsive to methanol therefore showing a selectivity over the other gases.

Graphene oxide is commonly used in gas sensor applications as it is easy producible and scalable. Lee and Wang employed conductive polyaniline together with reduced graphene oxide (rGO) for room temperature ammonia sensing with a sub-ppm detection limit of 0.3 ppm [28]. The response of the composite was higher than the sum of the individual responses. The response and recovery time also change with the material composition. The compound exhibited lower response time of 1.6 min than either of the base materials (2 min and 3.4 min), whereas pure rGO has the lowest recovery time with 8 min. The decrease of response time is due to the higher sensing surface area by preventing aggregation of polyaniline. To detect VOCs rGO [29] and functionalization such as Si-nanowires [30], polymer nanowires [31] or by amino-groups [32] are in use and show sensitivities down towards sub-ppm level.

As well as graphene and MOX modifications there is also plenty of research towards rGO and MOX modification. Ternary nanocomposites of $Ag/SnO_2/rGO$ [33] and $Pt/WO_3/rGO$ [34] are used for VOC detection as well as selective triethylamine (TEA) detection in the first case (Figure 1.11).

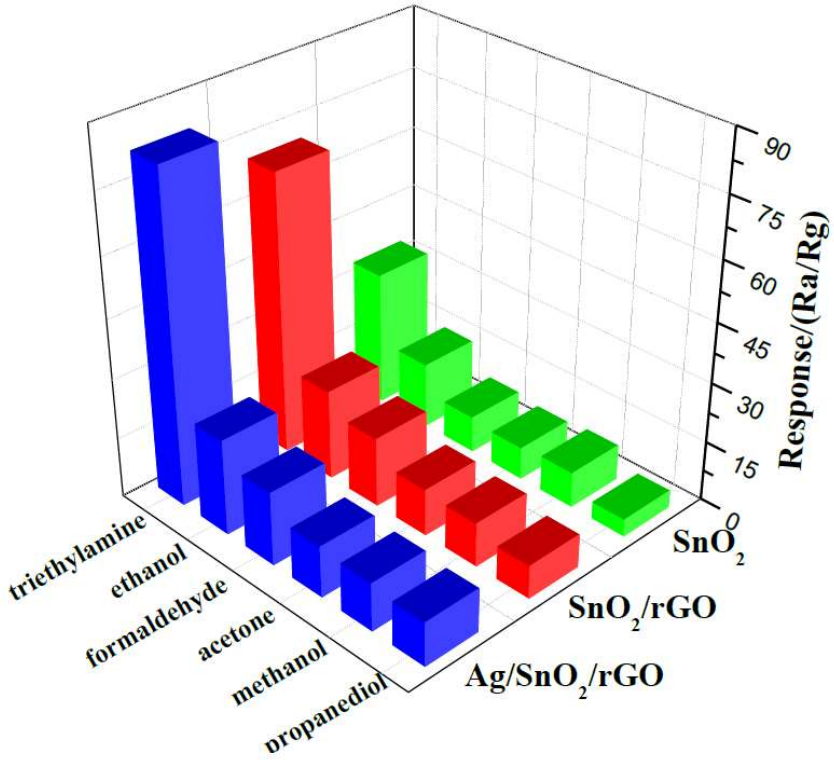

Figure 1.11. Sensitivity of three different sensors (SnO_2, SnO_2/rGO and Ag/SnO_2/rGO) to different gases. It is clearly visible that Ag/SnO_2/rGO shows the highest selectivity to triethylamine. Reprinted from [32] with permission from Elsevier.

Selectivity towards ethanol over other similar gases is the topic of Tian *et al.* who worked with rGO and Co_3O_4 NPs [35]. The higher sensitivity of the composite towards ethanol is owed to low oxidation potential of adsorbed oxygen, which is beneficial to selection of ethanol (Figure 1.12). Due to more defects in the synthesis Co_3O_4 adsorbed acetone molecules easily. Through heterojunctions between rGO and Co_3O_4 in turn reduced the possibility of adsorption of acetone and decreased the response accordingly. The same MOX nanomaterial was also used by Cao *et al.*, Jin *et al.*, and Gui *et al.* to detect VOCs [36-38].

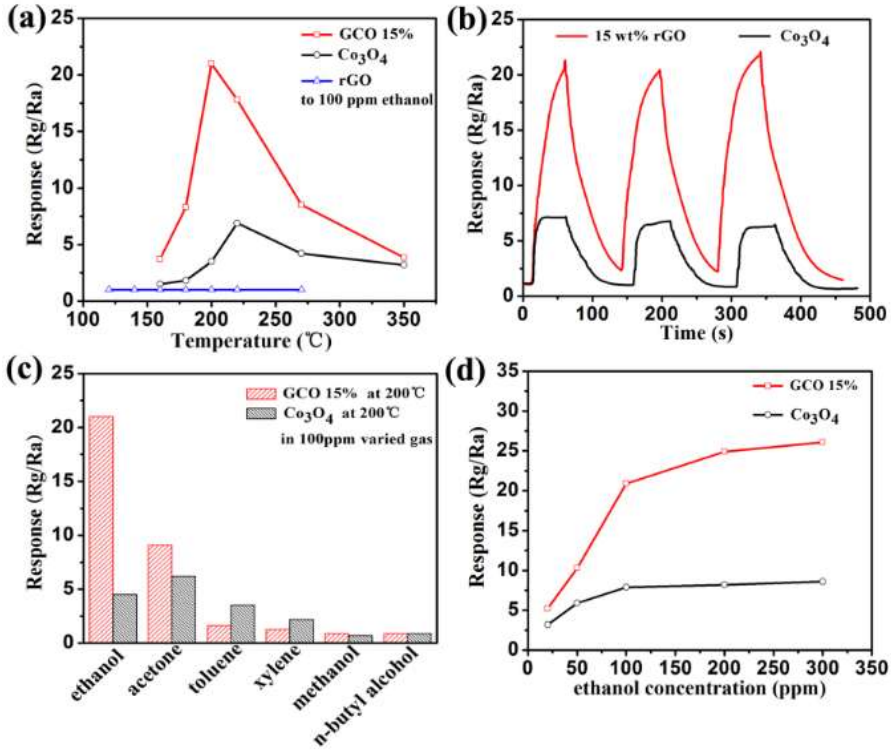

Figure 1.12. a) Temperature dependence of sensor response to ethanol; b) response and recovery with 100 ppm ethanol at 200°C; c) selectivity of GCO 15% to ethanol over other gases; d) response dependent on ethanol concentration Reprinted from [34] with permission from Elsevier.

In Table 1.2 different carbon-based devices are compared towards several factors critical in sensor development such as material combinations, sensitivity, target analytes as well as response, recovery times and operating temperature.

Table 1.2. Material combinations based on carbon nanomaterials for chemiresistive gas sensors for harmful gases.

Material	Response Definition	Sensitivity	Gas	Detection Limit	Operation Gases	Response/ Recovery Time	Operating Temperature	Identifier
graphene / V_2O_5	$\frac{G-G_0}{G_0}$	131%	NH_3	0.1 ppm	N_2	1887 s / 1607 s 329 s / 43 s 695 s / 658 s 474 s / 41 s	R.T.	[21]
graphene / Fe_3O_4	$\frac{R_g-R_0}{R_0}$	0.04% / 0.02%	formaldehyde benzene	1 ppb	synth. air	50 s / 70 s	150 °C	[22]
graphene / Pd / SnO_2	$\frac{R_{test}-R_{inert}}{R_{inert}} * 100$	10.5% H_2 / 6.8% ethanol	H_2 / ethanol	2% / -	N_2	27 s / 10 s 20 s / 27 s 35 s / 30 s	R.T.	[23]
GF / GO	$\frac{R_a-R_g}{R_a} * 100$	1500 ppm: 12.5% / 11.4% / 11%	isopropanol / ethanol / methanol	100 ppm	air	2 min/2 min	R.T.	[24]
CNT / GNS	$\frac{R_{Ethanol}-R_{N_2}}{R_{N_2}} * 100$	0.69%	ethanol	257 ppm 13 ppm	N_2	480 s / 525 s 428 s / 2000 s	R.T.	[25]
MWCNT / GNS	$\frac{\Delta R}{R_0}$	200 ppm hexanal: 2.5%	VOCs	10 ppm	pure analyte	450 s / 450 s	R.T.	[39]
Ag/ SnO_2 / rGO	$\frac{R_a}{R_g}$	80	VOCs/ triethylamine	0.5 ppm		30 s / 80 s 14 s / 70 s 11 s / 70 s	220 °C	[34[

1.5 Multigas Sensing

Even more challenging compared to the determination of a single gas is the simultaneous analysis of different gases in a complex mixture. VOCs, NO_2, O_3 and CO are all harmful and need to be detected all at once. Inherently, the high sensitivity of chemiresistive sensors is a positive trait. Here, so-called electronic noses come into play, which combine multiple sensors with different sensing materials to detect a specific fingerprint of a gas. Generally, the more different sensing fields there are the more gases can be discriminated. The optimal sensor array should be able to discriminate gases with the least required sensing fields through combination of data analysis. Sun et al. used this approach by combining an array of MWCNTs with non-covalently functionalization to selectively detect ozone [40]. The functionalization improved the response to 5 ppm ozone up to 34.4% Using principal component analysis (PCA) enables the classification of different. As shown in Figure 1.13, the sensor responses towards gases are clustered together for the individual gases, which proves that it is possible to distinguish the gases with the sensor array. The authors prove the selective determination of single harmful gases. Another example for the use of multiple receptors on one sensor is given by Freddi et al. who used an array of carbon nanotubes with nanoparticle decoration to detect different target molecules [41]. The array of sensors can detect gases and distinguish them through a PCA approach (Figure 1.14). When the sensor amount is increased to six by a humidity sensor the discrimination via PCA works better, especially for VOCs.

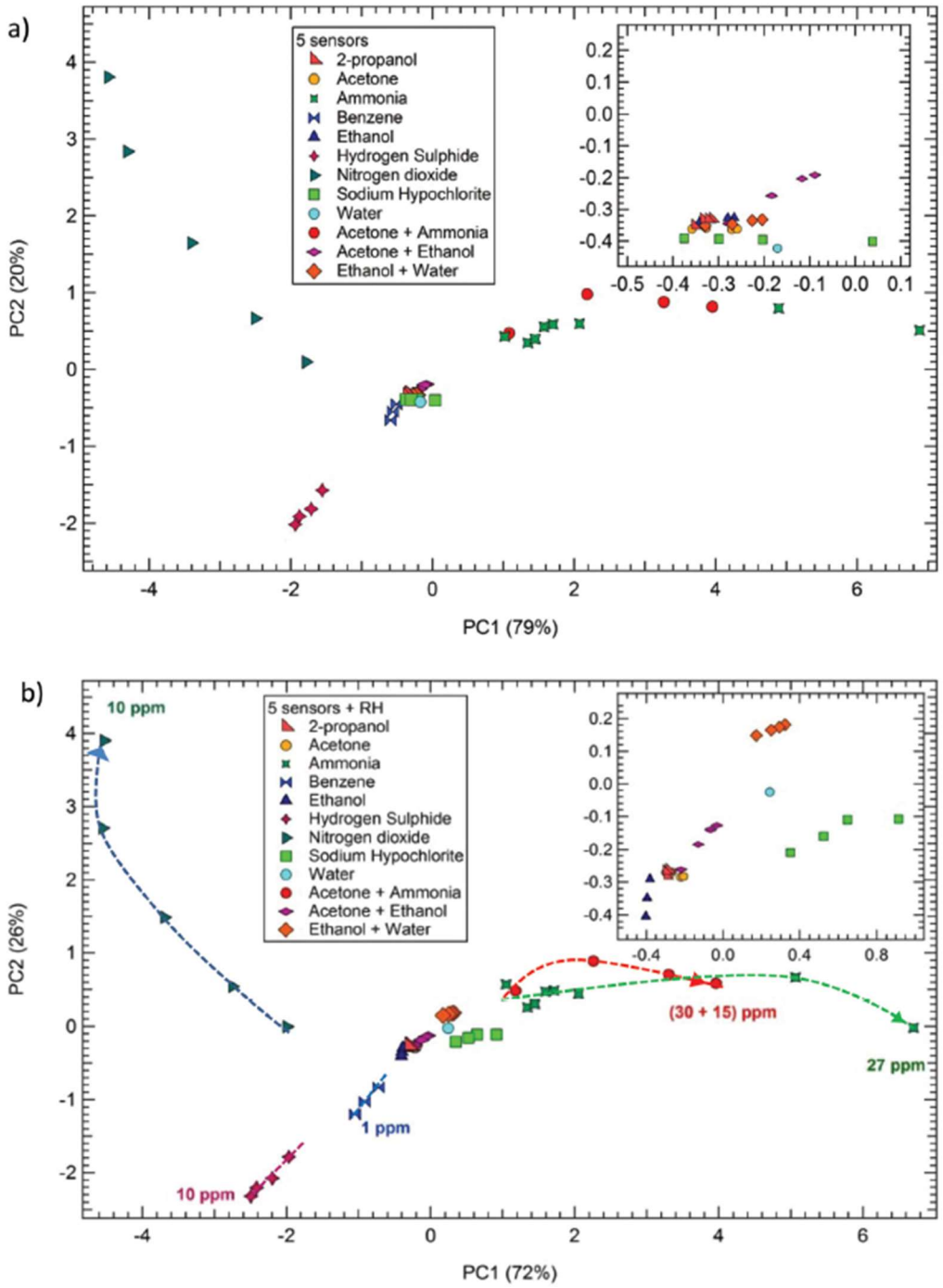

Figure 1.13. Results of PCA analysis with a) five gas sensors and b) five gas sensors and a humidity sensor. By adding the humidity sensor the discrimination ability increases, especially towards VOCs. Reproduced from [40] with Permission from Royal Society of Chemistry.

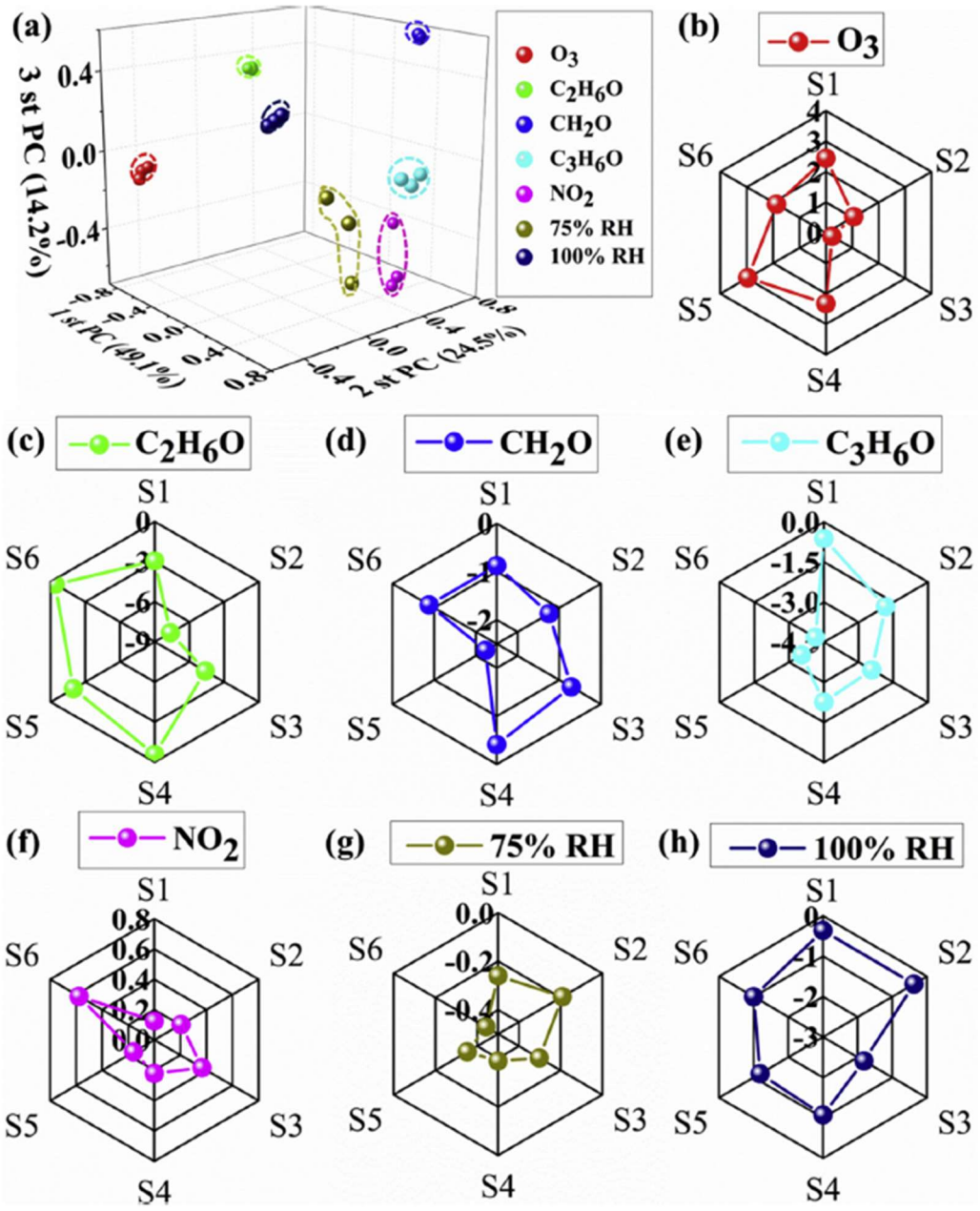

Figure 1.14. a) PCA chart with average sensor response of six sensors. Responses to gases b) O_3, c) ethanol, d) formaldehyde, e) propanol, f) NO_2, g) 75% r.h. and h) 100% r.h. Reprinted from [39] with permission from Elsevier.

1.6 Conclusion and Outlook

In this article, we compared current research papers about chemiresistive gas sensors based on nanomaterials. We conclude that there are various papers regarding research towards gas sensors in general. Nanomaterials of different elements and theircombinations are used in gas sensors and show valuable

properties for sensor applications. We can conclude that the main topics of research in chemiresistive gas sensors are a) increasing sensitivity, b) increasing selectivity, c) lower response and recovery times, and d) data evaluation and post processing for selectivity.

Graphene, CNTs, and derivatives like GO or rGO play a huge role due to their easy fabrication and manageability. This is true for their combination and interactions between nanomaterials. However, for gas sensing the interest in bare materials is slowing. Nowadays research is directed towards material composites from two or more materials. Many researchers use metal oxides in combination with the outstanding graphene properties to combine them into a device that in most cases achieves a result that the individual components could not achieve on their own. It is important to state that the properties of material mixtures differ from the initial material parameters and often overtake the sum of the initial parameter's sensitivities.

For harmful gases like ammonia, methanol, formaldehyde, and VOCs graphene and graphene-like materials are still the most used base materials while for NO_2 detection the base materials vary. Combination of nanomaterials also include conductive polymers, metal oxides and sulfides, as well as combination of two different metal oxides. Some research is also towards ternary composites in the form of noble metal, metal oxide and carbon-based nanoparticle where the noble metal acts as catalyst to facilitate the reaction while the sensitivity derives from the other two materials. It is palpable from the evaluated data that the sensitivity changes by combining different materials together in one sensor element. This trend is also noticeable for not only metal oxides and sulfides but also conductive polymers like polyaniline. Moreover, the sensitivity towards only one specific gas can be increased by combining materials, thereby increasing the selectivity of the sensor. This is especially striking for distinctly measuring VOCs.

Besides those improvements, the response and recovery time can be modulated. These reductions often originate from increase in active surface as well as reactivity due to changes in surface energy. It is desired to modulate the sensing behavior in such a way that the response and recovery time are minimal.

A different approach towards selectivity is the use of multiple sensing fields on the same chip. Each sensor field has a different material that reacts in a certain way towards analyte gases. The separation of gases happens in a later stage by evaluating the response with statistical approaches like PCA. This is the least published and yet most promising approach for integration in smart device later in the development cycle.

1.7 References

1 Meunier, C.; Ittershagen, M. Aktuelle Luftdaten. Umweltbundesamt, Fachgebiet II 4.2 Beurteilung der Luftqualität August 13, **2019**, accessed: 13.08.2019.

2. Otto, A. Aktuelle Messwerte der bayerischen Luftmessstationen. Bayerisches Landesamt für Umwelt August 23, **2019**., accessed: 23.08.2019.

3. Ou JZ, Ge W, Carey B, Daeneke T, Rotbart A, Shan W, Wang Y, Fu Z, Chrimes AF, Wlodarski W, Russo SP, Li YX, Kalantar-zadeh, K. Physisorption-Based Charge Transfer in Two-Dimensional SnS_2 for Selective and Reversible NO_2 Gas Sensing. *ACS Nano*. **2015**, 9(10), 10313–23.

4. Zhang H-F, Wu D-P, Ning X-J. Atomistic mechanism for graphene based gaseous sensor working. *Appl Surf Sci.* **2019**, 470, 448–53.

5. Choi SJ, Kim ID. Recent Developments in 2D Nanomaterials for Chemiresistive-Type Gas Sensors. *Electron. Mater. Lett.* **2018**, 14 (3), 221–260.

6. 1988 OSHA PEL Project Documentation Nitrogen Dioxide. The National Institute for Occupational Safety and Health (NIOSH) January 19, **1989**, accessed: 20.07.2021.

7. Zhang, L.; Shi, J.; Huang, Y.; Xu, H.; Xu, K.; Chu, P. K.; Ma, F. Octahedral SnO_2/Graphene Composites with Enhanced Gas-Sensing Performance at Room Temperature. *ACS Appl. Mater. Interfaces* **2019**, 11 (13), 12958–12967.

8. Fei, H.; Wu, G.; Cheng, W.-Y.; Yan, W.; Xu, H.; Zhang, D.; Zhao, Y.; Lv, Y.; Chen, Y.; Zhang, L.; Ó Coileáin, C.; Heng, C.; Chang, C.-R.; Wu, H.-C. Enhanced NO_2 Sensing at Room Temperature with Graphene via Monodisperse Polystyrene Bead Decoration. *ACS Omega* **2019**, 4 (2), 3812–3819.

9. Jang, J.-S.; Yu, H.; Choi, S.-J.; Koo, W.-T.; Lee, J.; Kim, D.-H.; Kang, J.-Y.; Jeong, Y. J.; Jeong, H.; Kim, I.-D. Heterogeneous Metal Oxide–Graphene Thorn-Bush Single Fiber as a Freestanding Chemiresistor. *ACS Appl. Mater. Interfaces* **2019**, 11 (10), 10208–10217.

10. Chen, T.; Yan, W.; Xu, J.; Li, J.; Zhang, G.; Ho, D. Highly Sensitive and Selective NO_2 Sensor Based on 3D MoS_2/rGO Composites Prepared by a Low Temperature Self-Assembly Method. *J. Alloys Cmpd.* **2019**, 793, 541–551.

11. Tung, T. T.; Chien, N. V.; Van Duy, N.; Van Hieu, N.; Nine, M. J.; Coghlan, C. J.; Tran, D. N. H.; Losic, D. Magnetic Iron Oxide Nanoparticles Decorated Graphene for Chemoresistive Gas Sensing: The Particle Size Effects. *J. Colloid Interface Sci.* **2019**, 539, 315–325.

12. Liu, B.; Liu, X.; Yuan, Z.; Jiang, Y.; Su, Y.; Ma, J.; Tai, H. A Flexible NO_2 Gas Sensor Based on Polypyrrole/Nitrogen-Doped Multiwall Carbon Nanotube Operating at Room Temperature. *Sens. Actuators, B* **2019**, 295, 86–92.

13. Casanova-Cháfer, J.; Navarrete, E.; Noirfalise, X.; Umek, P.; Bittencourt, C.; Llobet, E. Gas Sensing with Iridium Oxide Nanoparticle Decorated Carbon Nanotubes. *Sensors* **2018**, 19 (1), 113.

14. Kulkarni, S. B.; Navale, Y. H.; Navale, S. T.; Stadler, F. J.; Ramgir, N. S.; Patil, V. B. Hybrid Polyaniline-WO_3 Flexible Sensor: A Room Temperature Competence towards NH3 Gas. *Sens Actuators, B* **2019**, 288, 279–288.

15. Fort, A.; Panzardi, E.; Vignoli, V.; Hjiri, M.; Aida, M.; Mugnaini, M.; Addabbo, T. Co_3O_4/Al-ZnO Nano-Composites: Gas Sensing Properties. *Sensors* **2019**, 19 (4), 760.

16. Yan, X.; Wu, Y.; Li, R.; Shi, C.; Moro, R.; Ma, Y.; Ma, L. High-Performance UV-Assisted NO_2 Sensor Based on Chemical Vapor Deposition Graphene at Room Temperature. *ACS Omega* **2019**, 4 (10), 14179–14187.

17. Bhadra J, Popelka A, Abdulkareem A, Ahmad Z, Touati F, Al-Thani N. Fabrication of polyaniline–graphene/polystyrene nanocomposites for flexible gas sensors. *RSC Adv.* **2019**, 9(22), 12496–506.

18. Kanaparthi S, Singh SG. Chemiresistive Sensor Based on Zinc Oxide Nanoflakes for CO_2 Detection. *ACS Appl Nano Mater.* **2019**, 2(2), 700–6.

19. George, R.; Kumar, L. A.; Alagappan, M. Synthesis of Nanotubular NiO-CNT Composite and Its Application in Temperature Independent CO_2 Gas Sensors Fabricated Using Interdigitated Silver Electrode. *Dig. J. Nanomater. Bios.* **2019**, 14, 213–224.

20. 1988 OSHA PEL Project Documentation Ammonia. The National Institute for Occupational Safety and Health (NIOSH) January 19, **1989**, accessed: 20.07.2021.

21. Formaldehyde; International Programme on Chemical Safety, Ed.; Concise international chemical assessment document; World Health Organization: Geneva, **2002**, accessed: 20.07.2021.

22. Kodu, M.; Berholts, A.; Kahro, T.; Eriksson, J.; Yakimova, R.; Avarmaa, T.; Renge, I.; Alles, H.; Jaaniso, R. Graphene-Based Ammonia Sensors Functionalised with Sub-Monolayer V_2O_5: A Comparative Study of Chemical Vapour Deposited and Epitaxial Graphene. *Sensors* **2019**, 19 (4).

23. Rodner, M.; Puglisi, D.; Ekeroth, S.; Helmersson, U.; Shtepliuk, I.; Yakimova, R.; Skallberg, A.; Uvdal, K.; Schütze, A.; Eriksson, J. Graphene Decorated with Iron Oxide Nanoparticles for Highly Sensitive Interaction with Volatile Organic Compounds. *Sensors* **2019**, 19 (4), 918.

24. Dhall S, Kumar M, Bhatnagar M, Mehta BR. Dual gas sensing properties of graphene-Pd/SnO_2 composites for H_2 and ethanol: Role of nanoparticles-graphene interface. *Int J Hydrog Energy*. **2018**, 43(37), 17921–7.

25. Aslam S, Bokhari TH, Anwar T, Khan U, Nairan A, Khan K. Graphene oxide coated graphene foam based chemical sensor. *Mater Lett.* **2019**, 235, 66–70.

26. Muangrat W, Wongwiriyapan W, Morimoto S, Hashimoto Y. Graphene nanosheet-grafted double-walled carbon nanotube hybrid nanostructures by two-step chemical vapor deposition and their application for ethanol detection. *Sci Rep.* **2019**, 9(1), 7871.

27. Janfaza, S.; Banan Nojavani, M.; Nikkhah, M.; Alizadeh, T.; Esfandiar, A.; Ganjali, M. R. A Selective Chemiresistive Sensor for the Cancer-Related Volatile Organic Compound Hexanal by Using Molecularly Imprinted Polymers and Multiwalled Carbon Nanotubes. *Microchim. Acta* **2019**, 186 (3), 137.

28. Lee C-T, Wang Y-S. High-performance room temperature NH_3 gas sensors based on polyaniline-reduced graphene oxide nanocomposite sensitive membrane. *J Alloys Compd.* **2019**, 789, 693–6.

29. Şen Z, Öztürk S, Harbeck M, Öztürk ZZ. Room-temperature Sensing of Volatile Organic Compounds Using Graphene. *Sens. Mater.* **2019**, 31(4), 10.

30. Song, L.; Luo, L.; Xi, Y.; Song, J.; Wang, Y.; Yang, L.; Wang, A.; Chen, Y.; Han, N.; Wang, F. Reduced Graphene Oxide-Coated Si Nanowires for Highly Sensitive and Selective Detection of Indoor Formaldehyde. *Nanoscale Res. Lett.* **2019**, 14 (1), 97.

31. Tang N, Jiang Y, Qu H, Duan X. Graphene Oxide-Doped Conducting Polymer Nanowires Fabricated by Soft Lithography for Gas Sensing Applications. *IEEE Sens. J.* **2018**, 18(19), 7765–71.

32. Liu, B.; Huang, Y.; Kam, K. WL.; Cheung, W.-F.; Zhao, N.; Zheng, B. Functionalized Graphene-Based Chemiresistive Electronic Nose for Discrimination of Disease-Related Volatile Organic Compounds. *Biosens. Bioelectron.: X* **2019**, 1, 100016.

33. Zhang, S.; Zhang, B.; Sun, G.; Li, Y.; Zhang, B.; Wang, Y.; Cao, J.; Zhang, Z. One-Step Synthesis of Ag/SnO_2/rGO Nanocomposites and Their Trimethylamine Sensing Properties. *Mater. Res. Bull.* **2019**, 114, 61–67.

34. Chen, L.; Huang, L.; Lin, Y.; Sai, L.; Chang, Q.; Shi, W.; Chen, Q. Fully Gravure-Printed WO_3/Pt-Decorated rGO Nanosheets Composite Film for Detection of Acetone. *Sens. Actuators B* **2018**, 255, 1482–1490.

35. Tian M, Miao J, Cheng P, Mu H, Tu J, Sun J. Layer-by-layer nanocomposites consisting of Co_3O_4 and reduced graphene (rGO) nanosheets for high selectivity ethanol gas sensors. *Appl Surf Sci.* **2019**, 479, 601–7.

36. Cao J, Wang S, Zhang H, Zhang T. Facile construction of Co_3O_4 porous microspheres with enhanced acetone gas sensing performances. *Mater. Sci. Semicond. Process.* **2019**, 101, 10–5.

37. Jin, Z.; Wang, L.-P.; Zhang, Y.; Fan, J.; Liao, M.-H.; Wang, X.-F.; Ding, Y. Highly sensitive and selective ethanol sensors based on porous Co_3O_4 nanobelts synthesized through a facile wet-chemistry method. *J. Nanoparticle Res.* **2019**, 21(6), 115.

38. Gui Y, Yang L, Tian K, Zhang H, Fang S. P-type Co_3O_4 nanoarrays decorated on the surface of n-type flower-like WO_3 nanosheets for high-performance gas sensing. *Sens. Actuators B* **2019**, 288, 104-112.

39. Janfaza, S.; Banan Nojavani, M.; Nikkhah, M.; Alizadeh, T.; Esfandiar, A.; Ganjali, M. R. A Selective Chemiresistive Sensor for the Cancer-Related Volatile Organic Compound Hexanal by Using Molecularly Imprinted Polymers and Multiwalled Carbon Nanotubes. *Microchim. Acta* **2019**, 186 (3), 137.

40. Sun, Q.; Wu, Z.; Cao, Y.; Guo, J.; Long, M.; Duan, H.; Jia, D. Chemiresistive Sensor Arrays Based on Noncovalently Functionalized Multi-Walled Carbon Nanotubes for Ozone Detection. *Sens. Actuators B* **2019**, 297, 126689.

41. Freddi S, Drera G, Pagliara S, Goldoni A, Sangaletti L. Enhanced selectivity of target gas molecules through a minimal array of gas sensors based on nanoparticle-decorated SWCNTs. *Analyst* **2019**, 144(13), 4100–10.

2 Carbon Nanomaterials for Miniaturized Gas Sensors

2.1 Abstract

Nanomaterials are in the focus of research due to their outstanding chemical, physical and electrical properties [1]. Society is also becoming more aware of air pollution and its negative effects due to numerous debates. As interest is growing to unite these two areas, the interest in materials for miniaturized gas sensors is growing as well. This is a key step to enable the later integration of gas sensors into portable electronics. Within the scope of this work, carbon nanomaterials prepared by a modified Hummers method were tested and compared for their suitability as sensor materials for miniaturized, low-power consuming chemiresistive gas sensors. The graphene flakes have been characterized by optical flake size analysis, defects were compared using Raman spectroscopy and interpretations are given. Furthermore, the sensors response to NO_2 was evaluated. The temperature dependence of the signal was investigated as well as calculations towards the power consumption were done. The results provide a comparison of the graphene-based materials and indicate their usefulness in low-power miniaturized gas sensing.

This chapter has been published. Fabian Aumer, Fabian Hecht, Anton Kröner, Patrick Recum, Dr. Thomas Hirsch. *Mikrosystemtechnikkongress,* **2019**.

Author contributions: This manuscript was published in the proceedings of the Mikrosystemtechnikkongress 2019. PR and AK synthesized the materials. FH deposited the materials onto the sensor devices supervised by FA. FA performed the flake size characterization and the gas measurements. PR performed Raman

spectroscopy of the sensor surfaces. The manuscript was written by FA and revised by TH. FA is the corresponding author.

2.2 Introduction

The market of gas sensors offers several options mainly based on electrochemical transduction. Semiconductor materials allow the detection of gases with extreme low limit of detection down to about 100 parts per billion (ppb) and even the selectivity is excellent [2]. Nevertheless, the products available so far often suffer from poor robustness or complex calibration, and especially the ones with resistive readout need to be operated at high temperatures of 200 °C and higher, or bulky filters need to be applied to exclude humidity [3,4]. These features are accompanied by a large form factor and moderate energy consumption. Both are in contradiction to the need of portable sensing devices which can be integrated in wearables to improve the quality of life or for safety reasons. Two-dimensional carbon materials are well known for their outstanding electrochemical properties, especially their excellent conductivity [5]. Therefore, these materials are promising candidates in the development of gas sensors operated at low temperature. In this study we focused on the optimization of those materials in terms of fabricating them with a low number of defects and large flake size dispersed in inks to be compatible with the production lines of highly integrated gas sensors. This is the first report which demonstrates the benefit of such materials to be applied in gas sensors with low power consumption for a proof of concept study to detect NO_2 in air.

2.3 Experimental

2.3.1 Material synthesis

2.3.1.1 High Temperature Graphene Oxide (HTGO)

The synthesis of HTGO was performed by a modified Hummer's method [6]. 6 g flake graphite with 4.5 g $NaNO_3$ were suspended in 450 mL of 95% (v/v) H_2SO_4. The mixture was cooled in an ice bath, while 27 g $KMnO_4$ were added in small portions over a duration of 2 h under vigorous stirring whereby the temperature reached a maximum of 3 °C. The mixtures color changed from the graphite-grey to a dark green. During a sonication step the temperature went up to 60 °C. After 3 days of stirring at room temperature (RT) the color changed to violet. Yet, the end-temperature was approx. 30 °C. While cooling on ice, 450 mL of 5% (v/v). H_2SO_4 were added to the mixture, reaching a temperature of 45 °C. Heating at 100 °C for 2 h changed the color via yellow to a light-brown. After cooling to RT, 80 mL of 34% (v/v) H_2O_2 were added, resulting in heavy foaming. The brown dispersion of graphene oxide (GO) was centrifuged at 3000 g for 5 min and the supernatant was removed. The residue was washed three times with 3% (v/v). H_2SO_4 containing 0.5% (v/v) H_2O_2, two times with 1 M HCl and once with water. Then, the GO did no longer precipitate during centrifugation. As a final step about 1/3 of the mixture was dialyzed for 11 d against 8 L of water, which was changed three times. When the conductance reached a constant value the dialysis was stopped. The resulting GO suspension had a mass concentration of 2.6 $mg \cdot mL^{-1}$ which was determined by gravimetry.

2.3.1.2 Low Temperature Graphene Oxide (LTGO)

In comparison, also LTGO was fabricated by an adapted method as described by Eigler et al. which is also based on Hummer's method [7]. 2 g flake graphite with 1.5 g $NaNO_3$ were suspended in 150 mL of 95% (v/v) H_2SO_4. The mixture was

cooled to 0 °C in an ice bath, while 9 g $KMnO_4$ were added in portions over a duration of 8 h under stirring at 400 rpm. During that time, the temperature reached a maximum of 0.8 °C. The mixtures color changed from the graphite-grey to dark green. After permanently cooling by an ice bath overnight, the mixture was sonicated for 3 h at a maximum temperature of 8 °C, and stirred for 6 days at 4 °C in a cold water bath. No change in color was observable, as it was the case with the synthesis at high temperature. Water (200 mL) was added very slowly over a duration of 7 h to the mixture cooled by an ice bath to maintain the temperature below 10 °C. When the mixture starts to thicken, the color changes to violet and water was added to keep the suspension liquid. At the end of the hydrolysis the mixture had a brown color. After an additional night of stirring, 30 mL of 35% (v/v) H_2O_2 were added to the mixture very slowly, to prevent excessive foaming. The mixture got clear. The LTGO was then washed in the same manner, as for HTGO, but using cold solvents, storing the LTGO on ice and centrifuging at 0 °C. After dialysation for two weeks against 8 L of water, which was changed 5 times, conductance of the dispersion reached a constant and the dialysis was stopped. The final LTGO-solution had a concentration of 3.2 mg·mL^{-1}, which was determined by gravimetry.

2.3.2 Sensor Fabrication

For simplicity the suspensions will be referred to as inks from now on. The inks were diluted with water to a concentration of 0.1 mg·mL^{-1} and 1.0 mg·mL^{-1} for LTGO and HTGO respectively to ensure processability. Higher concentrations lead to clogging of the deposition device, while lower concentrations didn't result in a reproducibly continuous film. The sensor substrates are interdigitated gold electrodes on silicon nitride. They were cleaned and hydrophilized in a 30 s O_2 plasma step at 50 W. The inks were treated with an ultrasonic bath for 5 min to improve the dispersion of the particles. Following that they were drop-casted

with a semi-automated tool while heating the sensor surface to 50 °C to ensure uniform evaporation. The sensor substrate consists of eight sensor fields that can be separately read out. HTGO was applied to the four outer sensor fields while LTGO was applied to the four inner ones as shown on the bottom right hand side in Figure 2.1. After the deposition the carbon nanomaterials were thermally reduced from GO to rGO under N_2 atmosphere at 400 °C for 10 min. Afterwards the sensors substrates were bonded on a printed circuit board for further evaluation.

2.3.3 Characterization Techniques

For the flake size analysis Scanning Electron Microscope (SEM) pictures were taken at a Zeiss SEM 500 with an acceleration voltage of 1 kV. The pictures were taken with a back scattered electron detector. Raman measurements were taken on a DXR Raman Microscope from Thermo Scientific with a wavelength of 532 nm at a magnification of 10.

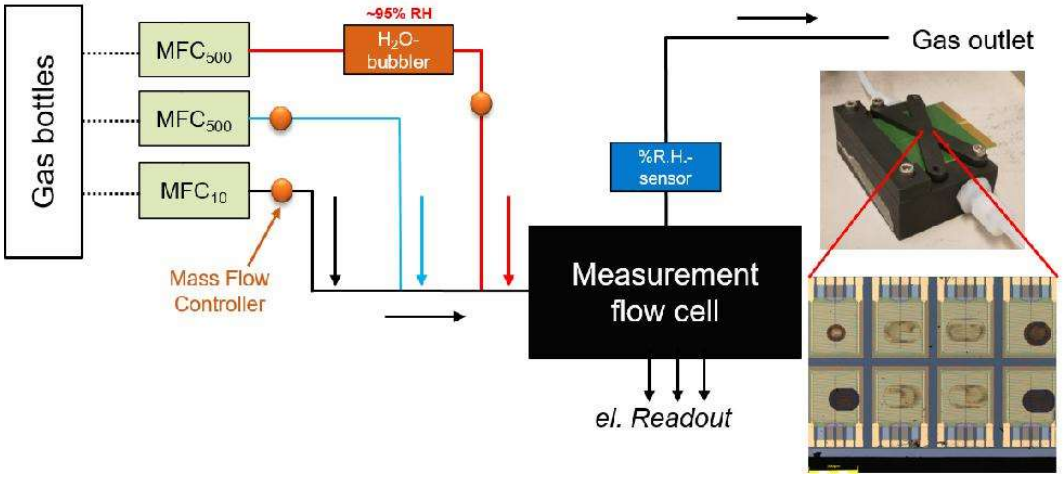

Figure 2.1. Scheme showing the mixture and application of test gases to the sensor. The measurement cell is depicted in the photograph. The inset shows the eight individual sensor fields. All sensor fields are connected to an electrical read-out system recording the resistance of the sensor material applied on the interdigitated electrodes.

Resistances with and without the presence of an analyte gas were measured at a self-built, fully automated gas characterization setup which is shown in

Figure 2.1. Target analyte gases were diluted by synth. air to the desired concentration values by mass flow controllers (MFC). Relative humidity (R.H.) was controlled by bubbling one stream of synth. air through a water bath and mixing the humid air with another stream of dry synth. air. The humid target gas/synth. air mixture was led into a small testing chamber of around 4 cm^3 were the sensor was located. For the first 1200 s the sensor was heated up to the target temperature and the measurement chamber was flooded with a constant stream of 100 sccm of synth. air in order to allow the sensor and setup to settle. Thereafter, a total flow of 100 sccm of target gas and synth. air at a specific concentration followed for 1200 s. Lastly came a step with 100 sccm flow of synth. air to regenerate the sensor for 1200 s. The last two steps were repeated for every tested concentration.

2.4 Results

2.4.1 Flake Size Analysis

The flake size distribution is one of the most influential parameters on the conductivity of the sensor films. Therefore, SEM images (Figure 2.2) of the diluted inks have been investigated by an image processing software to estimate average flake sizes. As visualized in Figure 2.3, the flake size distribution of HTGO ranges from ≤ 0.5 μm2 to 2 μm2. 90% of all flakes have an area of 0.5 μm^2 or lower, while the other 10% are spread out to higher areas with <1% at 2 μm^2. On the contrary, the flake size distribution of LTGO looks a lot different. The area range is wider and more big flakes were detectable. 90% of the flakes were between 0.5 μm^2 and 3 μm^2 in size. The rest of the flakes was larger with almost 9% showing an area of >4 μm^2, with the largest one being 60 μm^2. This shows that the low-temperature manufacturing process for GO flakes results in bigger flakes than the high-temperature method.

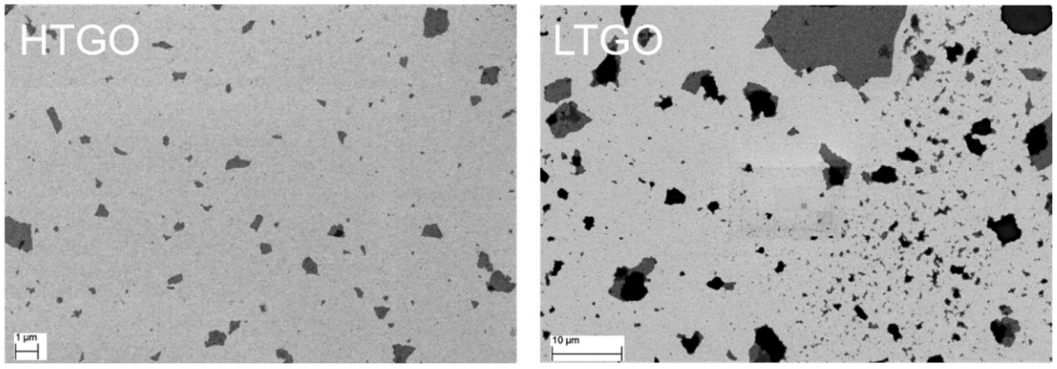

Figure 2.2. SEM pictures of HTGO and LTGO flakes on a gold film on a silicon wafer.

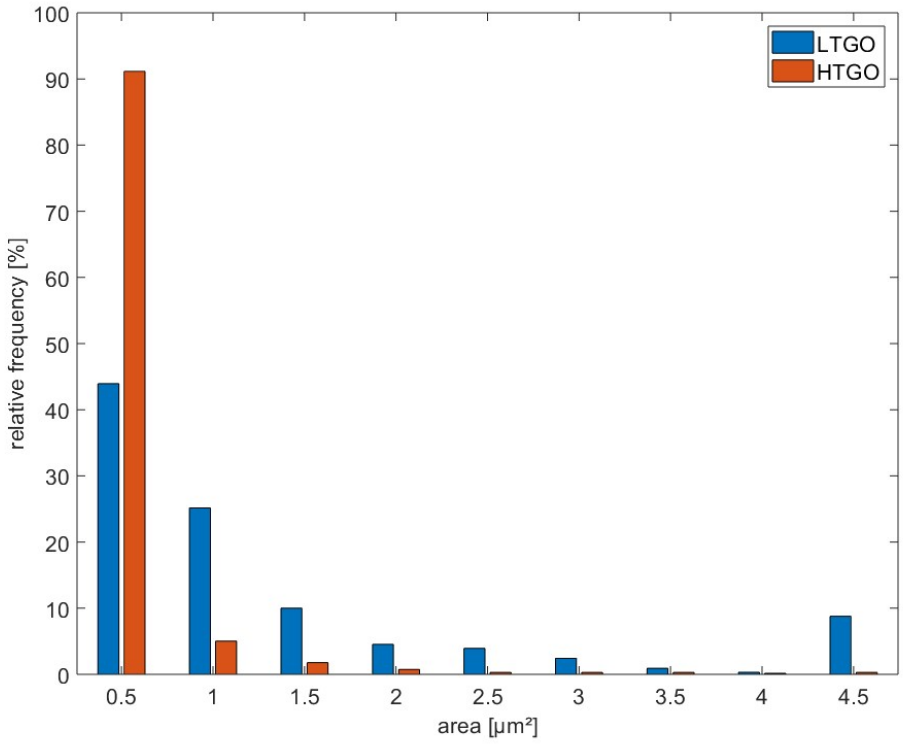

Figure 2.3. Flake size distribution of LTGO and HTGO. All flakes >4 µm² were sorted in the 4.5 µm² bin, even though their real dimension can be bigger.

2.4.2 Defect Analysis

GO modified surfaces are often thermally treated to cure the defects. The material is called reduced graphene oxide (rGO). So as to get an overview of the defect density Raman spectra were taken of the rGO surfaces after thermal reduction. From each sample 3 line scans with 50 spectra each were taken. Afterwards the

mean value was taken and the spectra were normalized to the G-Peak at approx. 1600 cm^{-1}. While the rLTGO exhibits a peak ratio (I_D/I_G) of 0.77 the rHTGO shows a ratio of 0.85. The lower peak ratio in rLTGO indicates a lesser defect density compared to the rHTGO [8]. This is in agreement with the results from the flake size analysis. The smaller flakes of rHTGO possess a higher amount of edges and therefore more defects.

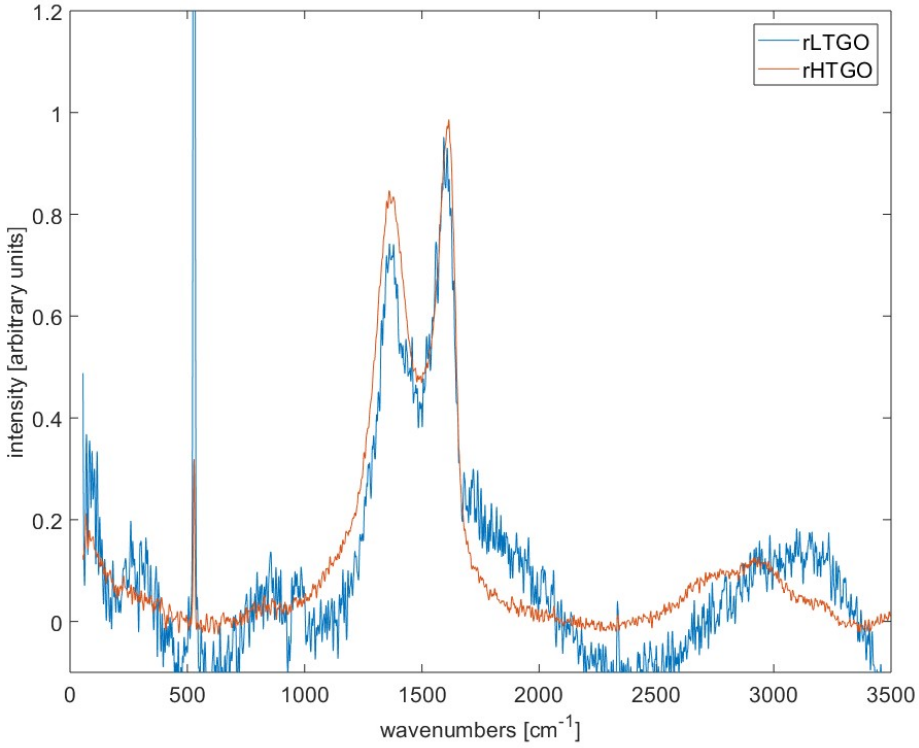

Figure 2.4. Raman spectra of rLTGO (in blue) and rHTGO (in orange) The lower concentration of rLTGO is the reason for the noisier signal and the prominent peak at 500 cm^{-1} representing vibrations from the silicon substrate.

2.4.3 Sensing Properties

The normalized sensor response *S* for changes in the resistivity upon the change in the composition of the gas mixture is defined in Eq. 1 as:

$$\boldsymbol{S = \frac{R - R_0}{R_0} * 100\%} \qquad 1$$

The resistances of the carbon material refer to the absence (R_0) and to the presence (R) of a certain amount of analyte gas. The change of resistance ΔR depends on the amount of adsorbed molecules n on the sensor surface following Eq. 2.

$$\Delta \boldsymbol{R} = \frac{\mathbf{1}}{\boldsymbol{q} * \boldsymbol{\mu} * (\boldsymbol{n_a} - \boldsymbol{n_d})} \qquad 2$$

The raw data from the measurements was normalized for better comparability and a moving average filter using 5 data points was applied to smooth the data.

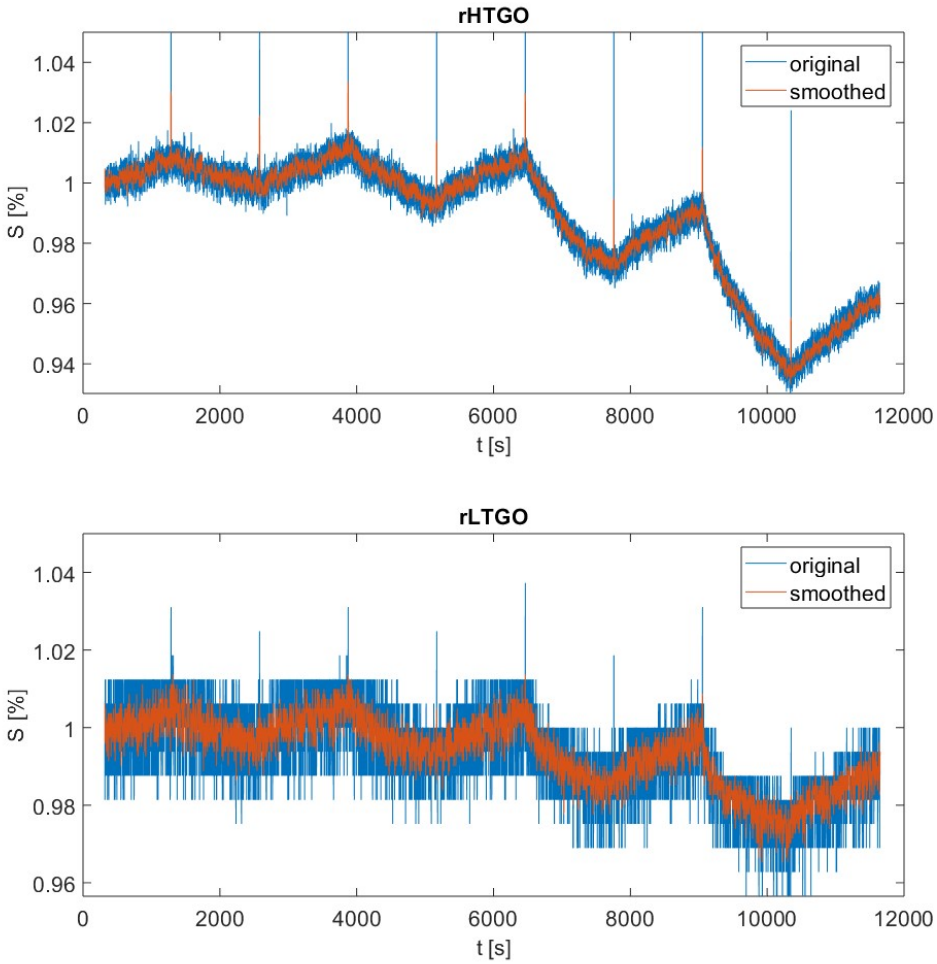

Figure 2.5. Response to 500, 1000, 2500 and 5000 ppb of NO_2 while the sensor surface was kept at a constant temperature of 50 °C. Humidity was fixed at 40%r.h.. rHTGO sensor on top, rLTGO on bottom.

The sharp periodic peaks are caused by the MFCs switching. For the collected response data at 50 °C and varying concentrations of NO_2 shown in Figure 2.5, the maximum response is 1.5% at 5000 ppb NO_2 for rLTGO and 7% for rHTGO. For the response of rLTGO it is visible that the signal is noisier compared to rHTGO response. At analyte gas concentrations of 500 ppb to 1000 ppb both materials can fully recover to the initial resistance values after flushing with synth. air. Whereas with higher concentrations of 2500 ppb to 5000 ppb the recovery is not completed within the given time before the next concentration step starts. Both materials react to NO_2 at temperatures slightly above room temperature. A temperature dependence of the sensor signal was detected and offers potential for further improvement. Again the findings are consistent and the more defective material shows a higher response to the analyte implying that the NO_2 more prone to bind at defective sites and induce a conductance change as proposed by [9].

2.4.4 Power Consumption

For later application in low energy systems it is of utmost importance to have a device that can be operated at low power. Most of the consumed energy comes from heating the sensor to operating temperature during the measurement. Following Eq. 3, the power for operating the system at different temperatures can be calculated.

$$\boldsymbol{P = U * I} \qquad \mathbf{3}$$

The power increases steadily from 7 mW at 30 °C to around 500 mW at 250 °C with a slope of 2.4 mW $°C^{-1}$ making a lower operating temperature of 50 °C consume only 15% of the power at 200 °C.

2.5 Conclusion and Outlook

Two differently produced Graphene Oxide materials were compared for low power gas sensing capabilities. We were able to manufacture miniaturized gas sensors that are able to detect NO_2 concentrations down to ppb levels while operating at slightly above room temperature. The possibility to operate the sensors at such low temperatures drastically facilitates future application in low-energy devices. Compared to one another, the rHTGO material showed better possibilities for sensing applications in the current state. A future challenge is to further optimize the sensor fabrication process in order to create rLTGO sensors with higher electrical resistance to make them viable for low power sensing. This could be done by operating the sensor without heating. As a result, the selectivity can suffer as well as the influence of humidity can increase. In order to counter that, additional research towards nanoparticles and material composites is required. They can be used as alternatives or functionalizations in miniaturized gas sensing to enhance sensitivity, selectivity and power consumption.

2.6 References

[1] Yang S, Jiang C, Wei S. Gas sensing in 2D materials. *Appl. Phys. Rev*. **2017** Jun;4(2):021304.

[2] Hossain M, Saffell J, Baron R. Differentiating NO_2 and O_3 at Low Cost Air Quality Amperometric Gas Sensors. *ACS Sens*. **2016** Nov 23;1(11):1291–4.

[3] Mead, M. I.; Popoola, O. A. M.; Stewart, G. B.; Landshoff, P.; Calleja, M.; Hayes, M.; Baldovi, J. J.; McLeod, M. W.; Hodgson, T. F.; Dicks, J.; Lewis, A.; Cohen, J.; Baron, R.; Saffell, J. R.; Jones, R. L. The Use of Electrochemical Sensors for Monitoring Urban Air Quality in Low-Cost, High-Density Networks. *Atmos. Environ.* **2013**, 70, 186–203.

[4] Cross, E. S.; Williams, L. R.; Lewis, D. K.; Magoon, G. R.; Onasch, T. B.; Kaminsky, M. L.; Worsnop, D. R.; Jayne, J. T. Use of Electrochemical Sensors for Measurement of Air Pollution: Correcting Interference Response and Validating Measurements. *Atmos. Meas. Tech*. **2017**, 10 (9), 3575–3588.

[5] Kochmann, S.; Hirsch, T.; Wolfbeis, O. S. Graphenes in Chemical Sensors and Biosensors. *TrAC* **2012**, 39, 87–113.

[6] Zöpfl A, Lemberger M-M, König M, Ruhl G, Matysik F-M, Hirsch T. Reduced graphene oxide and graphene composite materials for improved gas sensing at low temperature. *Faraday Discuss.* **2014**;173:403–14.

[7] Eigler S, Enzelberger-Heim M, Grimm S, Hofmann P, Kroener W, Geworski A, et al. Wet Chemical Synthesis of Graphene. *Adv Mater.* **2013** Jul 12;25(26):3583–7.

[8] Muzyka R, Drewniak S, Pustelny T, Chrubasik M, Gryglewicz G. Characterization of Graphite Oxide and Reduced Graphene Oxide Obtained from Different Graphite Precursors and Oxidized by Different Methods Using Raman Spectroscopy. *Materials*. **2018** Jun 21;11(7):1050.

[9] Zhang H-F, Wu D-P, Ning X-J. Atomistic mechanism for graphene based gaseous sensor working. *Appl. Surf. Sci*. **2019** Mar;470:448–53.

3 Electrical Impedance Spectroscopy on 8-channel PSoC-Based Miniaturized Board to Enable Data-Rich Environmental Sensing

3.1 Abstract

A variable signal generation and data readout board for miniaturized biochemical and chemical sensors for application in environmental monitoring, agro-food or biomedical applications is presented. The PSoC 5LP-based board is able to deliver DC as well as AC voltage or current of up to 62.5 kHz to a maximum of 8 different sensing fields as well as read back the resulting data and processing it on-board. A sensible use therefore is Electrical Impedance Spectroscopy (EIS). The data received from EIS carries a lot more information about the sensor surface or interaction with the surroundings compared to DC resistance measurements found in literature. Through the frequency-dependent response of the system one receives a much more detailed description of the sensor-analyte-interaction. This enables the use of more complex biological or chemical sensors as well as mixed sensors arrays. The system is evaluated using a gas sensor featuring an array of 8 sensor fields with different μ-dispensed functionalities and following algorithm-assisted data evaluation which can later be integrated on chip level.

This chapter has been published. Fabian Aumer, Torsten Hinz. *Smart Systems Integration Conference,* **2021**. Publication pending July 2021.

Author contributions: FA designed the system in cooperation with Torsten Hinz. FA built the system and validated it in cooperation with Torsten Hinz. FA is the corresponding author.

3.2 Introduction

With increasing pollution of surrounding in air, water and soil the need for environmental sensing is growing. Fine particles as well as harmful chemicals polluting air, water and soil. Extending on that, people's awareness for their surroundings, food and sustainability is growing as strong as never before in history. With ecological products more and more prominent in everyday life and the will towards a healthy life the need for environmental sensing is ever growing. In order to fulfill this need many different approaches are available. From devices to control air quality coupled with air purifiers and smart HVAC systems to the supervision of meat quality in super markets and testing the water quality in homes. Our motivation is to ensure the need for further testing devices can be met by using our newly designed, miniaturized board targeted towards use in predevelopment by enabling on-site testing through its small footprint and integrated data acquisition possibilities.

While many applications in e.g. gas sensing rely on resistance change for target analyte detection other uses like histamine sensing [1] require more complex methods as electrical impedance spectroscopy (EIS) for their detection. In order to increase sensor sensitivity many sensors are targeted to specific analytes and are therefore covered in analyte-specific functionalizations [2], [3]. With as many possibilities for sensor sensitivity increase there are also ways to increase the sensors unspecific sensitivity or selectivity. The selectivity of the sensor is of utmost importance to make sure the right harmful analyte is detected without sounding a false alarm. One way to achieve that is use different functionalizations combined in to an array on a single sensor device. This leads to fingerprint-like responses for each analyte if the surface modifications show different behavior towards the analytes if an array of different materials is used

for the sensing device [4]. On top of that, the sensor response as well as the validity of data can be enhanced by post processing of the data. Another approach to enhance the sensor selectivity is to use EIS to simultaneously detect analytes as well as interfering environmental factors as humidity [5]. While the sensitivity depends mostly on the specific material and the preparation parameters, the selectivity can be increased by a number of ways like EIS and sensor arrays.

However, a combined approach is not shown yet. In this paper we target this issue with our newly developed miniaturized data acquisition board based on PSoC component. Through the combination of EIS and multivariate data analysis we ensure the sensor selectivity. The board is validated on a gas sensor equivalent array but can also be transferred to applications in liquid sensing or other biomonitoring applications that require EIS on multiple sensor fields to enhance their use.

3.3 Board Design

3.3.1 Hardware

In order to make EIS possible we used the PSoC 5 LP from Cypress as the processing unit as its many integrated components allow for quick changes without the need for redesign. The setup is designed for galvanostatic EIS and positive voltage amplitude as well as DC offset voltages between 0-1 V. First, a sine wave is generated by the 8-bit WaveDAC component on board the PSoC 5 LP device. For DC-resistance measurement V_{AC} remains 0 V and only V_{DC} is applied. That sine wave is then filtered with a two stage Low-Pass-filter (blue in Figure 3.1) with f_c = 200 kHz to reduce aliasing at the ADC avoid current ripples affecting the EIS. ($R_1 = R_2 = 5.1$ kΩ; $C_1 = C_2 = 150$ pF) After filtering the current is

generated by an operation amplifier (OpAmp) in a voltage to current setup. The sensing current can be changed by switching either one of the three high precision (∓ 0.1%) reference resistors (R_{ref1} = 2 kΩ, R_{ref2} = 20 kΩ; R_{ref3} = 200 kΩ; red in Figure 1) to ground via connection to a pin in open drain, drives low configuration and leaving the other two floating. Therefore, a wide range of possible sensor resistances R_{sense} can be accurately measured. The voltage over R_{sense} (8 fields, green in Figure 1) can, if necessary, be amplified by a programmable gain amplifier (PGA, orange in Figure 1) and is fed into a 12-bit ADC for detection. Figure 1 shows the signal path from generation to detection. The ADC is synced to the waveform output and is oversampling the sine wave 16 times to ensure accurate sampling following Shannon-Nyquist theorem. For reference purposes we applied a nine-channel Multiplexer (MUX) for eight sensor signals as well as one additional reference resistor R_3 to determine phase delay offset in the system. Each sensor field is exposed to a continuously increasing frequency range. Most of the components, except the filter and reference resistor could be integrated onboard the PSoC 5LP device without the need for additional external setup. The integration of these onboard components allows for a small footprint of the sensor board. Each sensor field is exposed to a rising frequency range until the set number of frequencies (100 Hz – 62.5 kHz) have occurred and were detected at the ADC. Afterwards the active sensor is switched to the next channel in the MUX. This relatively high frequency range (>100 Hz) was chosen in order to be able to detect changes in the sensor system with high temporal resolution. For the detection of other processes e.g. food sampling the frequency range can be extended to lower ranges to accommodate for slower processes. This frequency spectrum is applied and the response detected for each sensor element on the board in series.

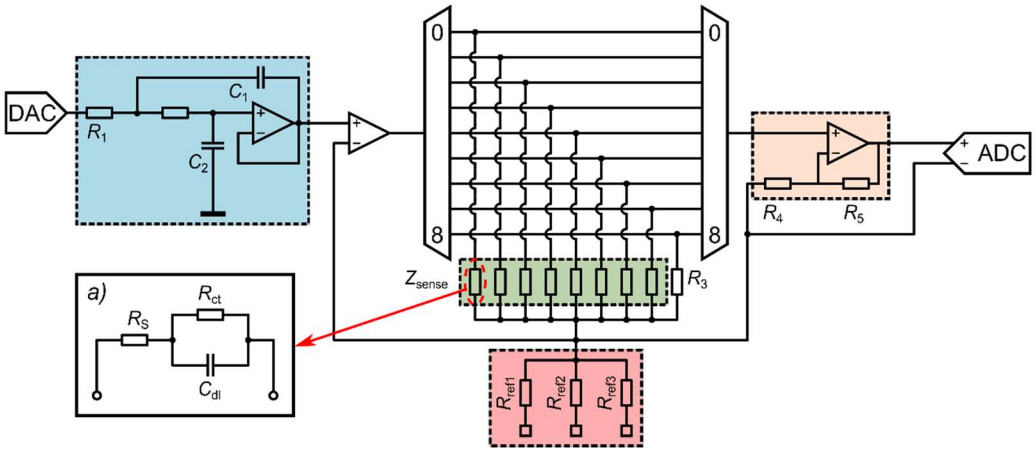

Figure 3.1. Schematic of board setup. Low-pass filter with fc = 200 kHz (left, blue); 8 connections for Devices under test (DUT) with equivalent test circuit of a sensor in inset a) + additional reference resistor R_3 for debugging (middle; green), 3 high precision reference resistors (red, middle), Programmable Gain Amplifier (PGA) for signal amplification (orange, right).

The board offers a 50 pin 2 slot board to board connector to easily add interchangeable sensor boards to it. Data acquisition and power is delivered via USB connection on board. Data is transmitted using USB UART and multivariate data analysis is done off-board. This step can later be integrated on-board as well. Additionally an SHTC3 sensor was added on board to measure humidity and temperature during the EIS measurement and allow for correction. The board is shown in Figure 3.2.

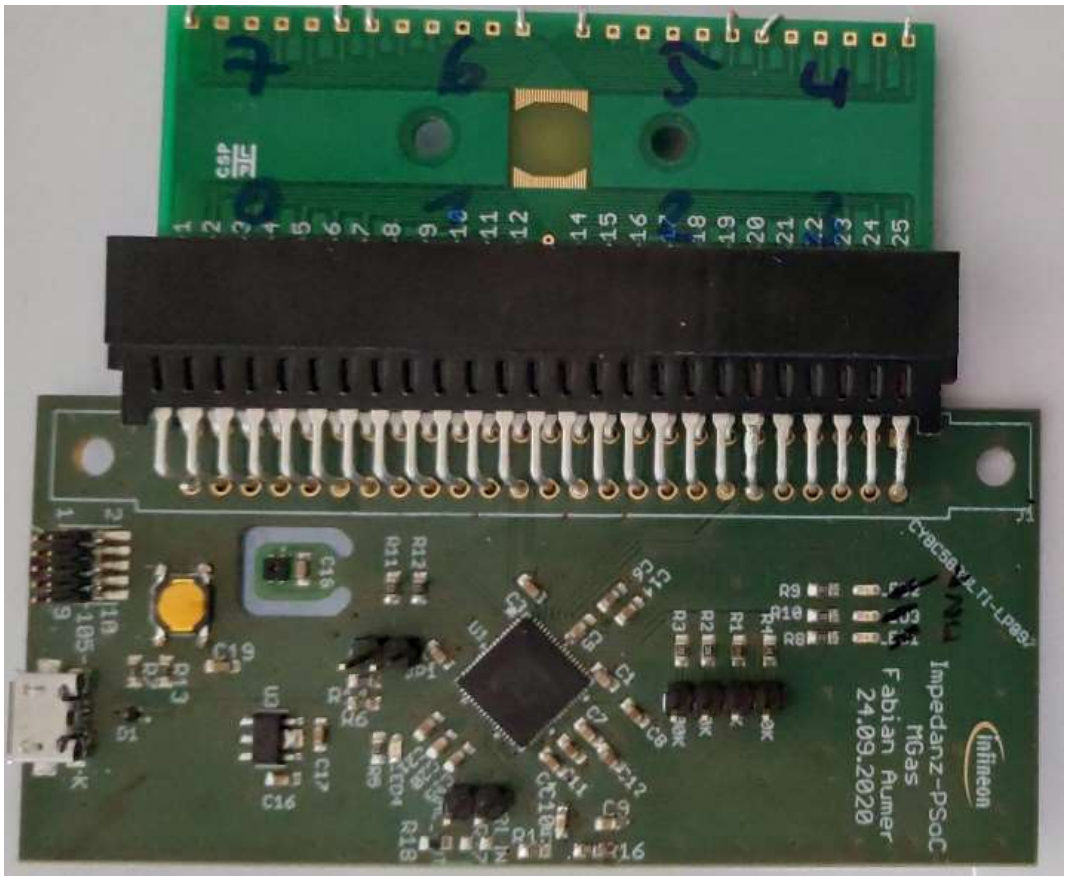

Figure 3.2. Physical version of the measurement board on the bottom including a 50 pin adapter for possible sensor devices on top

3.3.2 Firmware

In order to get the Impedance spectra at reasonable speed and low computing power we employed a simplified Discrete Fourier Transformation (DFT) targeted to each individual frequency, the Goertzel algorithm. This algorithm is commonly used in touch tone detection (DTMF) but can also be applied with little tweaking to work for EIS. The method uses less processing power than a Fast Fourier Transform (FFT) while still delivering the desired outcome. With little precomputing the required constants can be calculated once at the start of the program and do not have to be changed afterwards [6]. These constants are shown in the following equations (1) through (3):

$$\boldsymbol{k = 0.5 * \frac{N * f_{target}}{f_{sample}}} \quad \mathbf{1}$$

$$\omega = 0.5 * \frac{2\,\pi}{N} * k \quad 2$$

$$sine = sin(\omega); cosine = cos(\omega); coeff = 2 * cos(\omega) \quad 3$$

Here, *N* is the number of samples taken into calculation and the ratio of f_{sample} : f_{target} is a constant factor of 16:1, thereby ensuring an oversampling of 16x. As the target frequency f_{target} as well as the sampling frequency f_{sample} are the same ratio for each step and sample number *N* (=800) not changing, the Goertzel algorithm is perfectly suited for this application. Following the previous calculations each sample is then processed individually and at the end the final results are calculated. In practice this means that after 52 periods of sine generation with 16 samples per sine wave 832 samples arrive at the ADC. To ensure reliability the first 18 samples and last 14 samples of each sine wave are discarded and 800 samples are used to calculate the real (Z′) and imaginary part (Z′′) of each frequency response as well as magnitude (|Z|) and phase angle (φ). Three operation modes were integrated. Single acquisition of one sensor field (see Figure 3.3), single acquisition of each sensor field as well as continuous acquisition of each sensor field.

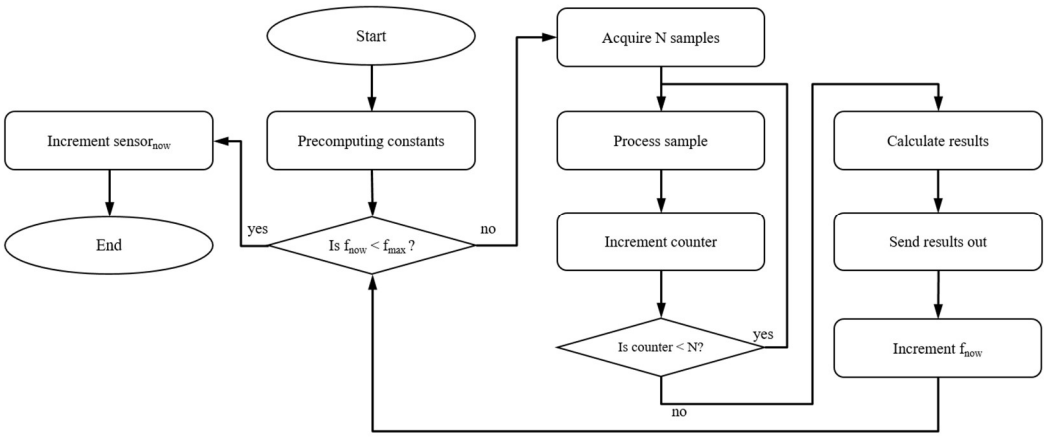

Figure 3.3 High level flow chart of a frequency sweep including data output on a single sensor field

The last one is the preferred method to ensure the highest temporal resolution of acquired data in a sensing system. The board communicates with the master device (PC) and opens a virtual COM-Port and waits for user input in an endless loop. The communication with the board is implemented via terminal program HTerm. Single char commands (1; 8 and c respectively) can be sent to the board and the board responds with the corresponding spectra of the active sensor field. After receiving a command, the board starts an EIS measurement and returns the values to the PC.

3.4 Testing and Capabilities

In order to test the functionality of the developed board we examined the phase response of a common equivalent circuit diagram used in electrochemistry, the Randles circuit seen in Figure 3.1, inset a). Where R_1 = 560 (±1%) Ω; R_2 = 10 (±1%) kΩ and C_1 = 33 (±5%) nF. As well as being a common circuit in electrochemical systems this circuit also exhibits a phase shift of about 56° in the delimited frequency range, making it perfect for testing purposes. First, the system was simulated in LTSpice XVII and afterwards the developed PSoC-

board was tested and the results were compared to gain insight on the performance. In Figure 3.4 the results of the benchmark are shown.

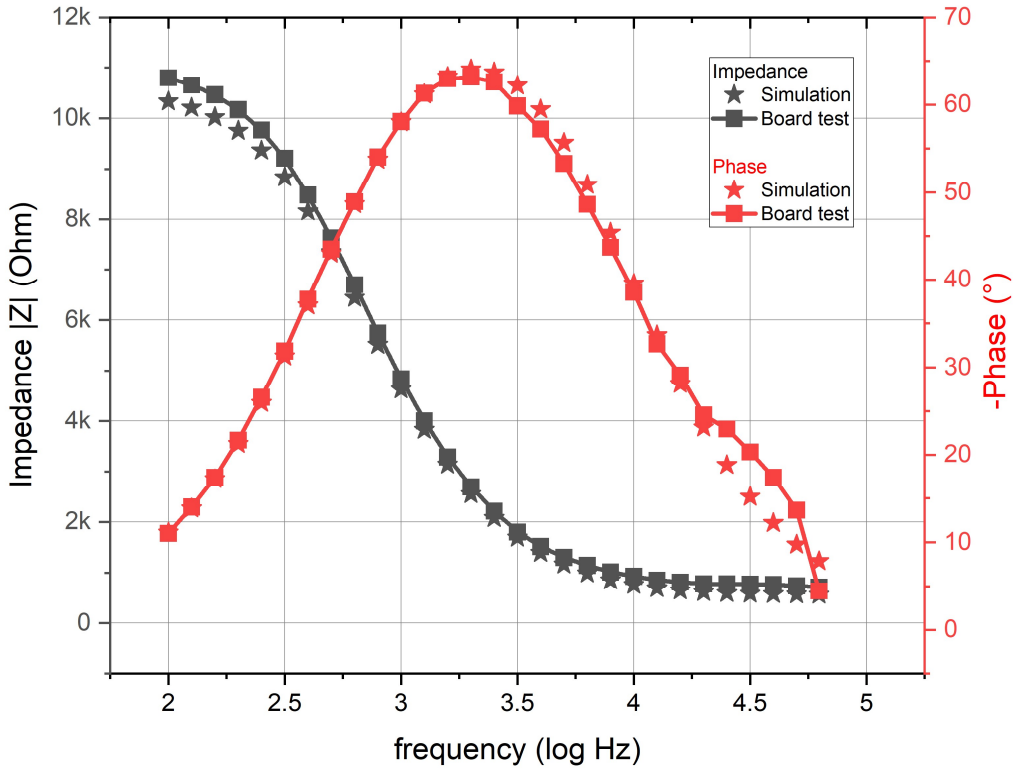

Figure 3.4. Frequency dependent phase behavior of test circuit. Simulated values (stars), and measured results (squares) for magnitude |Z| (black) and phase φ (red).

The board results pose the mean of 8 sensor fields tested. Firstly, there is no noticeable deviation between sensor fields, resulting in a low standard deviation. The median deviation for the magnitude |Z| with the board compared to the simulation results is -6.39%, whereas for the phase φ the value is -5.55E-1%. The most deviation for the phase occurs at higher frequencies, while the most deviation in magnitude occurs at lower frequencies. Table 3.1 shows a summary of the deviation from simulation results.

Table 3.1. Median deviation of Magnitude |Z| and Phase φ of measured values compared to simulation.

	Developed Board
Median Δ |Z| (%)	-6.39
Mean Δ phase φ (%)	-5.55E-1

3.5 Discussion and Outlook

We developed and tested a novel readout board that can perform Electrical Impedance Spectroscopy (EIS) on up to 8 sensor fields that can be interchangeably connected to the board via board connector. These results show that the board can be used for EIS in the given frequency range with a median deviation of -6.39% for impedance as well as -5.55E-1% median deviation for the phase angle φ. The findings indicate a usefulness for application of the developed board in a multitude of areas where EIS ma by relevant as e.g. environmental monitoring, agricultural or food testing or biomedical applications as well as water contamination testing. Furthermore the board is suitable for applications that benefit from an array of sensors to increase their analytic performance. While technically the lower limit for target frequencies is 2.61E-4 Hz with the current configuration, there is no practical use due to time critical processes on the sensor surface. The range at higher frequencies is capped at 62.5 kHz due to the maximum sampling speed of the onboard ADC of the PSoC device of 1 MHz In terms of precision, an improvement can be made in future iterations by sampling multiple time and applying a digital filter afterwards to improve the data. All in all this system offers a low-cost and miniaturized testing system for EIS in many different areas. The future potential of a combining the aforementioned array of functionalized material as well as an EIS based readout should be targeted next.

3.6 References

[1] Parate, K.; Pola, C. C.; Rangnekar, S. V.; Mendivelso-Perez, D. L.; Smith, E. A.; Hersam, M. C.; Gomes, C. L.; Claussen, J. C. Aerosol-Jet-Printed Graphene Electrochemical Histamine Sensors for Food Safety Monitoring. *2D Mater.* **2020,** 7 (3), 034002.

[2] Chen, Q.; Wang, Y.; Wang, M.; Ma, S.; Wang, P.; Zhang, G.; Chen, W.; Jiao, H.; Liu, L.; Xu, X. Enhanced Acetone Sensor Based on Au Functionalized In-Doped $ZnSnO_3$ Nanofibers Synthesized by Electrospinning Method. *J. Colloid Interface Sci*. **2019**, 543, 285–299.

[3] B. Alfano, E. Massera, T. Polichetti, M. L. Miglietta, and G. Di Francia, "Effect of palladium nanoparticle functionalization on the hydrogen gas sensing of graphene based chemi-resistive devices," *Sens. Act. B*, **Dec. 2017**,vol. 253, pp. 1163–1169.

[4] Liu, B.; Huang, Y.; Kam, K. WL.; Cheung, W.-F.; Zhao, N.; Zheng, B. Functionalized Graphene-Based Chemiresistive Electronic Nose for Discrimination of Disease-Related Volatile Organic Compounds. *Biosens. Bioelectron.: X*, **2019**, 1, 100016.

[5] Falco, A.; Loghin, F. C.; Becherer, M.; Lugli, P.; Salmerón, J. F.; Rivadeneyra, A. Low-Cost Gas Sensing: Dynamic Self-Compensation of Humidity in CNT-Based Devices. **ACS Sens.** *2019*, 4 (12), 3141–3146.

[6] E. Staff, "The Goertzel Algorithm," Embedded.com, Aug. 28, **2002**. https://www.embedded.com/the-goertzel-algorithm/ (accessed Jan. 29, 2021).

4 Impedimetric Sensing of NO2 with Carbon Nanomaterials at Ambient Temperatures and in Presence of Humidity

4.1 Abstract

Gas monitoring of hazardous volatile compounds is a highly discussed topic especially in times of continuously evolv-ing globalization. Many gas sensors targeting at NO_2 have been reported so far. Yet, most of them omit the influence of humidity, investigating the sensor's performance under laboratory conditions in dry environment or by measuring at high temperature coming at the cost of elevated power consumption. To address these drawbacks a recognition layer formed by various graphene materials, derived either mechanically, or synthesized by Hummer's method were examined upon layer thickness and defects on the sensitivity towards NO_2 sensing at room temperature. It turned out that the more defective reduced graphene shows a higher sensitivity which allows the determination of about 150 ppb NO_2 at variable relative humidity levels from 0 – 40%. Electrochemical impedance spectroscopy was chosen as read-out technology, as frequency dependent analysis in the range from 100 Hz to 1 MHz results in a data set which enables the clus-tering of the data points for NO_2, relative humidity and mixtures of both by principal component analysis. It is believed that this sensing technology together with improved electrode design and tailored nanomaterials can help to fabricate highly sensitive gas sensors to qualitatively and quantitatively detect individual gases within a complex mixture at ambient conditions.

This chapter is in revision for ACS Applied Nanomaterials. Fabian Aumer, Eva-Maria Kirchner, Sebastian A. Schober, Thomas Hirsch., **2021**.

Author contributions: EMK fabricated the nanomaterials and performed Raman Spectroscopy on the final samples. FA deposited the nanomaterials and performed electrical characterization under gas influence on the sensor surface. SAS helped process the data under supervision of FA. Further data analysis including PCA was done by FA. FA and TH wrote the manuscript and TH revised it. TH is the corresponding author.

4.2 Introduction

The progressing globalization leads to high emissions of potentially harmful gases, i.e., NO_2, which is mainly formed as combustion by-product of fossil fuels. Besides the traffic-based emission of NO_2, the main indoor source of toxic NO_2 is the combustion in stoves, heaters as well as tobacco smoke, which play a crucial role in terms of emerging health risk factors.[1] An increased uptake of NO_2 affects the respiratory system, which can lead to asthma and respiratory infections. The World Health Organization (WHO) recommends a maximum intake limit for 1 h of 100 parts per billion (ppb).[2] Poor air quality is a risk to health and environment, which makes gas monitoring inevitable.

Analytic devices based on optical spectroscopy or gas chromatography coupled with mass spectrometry provide reliable, accurate results with a low detection limit. Nevertheless, they suffer from bulky instrumentation, complex and cost-intensive analysis under operation of qualified personnel. The implementation of these devices into the everyday life of an ordinary consumer is simply impracticable.[3] To prevent individuals from putting themselves into a perilous situation caused by poor air quality, there is an urgent need for the wide

distribution of sensor systems in the environment.[4] Driving forwards the idea of Internet of Things technologies, mobile applications and automation, the need of miniaturized, cost-efficient, easy-operable, customized devices providing low detection limits, is more demanding than ever.[5] The simplicity of electrochemical gas sensors, i.e. based on the change of the intrinsic resistance of the sensor material upon gas exposure, lay the foundation for sensor technologies available for individual use.[6,7] Nevertheless, even if there is great attention in research on this field there are still hurdles to overcome to bring such sensors to market. A lot of studies investigate sophisticated composite materials to improve the sensitivity, but they still suffer from cross sensitivity and high-power consumption.[8] One major obstacle, which has to be ad-dressed is the omnipresent influence of humidity during monitoring of air quality.[9] The established metal oxide-based sensors deal with it by application of heating steps, desorbing water molecules from the sensor surface.[10,11] Yet, this does not fulfill the requirements of low power applications. A smart way to overcome these challenges is to use photoactivation, which was successfully demonstrated for the detection of NO_2 at low power and without interference with humidity.[12,13] Nevertheless, such sensors suffer from a complex setup and fabrication. Another possibility to minimize the sensor-humidity-interaction is to use 2D carbon nanomaterials as receptor layers.[14,15] They provide high surface-to-volume-ratio, low charge transfer resistance, facile synthesis and functionalization techniques.[16] To design a gas sensor based on 2D carbon nanomaterials offers a huge variation in the choice of materials. On the one hand there is almost perfect graphene, which consists of a single layer of sp^2 hybridized carbons only, not showing any band gap and therefore characterized by the behavior of a semimetal.[17] In contrast to this, a very ill-defined carbon lattice with many defects consisting of few to multilayer material, as it is presented by reduced graphene oxide (rGO), displays

semiconductor behavior.[18] In dependence of the material fabrication all intermediates are available and by screening the literature it becomes obvious that many of those materials have been used in gas sensors.[19,20] Still, there is a lack of information in comparing such materials regarding the advantages of either one type within this carbon material class in gas sensing. With this motivation we compare two different carbon nanomaterials in chemiresistive gas sensing for NO_2 at ambient temperature. Among the pool of graphite exfoliation techniques, the chemical synthesis is the most commonly used one. Promising results towards toxic gas analysis have been achieved so far, using reduced graphene oxide.[21,22] Nevertheless, the influence of humidity still plays a crucial role. On the one hand, it is targeted by operating the device under enhanced temperatures, subsequent thermal treatment or UV-illumination.[23] On the other hand, hydrophobic heterostructures are designed to reduce the impact of humidity.[24] In this work, the effect of humidity towards NO_2 sensing under ambient conditions is tackled by combining two approaches, a) choice of the proper material and b) frequency dependent read-out of the electrical properties during sensing.

Sensor characteristics on two of the most-suitable graphene allotropes to be integrated as sensor layer are conducted. Graphene, exfoliated by chemical synthesis, is compared to mechanical exfoliation upon their structural characteristics by Raman spectroscopy as well as contact angle measurements. From its morphology, mechanically derived graphene (meG), exfoliated by application of shear forces in an organic solvent is attractive as sensor material as it lacks oxygen residues and defective sites caused by oxidation procedures. With this, the sensing interface becomes hydrophobic which is expected to block water molecules more efficiently from absorbing to the surface. Reduced graphene oxide (rGO), as second studies material, is characterized by oxygen containing

groups which are beneficial in attracting the analyte gas and therefore to gain high sensitivity.

The chosen read-out technique in this approach is electrochemical impedance spectroscopy, as it allows to obtain information on the frequency dependent change of the resistivity. In contrast to a simple DC resistance measurement, in which the total signal is a sum of the signals generated by the individual gases, it is expected to get a better discrimination between the target gas and humidity. When graphene oxide is in contact with humid air the dielectric constant of the carbon material decreases linearly from 3.0 to 2.4 by an increase of the relative humidity (r.h.) from 0 to 60%.[25] This effect is attributed to hydroxyl groups binding to the defects within the carbon nanomaterial.[26] Changes in the dielectric properties of the material are known for their impact on the capacitive current and therefore on the imaginary part of the resistance when the impedance vector is analyzed in a Nyquist plot. Taking this into account, impedimetric gas sensing is expected to distinguish between NO_2 and humidity effects on the sensor signal already at room temperature.

4.3 Experimental Section

Reduced graphene oxide was prepared by a modified Hummer's method[27] with a subsequent reduction step based on hydrazine. China flake graphite (1 g) from K. W. Thielmann & Cie KG and $NaNO_2$ (0.75 g, 8.9 mmol) were mixed in conc. sulfuric acid (75 mL). The dispersion was stirred for 30 min, cooled in an ice bath and $KMnO_4$ (4.5 g, 28 mmol) was added. The mixture was sonicated for 4 h and afterwards stirred for 3 d at ambient conditions. After addition of H_2SO_4 (5% (w/v), 75 mL), the mixture was refluxed for 2 h at 115 °C. Excess $KMnO_4$ was precipitated by addition of H_2O_2 (30% (w/v), 15 mL). The suspension was centrifuged at 2,650 rcf and the supernatant was removed. The graphene oxide

was four times washed with H_2SO_4 (3% (w/v)) containing H_2O_2 (0.5%, (w/v)), two-times with HCl (3% (w/v)) and three times with H_2O followed by dialysis (pore size: 12 – 14 kDa) for 12 days. The graphene oxide dispersion (7 mL, β_{GO} = 0.5 mg mL^{-1}) was mixed with NH_3 (32% (w/v), 31 µL) and hydrazine monohydrate (98% (w/v), 5 µL). The mixture was refluxed for 1.5 h. The product was purified by three washing steps with H_2O.

Mechanically exfoliated graphene was prepared by shear exfoliation technique. A dispersion of 60 mg mL^{-1} China flake graphite in N-Methyl-2-pyrrolidone (NMP) (Honeywell) was exfoliated via ULTRA-TURRAX T25-S25N-18 G (IKA-Werke GmbH & Co KG) at 6,000 rpm for 1 h. The dispersion settled over night and was centrifuged at 500 rcf for 90 min. The supernatant was discarded, and the sediment resuspended in NMP. A second exfoliation step is performed at 6,000 rpm for 1 h. A centrifugation step at a speed of 1,000 rcf removed residual unexfoliated graphitic material. The meG dispersion (β = 0.126 mg mL^{-1}) was obtained after centrifugation at 9,000 rcf.

The sensor element consists of an array of eight inter-digitated gold electrodes on top of a silicon nitride wafer piece (Figure 4.S1). Before dispensing, the dispersions of the carbon nanomaterials (0.1 mg mL^{-1}) were sonicated for 5 min. The dispersions were drop-casted (6 nL for meG and 8 nL for rGO) on a single interdigitated electrode with a semi-automated VIEWEG F7000NV dispensing tool in combination with a micro dispensing valve VERMES MDV 3200+ while heating the sensor surface to 40 °C to ensure faster evaporation of the solvent. To vary the thickness of the carbon nanomaterial layer on top of the electrodes the dispensing was repeated. Finally, the sensor element was glued and bonded on a printed circuit board for further evaluation.

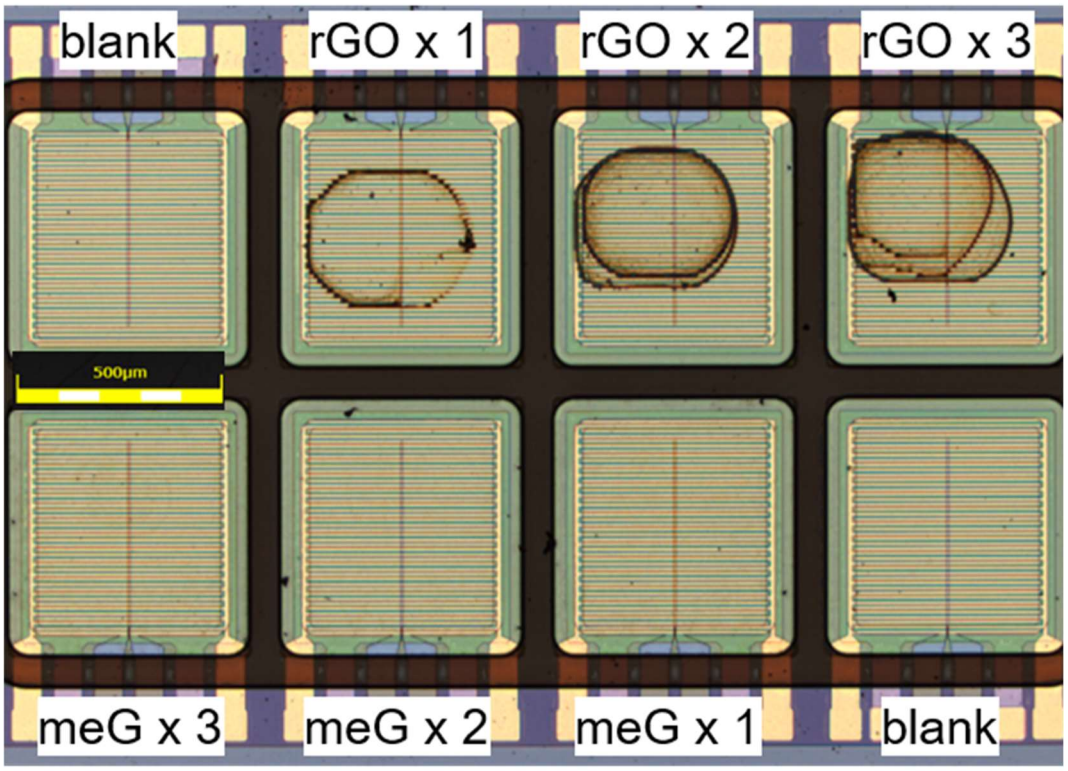

Figure 4.S1. Optical microscope image of the sensor element. It consists of eight interdigitated electrodes of 400 nm thick gold on top of 50 nm Si_3N_4. The length of the fingers is 500 µm and the width is 6 µm with 6 µm spacing in between. On the upper row rGO was dispensed on the lower row meG. The numbers indicate the number of dispensing steps. Due to different wettability, and smaller average flake size, meG cannot be visualized at this magnification. For rGO the larger flakes accumulate to a so-called coffee ring.

A DXR Raman microscope from Thermo Scientific was used for characterization of the carbon nanomaterials deposited on the sensor element. Raman spectra were recorded upon excitation at 532 nm at a power of 8 mW with a 50 µm slit at a 20-times magnification with an MPlan N objective (Olympus SE & Co. KG). The acquisition time is 0.8 s and spectra are averaged over 13 measurements.

Contact angle measurements via sessile drop technique with 0.2 µL H_2O were conducted on graphene-modified surfaces using a DataPhysics OCA 15EC (DataPhysics Instruments GmbH, Filderstadt, Germany). All contact angles given reflect the average value of three independent measurements.

Electrical impedance spectroscopy (EIS) at 51 frequencies ranging from 100 Hz up to 1 MHz was performed on a single interdigitated electrode applying an Agilent 4284A Precision LCR Meter coupled with a Hewlett Packard E5250 low leakage switch mainframe in order to record the data of individual sensors on the sensing element. The voltage amplitude V_{AC} was set to 50 mV at a bias voltage V_{DC} of +200 mV. When data points are presented together with error-bars, these values are the average of three measurements. The error bars are the standard deviations in these measurements.

For the DC resistance measurement, we used the same switch mainframe in combination with a digital multimeter (Hewlett Packard 3458A) to record each sensors response.

Gases were introduced to the measurement chamber by three mass flow controllers (Figure 4.S2). The first two supply dry and humid synthetic air respectively from in-house purified air, while the third one is used for the NO_2 gas, which is supplied from a pressurized bottle of 10 ppm NO_2 in synthetic air from Linde AG. The measurement cell consists of a custom-made 3D-printed flow cell with gas in- and outlet. Before the gases enter the flow cell, they are mixed in a passive mixer. Pneumatic valves ensure no reflow back in the gas pipes. Next to the sample outlet, a relative humidity sensor (Sensirion SHTx2) is installed in series to validate the relative humidity level in the chamber.

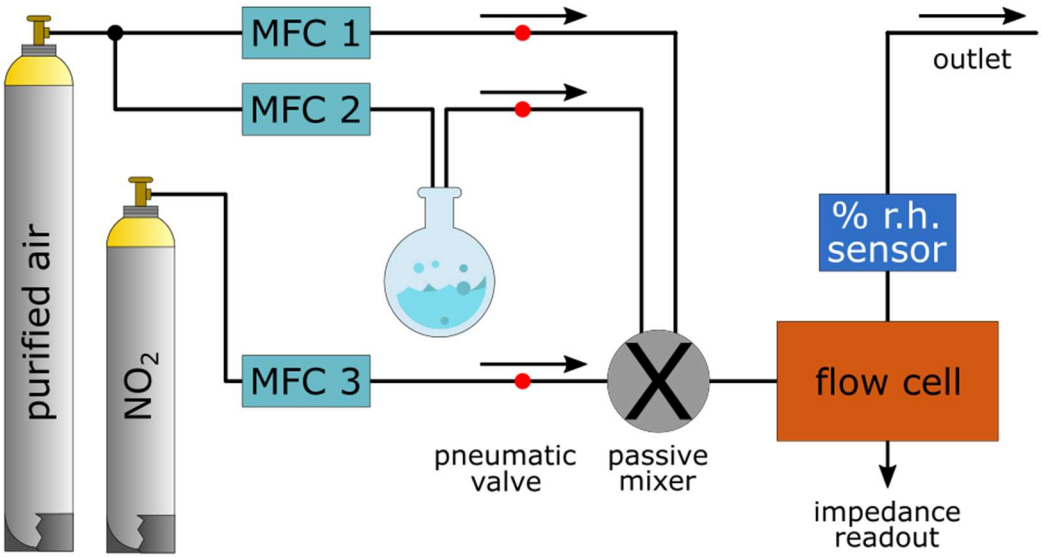

Figure 4.S2. The measurement setup consists of three mass flow controllers (MFC). The first two supply dry and humid synthetic air respectively, while the third one is used for the analyte gas. On the right-hand side is a custom-made 3D-printed flow cell with gas in- and outlet that can be plugged onto gas tubes. Before the gases enter the flow cell, they are mixed in a passive mixer. Pneumatic valves ensure no reflow back in the gas pipes. The sensor device was screwed on the chamber and sealed shut with silicon foil between the printed circuit board and the connection to the chamber. Behind the sample outlet, a relative humidity sensor is installed in series to validate the relative humidity level applied to the sensor element

4.4 Results and Discussion

The two graphene samples, rGO and meG, have been synthesized by a modified Hummers method and by mechanical shear exfoliation. After purification, a dispersion of rGO in water and meG in NMP with identical mass concentration of 0.1 mg mL^{-1} was used to apply the materials under identical conditions onto solid supports. Solvents have been evaporated at ambient temperature under vacuum before characterization. Raman spectroscopy allows to evaluate the structural details of the different graphene materials upon the number of intrinsic defects. Figure 4.1a shows the Raman spectra for rGO and meG. The D-band, located at around 1,350 cm^{-1}, the G-band at around 1,580 cm^{-1}, and the 2D-band at 2,700 cm^{-1} are the characteristic vibrations to be found. As no band of the solvent NMP (Figure 4.S3) was found, its removal was successfully proven.

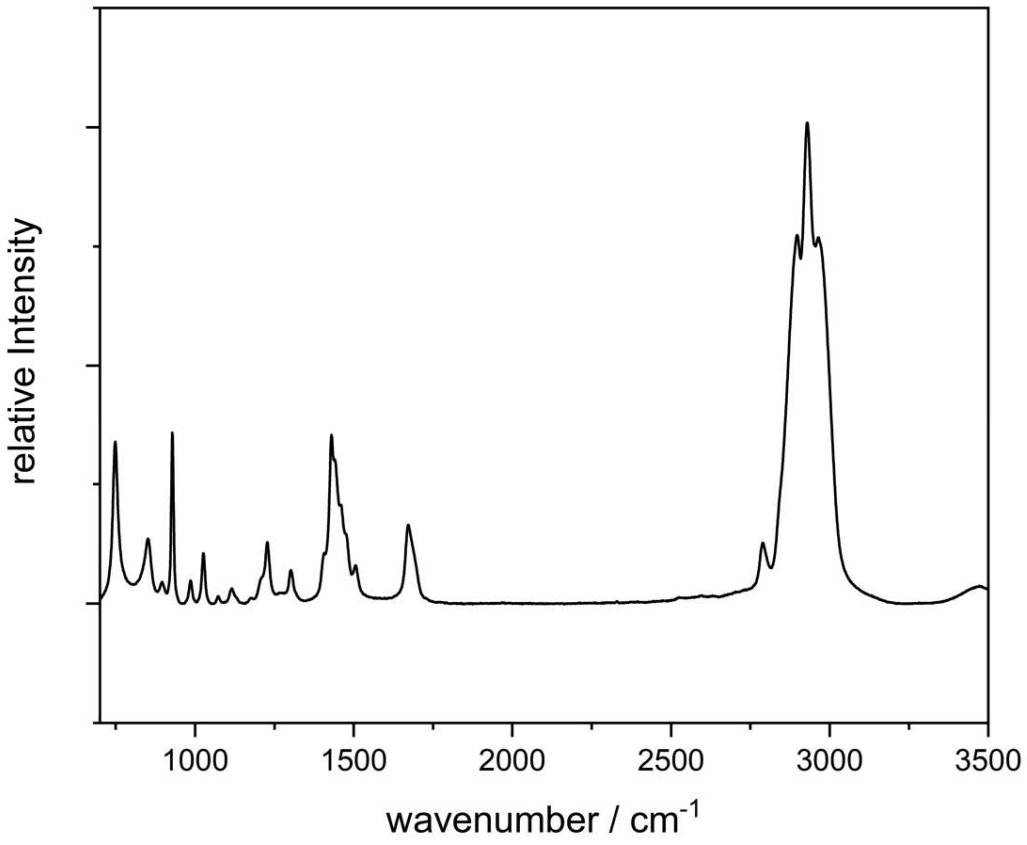

Figure 4.S3. Raman spectrum of N-methyl-2-pyrrolidone.

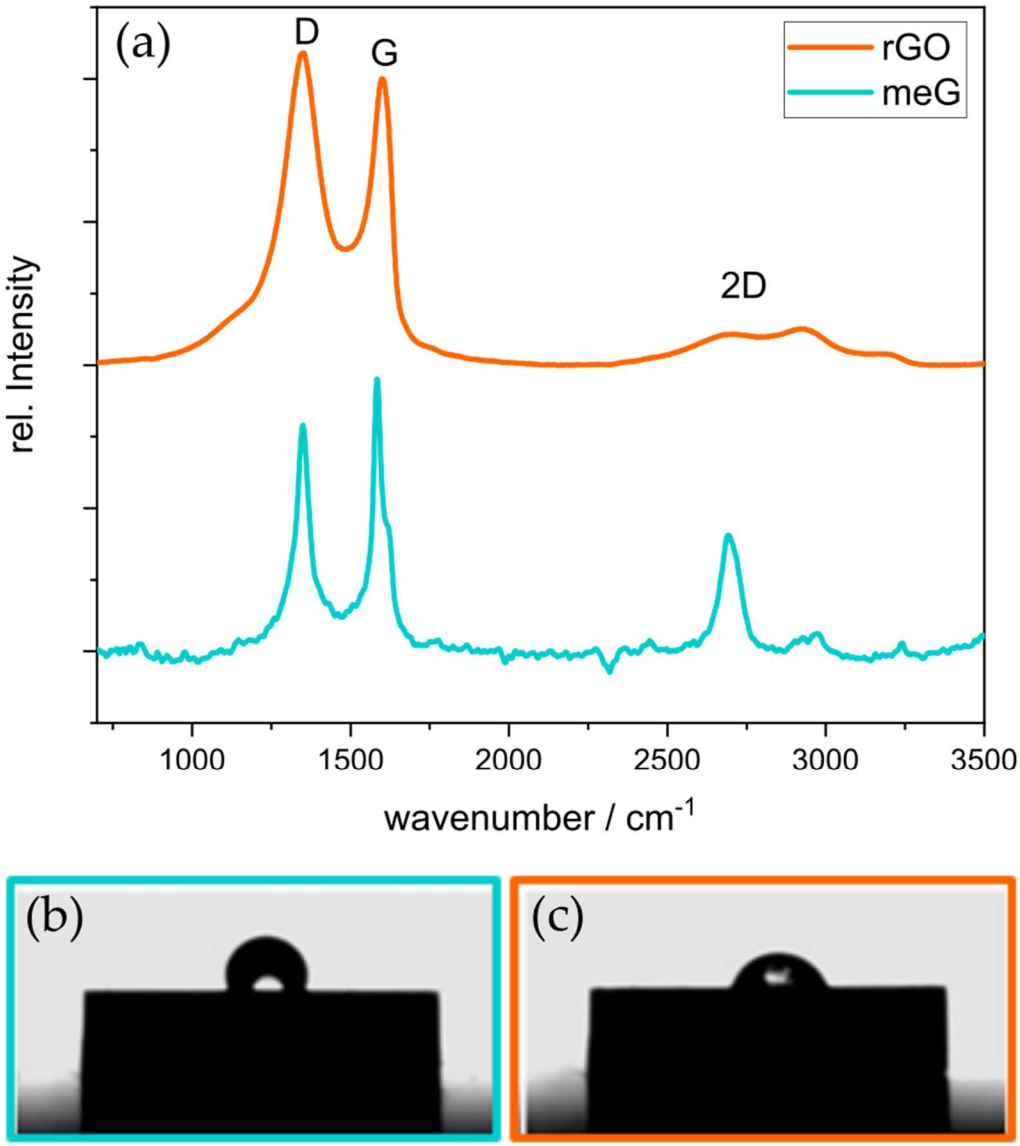

Figure 4.1. a) Raman spectra (n = 20) of meG (blue), and rGO (orange) deposited by single dispensing step on interdigitated electrodes (a). Images of surface wettability by water for meG (b) and rGO (c) deposited on a piece of a silicon wafer.

Furthermore, the intensity of the 2D band indicates the exfoliation efficiency of each preparation technique. The increase of 2D/G-peak ratio of meG compared to rGO indicates that the reduction of graphene oxide yielded a multilayered graphene compound ($(I_{2D}/I_G)_{rGO}$ = 0.08 ± 0.015), whereas mechanical exfoliation results in carbon flakes with few layers of graphene stacked together ($(I_{2D}/I_G)_{meG}$ = 0.31 ± 0.07). The structural defect distribution within the carbon lattice is

correlated to the intensity of the D/G-peak ratio, as the D-band is activated in presence of edges, defects or structural disorder within the sp^2-hybridized carbon lattice.[28] The low ratio of $(I_D/I_G)_{meG}$ = 0.69 ± 0.20 is attributed to the mechanical exfoliation, which does not introduce functional groups by additional exfoliation agents. In contrast, exfoliation techniques, which rely on oxidation steps during the processing introduce oxygen defects within the sp^2-hybridized carbon lattice giving rise to the D-band in the Raman spectra. Reduced graphene oxide resulting in $(I_D/I_G)_{rGO}$ = 1.10 ± 0.01. This is in accordance with literature findings and implies that the nanoflakes are decorated by oxygen residues mainly located at the flakes' edges as well as defects, such as vacancies.[29]

Investigations on the hydrophobicity of the materials were performed by contact angle measurements via sessile drop technique with H_2O (Figure 4.1B). Reduced graphene oxide shows hydrophilic character as it displays the lowest contact angle of (64 ± 3)°, which is attributed to the oxygen moieties and structural defects, still remaining after the reduction process. Mechanically exfoliated graphene with an increased contact angle of (109 ± 11)° is of hydrophobic character. The water-repelling behavior of this carbon material forms a good starting position in terms of humidity-insensitive gas monitoring.

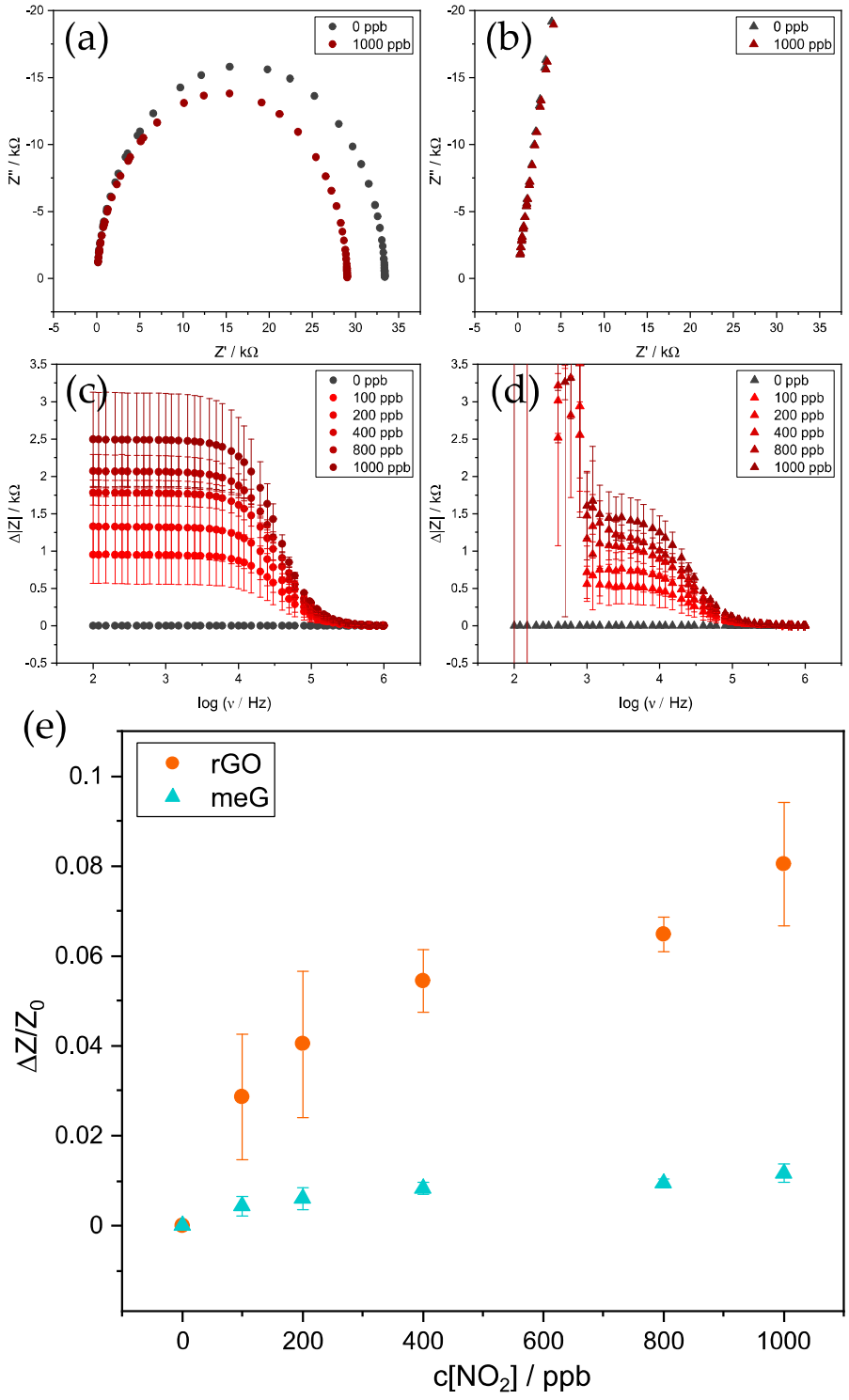

Figure 4.2. Impedance spectra of rGO (a, c) and meG (b, d) on inter-digitated electrodes in presence of different concentrations of NO_2. In (e) ΔZ (= $Z - Z_0$) is taken from (c and d) at 10 kHz while Z_0 is the impedance in dry synthetic air at the same frequency.

When applying both carbon materials in the same mass concentration on interdigitated electrodes, they clearly differ in their impedance spectra. From the Nyquist plots (Figure 4.2a, b) a full semi-circle is found at bias voltage of +200 mV and an amplitude of 50 mV in the frequency range from 100 Hz to 1 MHz for rGO. In synthetic air the impedance of rGO can be fitted by a Randles equivalent circuit of a resistance (~32 kΩ) and a capacitance (~13 nF) in parallel with a resistance (~151 Ω) in series. The characteristics are affected in their magnitude by applying the test gas NO_2. The situation is different for the case for meG. Here the Nyquist plot is described by a linear increase towards lower frequencies which is typical for diffusion dominated processes. One can assume that NO_2 is mainly detected by an association of the molecule to any of the defects or functional groups present in rGO. Due to the absence of these groups in meG the change in the impedance is mainly caused by diffusion of the gas molecules in between the individual graphene sheets. The Bode plots (Figure 4.2c, d) show that the magnitude of the impedance change in the low frequency range is significantly higher for rGO when comparing to meG. For both materials at frequencies higher than 0.1 MHz almost no change in the impedance in presence of NO_2 is detectable and at frequencies lower than 1 kHz, for meG the signal changes became not reproducible any longer as it can be seen from the huge error-bars. This might also be a consequence of the diffusion of the analyte in between the graphene layers. Detailed investigations are needed to clarify these findings, which are out of the scope of this study. In terms of sensing, one can conclude that rGO results in a relative impedance change of about 5.4% at a frequency of 10 kHz in presence of 400 ppb NO_2, which is 6.8-times higher than the sensitivity for meG.

To verify the influence of the thickness of the carbon layers on the interdigitated electrodes it was tried to deposit as low amount of material as possible. After op-

timization of the dispensing protocol approx. 7 nL (0.1 mg ml^{-1}) of the carbon material resulted in a complete layer, verified by line scans recorded by the Raman microscope. Upon repeating the dispensing for a second and a third time different layer thicknesses have been realized. In Figure 4.3 the impedance spectra of rGO and meG in the presence of 400 ppb NO_2 are depicted. The difference in the absolute change in the impedance at 10 kHz for both materials might be attributed to lower number of binding sites for the analyte in the less defective material. In both cases it is obvious that thinner layer result in higher signal changes. This clearly indicates that an emphasis needs to be put in sensor devel-opment to further reduce the layer thickness and to optimize the homogeneous deposition of rGO to further improve the sensitivity. Instrumental limitation hin-dered a further decrease of the amount of deposited carbon nanomaterials.

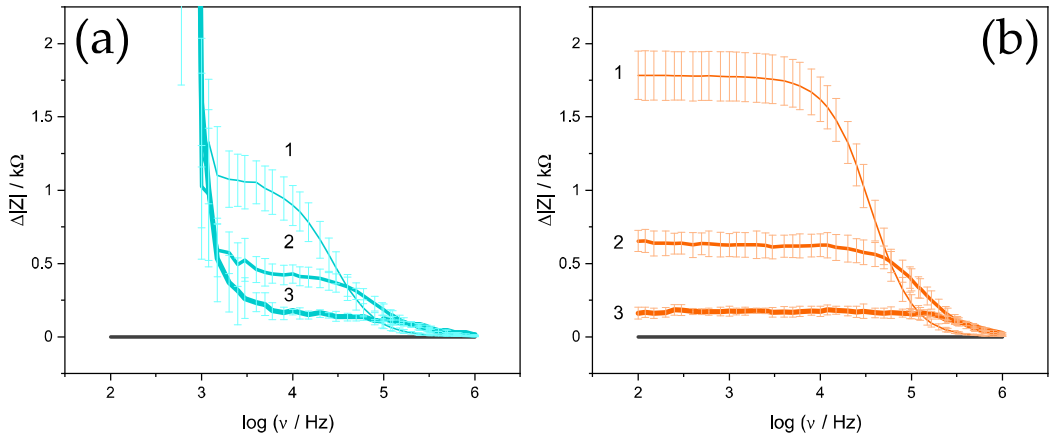

Figure 4.3. Impedance spectra of meG (a) and rGO (b) on interdigitated electrodes in presence of 400 ppb of NO_2. The numbers indicate the dispensing steps to apply thicker layers of the carbon material.

The advantage to use 2D carbon materials in gas sensing is ascribed to the fact that no heating of the sensor element is needed to obtain signal changes with ex-tremely high sensitivity. Even a concentration of 100 ppb NO_2 is easy to determine by rGO modified interdigitated electrodes. For smaller concentrations

the error in the gas mixing is getting too high to determine a limit of detection for this sensor. For an application in a miniaturized device humidity is known to seriously affect the most commonly used resistive-based signal read out. This leads to complex settings where the sensing element is placed below some materials adsorbing all the humidity. This is accompanied to slow diffusion of the analyte gas to the sensing element and long response times are the consequences. This is the reason why we used an impedimetric approach. The impedance of the sensor is also affected by humidity as one can see in Figure 4.4. Again, the performance to meG with only low number of defects shows slightly lower signal changes towards an increase in humidity as for rGO as sensing material.

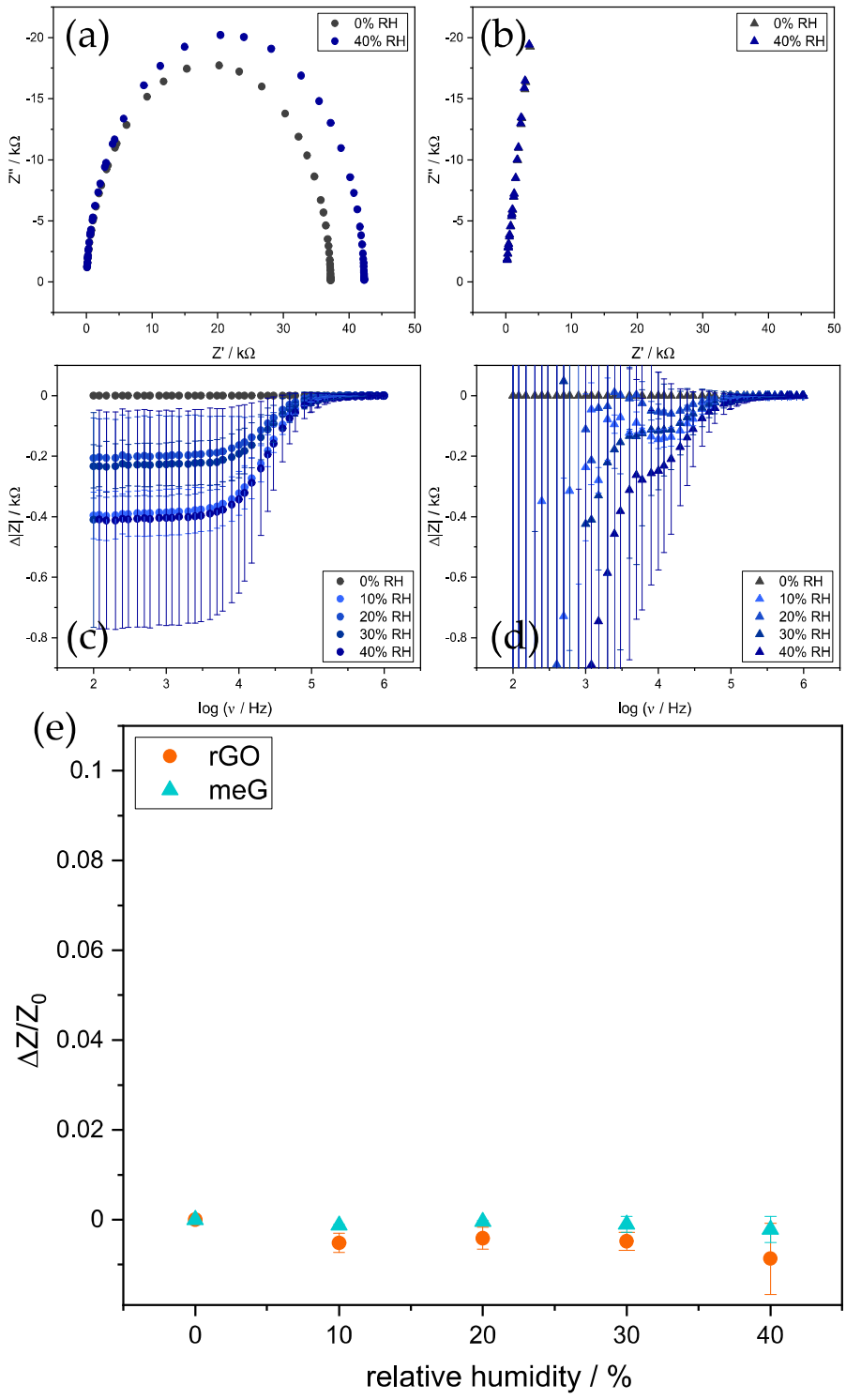

Figure 4.4. Impedance spectra of rGO (a, c) and meG (b, d) on interdigitated electrodes in in dry air and in presence of 40% relative humidity. In (e) ΔZ (= $Z - Z_0$) is taken from (c and d) at 10 kHz while Z_0 is the impedance in dry synthetic air at the same frequency.

In general, the impedance obtained at 10 kHz showed a much smaller impact of the humidity (Figure 4.4e) in respect to the presence of NO_2 (Figure 4.2e). For rGO the maximal increase in signal is about 8 times smaller in presence of 40% humidity in respect to the relative sig-nal decrease caused by 1000 ppb NO_2. The total signal change obtained for rGO covered electrodes is about 8% for impedimetric (AC) measurements and about 7% for resistive (DC) measurements. The benefit of AC measurements is clearly seen when humidity comes into play. Here the maximum signal change generated by NO_2 is only affected by about 1% by humidity whereas about 3.5% variation in the signal can be expected for the same scenario in DC measurements (Figure 4.S4).

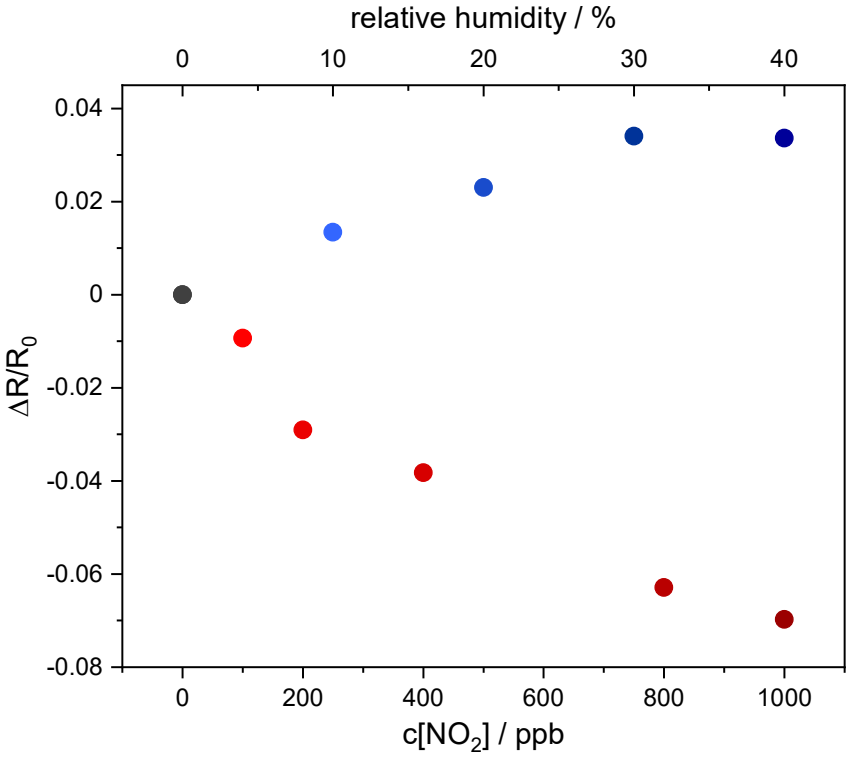

Figure 4.S4. Relative signal response of rGO towards NO_2 (red) and relative humidity (blue). ΔR (= R – R_0) was measured at a constant electrode potential of 200 mV. R_0 is the resistance in dry synthetic air at this potential.

This means that fluctuations in humidity by 40% will not allow to reliable detect NO_2 levels lower 400 ppb in DC measurements, but the same electrode in the same setup enables by switching to AC measurements the detection of levels down to about 150 ppb NO_2 by taking data ob-tained only at one frequency are considered. In AC measurements the recording of a full impedance spectrum, here for 51 frequencies within 2.5 minutes with a miniaturized homebuilt circuit board which additionally can operate eight individual sensors offers the potential of retrieving many datapoints compared to resistivity measurements performed upon a DC potential applied to the electrode.[30] In DC technique there is only one resistance for measurement point. Not only the total impedance is recorded in AC measurements, but together with the phase angle, a real part and an imaginary part of the impedance can be assigned for every measured frequency by vector analysis. Therefore, this technique enables the discrimination of gases which show different interactions with the sensing material, as the imaginary part of the impedance is affected by changes in the dielectric constant of the sensing material, whereas the real part of the impedance is not. To demonstrate this, a multivariate data analysis was applied to the data set recorded by AC technique at 51 different frequencies for changes in NO_2 concentration, the humidity and both parameters simultaneously. By principal component analysis, after normalization of the data set to a standard deviation of 1 and a mean value of 0, clustering was obtained (Figure 4.5).

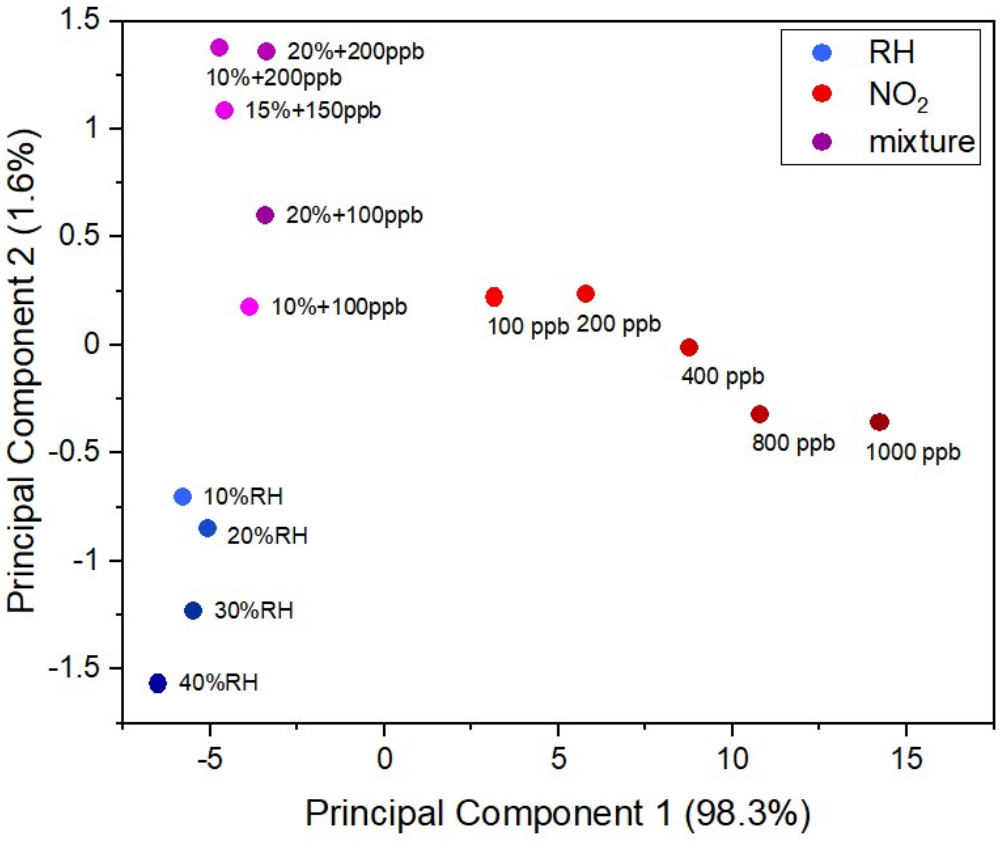

Figure 4.5. Principal component analysis of a data set obtained by impedimetric measurement of 51 frequencies ranging from 100 Hz to 1 MHz for rGO covered electrodes in presence of different concentrations of NO_2, different humidity levels and the simultaneous change of both parameters.

The rGO modified electrodes showed a fully reversible responds toward changes in NO_2 concentration as well as for humidity changes and within 6 months of storing at ambient conditions the sensor still is fully operational. Both parameters need to be further investigated in detail with an optimized sensor design. Especially the recovery rate of about 15 min which was observed when synthetic air was applied again after the signal was stabilized in presence of 400 ppb NO_2 is not acceptable for high precision online monitoring. Nevertheless, a slight increase in sensor temperature or a short heating pulse might overcome this drawback. It is also expected that a smaller gap and variations in size of the interdigitated electrodes together with an improved deposition of rGO on the

electrode will lead to faster response and recovery times and to better sensitivity. It is also suggested to control the defects of the carbon material for improving the sensitivity as well as to use an array of 2D carbon materials with different amounts of defects. This could lead to sensors identifying more than one gas qualitatively as well as quantitatively by pattern analysis.

4.5 Conclusion

In conclusion we demonstrate that it is possible by the use of 2D carbon materials to build a sensor for NO_2 with high sensitivity down to the 100-ppb range which can be operated at room temperature and therefore consumes low power. The 2D carbon sensing material needs to have defects within the carbon lattice to improve the sensitivity and the layer thickness should be as thin as possible to obtain the best results. Using AC impedimet-ric readout technique gains benefits compared to DC resistive measurements by enabling readout at certain measurement frequencies. Hereby it is possible, together with proper design of the sensing material to address different binding mechanism of different analytes at the same time, e.g., if one type of analyte affects the specific conductivity of the material whereas another analyte causes changes of the dielectric constant of the material due to the interaction or reaction at the surface. By introducing this concept, we hope to stimulate research in this direction also for other material and analyte combi-nations towards fast electrical sensing applications con-ducted at ambient conditions.

4.6 References

(1) Anenberg, S.C.; Miller, J.; Minjares, R.; Du, L.; Henze, D.K.; Lacey, F.; Malley, C.S.; Emberson, L.; Franco, V.; Klimont, Z.; Heyes, C. Impacts and Mitigation of Excess Diesel-related NO_x Emissions in 11 Major Vehicle Markets. *Nature* **2017**, 545, 467–471, DOI: 10.1038/nature22086

(2) World Health Organization. Occupational and Environmental Health Team. WHO Air Quality Guidelines for Particulate Matter, Ozone, Nitrogen Dioxide and Sulfur Dioxide: Global Update 2005: Summary of Risk Assessment. *World Health Organization* **2006**. https://apps.who.int/iris/handle/10665/69477 (accessed 13..03.2021)

(3) Kumar, P.; Morawska, L.; Martani, C.; Biskos, G.; Neophytou, M.; Di Sabatino, S.; Bell, M.; Norford, L.; Britter, R. The Rise of Low-cost Sensing for Managing Air Pollution in Cities. *Environ. Int.* **2015**, 75, 199–205, DOI: 10.1016/j.envint.2014.11.019

(4) Gooding, J. J.; Liu S. M. A New Year Period Emphasizing the Need for Better Sensors. *ACS Sens.* **2020**, 5, 597–598, DOI: 10.1021/acssensors.0c00456

(5) Mayer, M.; Baeumner, A. J. A Megatrend Challenging Analytical Chemistry: Biosensor and Chemosensor Concepts Ready for the Internet of Things. *Chem. Rev.* **2019**, 119, 7996–8027, DOI: 10.1021/acs.chemrev.8b00719

(6) Nazemi, H.; Joseph, A.; Park, J.; Emadi, A. Advanced Micro- and Nano-Gas Sensor Technology: A Review. *Sensors* **2019**, 19, 1285, DOI: 10.3390/s19061285

(7) Degler D.; Weimar U.; Barsan N. Current Understanding of the Fundamental Mechanisms of Doped and Loaded Semiconducting Metal-oxide-based Gas Sensing Materials. *ACS Sens.* **2019**, 4, 2228–2249, DOI: 10.1021/acssensors.9b00975

(8) Meng, G.; Zhuge, F.; Nagashima, K.; Nakao, A.; Kanai, M.; He, Y.; Boudot, M.; Takahashi, T.; Uchida, K.; Yanagida, T. Nanoscale Thermal Management of Single SnO_2 Nanowire: Pico-Joule Energy Consumed Molecule Sensor. *ACS Sens.* **2016**, 1, 997–1002, DOI: 10.1021/acssensors.6b00364

(9) Seiyama, T.; Kagawa, S. Study on a Detector for Gaseous Components Using Semiconductive Thin Films. *Anal. Chem.* **1966**, 38, 1069–1073, DOI: 10.1021/ac60240a031

(10) Wang, C.; Yin, L.; Zhang, L.; Xiang, D.; Gao, R. Metal Oxide Gas Sensors: Sensitivity and Influencing Factors. *Sensors* **2010**, 10, 2088–2106, DOI: 10.3390/s100302088

(11) Wilson, R.; Simion, C. E.; Stanoiu, A.; Taylor, A.; Guldin, S.; Covington, J. A.; Blackman, C. Humidity Tolerant Ultra-thin NiO Gas Sensing Films. *ACS Sens.* **2020**, 5, 1389–1397, DOI: 10.1021/acssensors.0c00172

(12) Espid, E.; Taghipour, F. UV-LED photo-activated chemical gas sensors: A review. Crit. Rev. *Solid State Mater. Sci.* **2017**, 42, 416–432, DOI: 10.1080/10408436.2016.1226161

(13) Cho, I.; Sim, Y.C.; Cho, M.; Cho, Y.-H.; Park, I. Monolithic Micro Light-Emitting Diode/Metal Oxide Nanowire Gas Sensor with Microwatt-Level Power Consumption. *ACS Sens.* **2020**, 5, 563–570, DOI: 10.1021/acssensors.9b02487

(14) Chatterjee, S.G.; Chatterjee, S.; Ray, A.K.; Chakraborty, A.K., Graphene–Metal Oxide Nanohybrids for Toxic Gas Sensor: A Re-view. *Sens. Actuators B* **2015**, 221, 1170–1181. DOI: 0.1016/j.snb.2015.07.070

(15) Joshi, N.; Hayasaka, T.; Liu, Y.; Liu, H.; Oliveira, O.N.; Lin, L. A Review on Chemiresistive Room Temperature Gas Sensors Based on Metal Oxide Nanostructures, Graphene

and 2D Transition Metal Dichalcogenides. *Microchim. Acta* **2018**, 185, 213, DOI: 10.1007/s00604-018-2750-5

(16) Kirchner, E.M.; Hirsch, T. Recent Developments in Carbon-based Two-dimensional Materials: Synthesis and Modification Aspects for Electrochemical Sensors. *Microchim. Acta* **2020**, 187, 441, DOI: 10.1007/s00604-020-04415-3

(17) Liu, Y.; Dong, X.; Chen, P. Biological and Chemical Sensors Based on Graphene Materials. *Chem. Soc. Rev.* **2012**, 41, 2283–2307, DOI: 10.1039/C1CS15270J

(18) Compton, O.C.; Nguyen, S.T. Graphene Oxide, Highly Reduced Graphene Oxide, and Graphene: Versatile Building Blocks for Carbon-Based Materials. *Small* **2010**, 6, 711–723. DOI: 10.1002/smll.200901934

(19) Liu, X.; Ma, T.; Pinna, N.; Zhang, J.; Two-Dimensional Nanostructured Materials for Gas Sensing. *Adv. Funct. Mater.* **2017**, 27, 1702168. DOI: 10.1002/adfm.201702168

(20) Malik, R.; Tomer, V.K.; Mishra, Y.K.; Lin, L. Functional Gas Sensing Nanomaterials: A Panoramic View. *Appl. Phys. Rev.* **2020**, 7, 021301, DOI: 10.1063/1.5123479

(21) Zhang, B.; Cheng, M.; Liu, G.; Gao, Y.; Zhao, L.; Li, S.; Wang, Y.; Liu, F.; Liang, X.; Zhang, T.; Lu, G. Room Temperature NO_2 Gas Sensor Based on Porous Co_3O_4 Slices/Reduced Graphene Oxide Hybrid. *Sens Actuators, B* **2018**, 263, 387–399, DOI: 10.1016/j.snb.2018.02.117

(22) Li, Q.; Chen, D.; Miao, J.; Lin, S.; Yu, Z.; Han, Y.; Yang, Z.; Zhi, X.; Cui, D.; An, Z. Ag-Modified 3D Reduced Graphene Oxide Aerogel-Based Sensor with an Embedded Microheater for a Fast Response and High-Sensitive Detection of NO_2. *ACS Appl. Mater. Interfaces* **2020**, 12, 25243–25252, DOI: 10.1021/acsami.9b22098

(23) Yang, C. M.; Chen, T. C.; Yang, Y. C.; Meyyappan, M. Annealing effect on UV-illuminated Recovery in Gas Response of Graphene-based NO_2 Sensors. *RSC Adv.* **2019**, 9, 23343–23351, DOI: 10.1039/C9RA01295H

(24) Huang, Y.; Jiao, W.; Chu, Z.; Wang, S.; Chen, L.; Nie, X.; He, X. High Sensitivity, Humidity-independent, Flexible NO_2 and NH_3 Gas Sensors Based on SnS_2 Hybrid Functional Graphene Ink. *ACS Appl. Mater. Interfaces* **2019**, 12, 997–1004, DOI: 10.1021/acsami.9b14952

(25) Salomão, F.C.; Lanzoni, E. M.; Costa, C. A.; Deneke, C.; Barros, E. B. Determination of High-Frequency Dielectric Constant and Surface Potential of Graphene Oxide and Influence of Humidity by Kelvin Probe Force Microscopy, *Langmuir* **2015**, 31, 11339–11343, DOI: 10.1021/acs.langmuir.5b01786

(26) Kavinkumar, T.; Sastikumar, D.; Manivannan, S. Effect of Functional Groups on Dielectric, Optical Gas Sensing Properties of Graphene Oxide and Reduced Graphene Oxide at Room Temperature, *RSC Adv.* **2015**, 5, 10816–10825, DOI: 10.1039/C4RA12766H

(27) Botas C.; Álvarez P.; Blanco P.; Granda M.; Blanco C.; Santamaría R.; Romasanta L.J.; Verdejo R.; López-Manchado M.A.; Menéndez R. Graphene Materials with Different

Structures Prepared from the Same Graphite by the Hummers and Brodie Methods, *Carbon* **2013**, 65, 156–164, DOI: 10.1016/j.carbon.2013.08.009

(28) Ferrari, A. C.; Basko, D. M. Raman Spectroscopy as a Versa-tile Tool for Studying the Properties of Graphene. *Nature Nanotech.* **2013**, 8, 235–246, DOI: 10.1038/nnano.2013.46

(29) Feicht, P.; Biskupek, J.; Gorelik, T. E.; Renner, J.; Halbig, C. E.; Maranska, M.; Eigler, S. Brodie's or Hummers' Method: Oxidation Conditions Determine the Structure of Graphene Oxide. *Chem. Eur. J.* **2019**, 25, 8955–8959, DOI: 10.1002/chem.201901499

(30) Aumer, F.; Hinz, T. Electrical Impedance Spectroscopy on 8-channel PSoC-Based Miniaturized Board to Enable Data-Rich Environmental Sensing, *Smart Systems Integrated*, **2021**.

5 Conclusion and Future Perspectives

The awareness of air pollution in the present day is increasing and its effect on human health is becoming clearer. More than 7 million casualties worldwide are attributed to the result of poor air quality each year according to the World Health Organization (WHO) (1). As the current monitoring methods are costly, bulky, and centralized they pose the bottleneck towards higher spatial coverage. In 2021, there are only 265 testing stations (2) for air quality in Germany, meaning that each station theoretically covers approximately 1,350 km². An area this large is not fit to tell the individual what the current level of pollution at their location is. The end user wants to know the current pollution level and is able to partially achieve his goal through measurement devices as shown in Figure 5.1 with the current infrastructure. The goal is to increase the mesh density of the air quality measurement by providing miniaturized, low-cost, highly sensitive and selective sensor devices for a wide range of pollutant gases in a high volume and still be sustainable. This will inevitably lead to further information and quality of life in various areas on the end user's side.

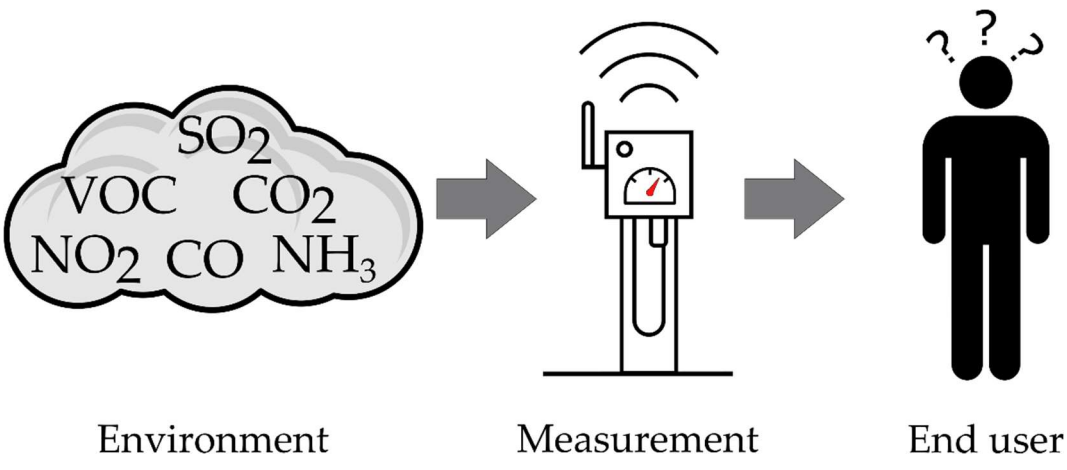

Figure 5.1. Schematic visualization of chain of information from the environment to the end user.

While the outdoor pollution poses a big threat with an attributed 4.2 million deaths annually there is also a not negligible pollution factor from indoor air with 3.8 million deaths per year (1). People in higher developed countries tend to spend 90% of their time in closed rooms. The main sources of pollution for indoor air are open cooking, smoking, outgassing of furniture and mold. Among the most common pollutants are CO, CO_2, NH_3, NO_2, SO_2, various volatile organic compounds as well as particulate matter and allergens.

The sampling of the environment can be classified in different areas. These are active, passive, intermittent and continuous sampling. Each excelling at their own application scenario.

Passive sampling means the passive accumulation of analytes such as gases, pathogens or allergens in testing devices or tubes through passive physical processes such as diffusion or permeation through membranes. This can be done cheaply and allows for widespread application. Collecting the accumulated analytes is simple and effective to monitor long-term changes in the measured system. The downside to this is that the analysis needs to happen off-site in a laboratory and thus reduces the time from pollution events to their discovery and possible countermeasures. Also, quick spikes in pollution cannot be seen with this method as only the average over the sampling period is detected. Another application of this is colorimetric dosimeters that change their color when they encounter a certain amount of analyte. They are simple to use and give clear and instant results but can only be used once before they need to be replaced. The preferred use for this in areas where the pollution levels are uncertain and the exposure to possibly lethal gases needs to be monitored closely without the need for active sampling or electricity. They are, however, limited in their use for continuous measurement by their common one-time use. **Active sampling** on the other hand describes the process that is prevalent in current measurement

stations across the globe. The concentration of pollutants is measured, and the results can be evaluated on-site leading to a high spatial resolution at the current site. This is limited by the amount of monitoring stations and expensive as the testing stations are large and complex. Furthermore, the devices need to be maintained and operated by experts further increasing their cost. **Cyclic monitoring** describes the process of taking samples at a given interval such as once per hour or once per day. This allows for lower power consumption of the measurement devices as the power only needs to be switched on periodically. The lower power consumption makes this a great way to include sensing devices in mobile applications. Analysis can be done on-site as well and allows for quick results and counteractions towards occurring events. The downside to this method is, that if a pollution event occurs too early or too late after the measurement the event will not be detected. The solution to this is **continuous monitoring** where the environment is permanently monitored. This allows for real time data if a pollution even were to occur with high temporal solution and spatial resolution near the device. On the other hand, continuous uptime of the measurement device comes with a reduced lifetime and a large amount of data that needs to be handled. Many data points can certainly be helpful in times when the pollution changes rapidly in other to find the source but are useless and cumbersome in times where the pollution level is stagnant. An environmental sensor on its own does not contribute to enhance air quality. However, the sensor can provide detailed information about the current air quality and can prompt an action following the results and inform the user of a possible drop in air quality. These actions can be an action taken by the user consciously such as opening a window or an automated action as turning on an air purifier or the Heating, Ventilation and Air Conditioning (HVAC) system in the building. Possible applications are summarized in Table 5.1 below.

Table 5.1. Summary of application scenarios for miniaturized gas sensors.

Application	Description	Example	Sampling
Dosimeter	Indicate harmful pollutants quickly and allow user to leave harmful environment	Colorimetric dosimeter can be attached to clothing and changes color to alarm the user of a perilous situation	passive
Action Warning	Using sensor to detect rising pollution level and infroms the user to take action	CO_2/ VOC monitoring through smart devices in schools, homes, offices	active cyclic/ continuous
Power Reduction	Use devices to turn on / off ventilation	Monitor pollution level an turn on HVAC system if required or turn off when no longer required	active continuous
Air Quality Tags	Small devices at pedestrian crossings deliver the air quality to the user after prompt	Cyclic or on-demand measurement of air quality to inform passing users of air quality level and gives instructions	active cyclic
Long-term health monitoring	Monitor users health	Long-term measurements of pollutants/ allergens at home/ site in order to be able to correlate or prevent disease	active continuous/ cyclic
Identify Pollution Sources	Use sensor grid to identify pollution sources	Sensor grid around busy intersections or factories and find areas of high pollution in correlation with weather conditions	active continuous/ cyclic
Equip vehicles/ transportation	Deploy sensors on cars, planes, ships and increase global pollution monitoring	Equip new cars, planes, ships and retrofit old ones with air quality monitoring devices in order to map the global air pollution	active continuous

Another possibility is to tell the user to avoid certain routes on their daily commute on bike or during sport activities when the body is most sensitive to pollution. One can think of an automated notification in meeting rooms where an air pollution management can be included to detect CO_2 level and warn meeting participants of a rising CO_2 concentration that could hinder their productivity and decision-making capabilities. Miniaturized devices can be integrated into smart home devices such as speakers that are already deployed in many homes and tend to grow further in the future. This solution can also be applied to class and lecture rooms in schools and universities or office buildings. The application of smart sensor devices in buildings can also help to bring more sustainability. The system can detect the occupant's presence in the form of a rising CO_2 level. Afterwards, the HVAC system can be turned on in the respective rooms while staying on standby in the other parts of the building. This can therefore reduce the overall energy consumption of the building by reducing useless air exchange. Furthermore, this also increases longevity of the system as its uptime is reduced. Another possibility are passive air quality tags around intersections in lamp posts or traffic lights. The system measures the air quality at certain intervals and if a user comes in close range with his mobile phone the data can be transferred to the user forwarding the relevant information.

Following up on that idea the sensors could also continuously monitor the air quality and if there is a relevant drop give that information to either pedestrians or another service provider such as Google that can use that information in their navigation tool maps to provide alternative routes for pedestrians, bikers, and drivers. With the wide spread of sensing technology one can use the collected data to study health effects that long-term pollution levels can have on people living in high pollution areas. Sicknesses and their probability to arise in certain residential areas can be monitored and their origin can be detected, and further sickness development can be negated. If a person lives in an area near a factory the pollution can be closely monitored over a long time to evaluate the long-term pollution and possible effects on people. Also, special care can be taken of persons that suffer from respiratory problems. Through small monitoring devices in a smartphone the level of pollution the person is exposed to can be tracked permanently and correlation to symptoms can be made. Another big aspect is the employment of environmental sensors on newly built vehicles, ships, and planes as well as retrofitting existing ones. As climate change plays a big role in today's world miniaturized devices can also play their part and deliver meaningful values towards current gas concentrations and temperature in the atmosphere as well as in bodies of water. On January 1st, 2021 there were 66.9 million vehicles registered in Germany (3). In a similar manner there are approximately 13,000 aircrafts in the air around the world (4) and approximately 56,000 commercial merchant ships around the oceans as of January 1st, 2020 (5). Now, if each of these were equipped with a small device to track certain environmentally critical parameter intermittently or permanently such as the temperature of the air or water as well as gas concentrations of harmful gases this would provide the world with many additional, more localized, spots for tracking the pollution level on a bigger scale. Filling the grid with many more

devices would allow for better transparency in-between existing stations as well as allowing for more in-depth analysis of atmospheric pollution for climate researchers and open the possibilities for further discoveries and understanding of the underlying processes.

Recently the pollution disparity has been coming more to light in the United States. Studies show that there is a difference in where different ethnicities in cities tend to reside that can also be linked to differing pollution levels with even more influence in race-ethnicity than in income. Even though pollution in general decreased from 2000 to 2010, people of color tend to live up to 2.5 times more likely in areas with higher NO_2 pollution than recommended by the WHO compared to whites (6). Not only NO_2 pollution but also fine particles with a diameter of 2.5 μm and below, which are a main cause of excess mortality in the US linked to pollution (7) are spread unequally (8). This increased exposure can lead to pediatric asthma stemming from increased NO_2 exposure (9), pneumonia-related deaths in adults (10) and increased mortality overall (11). There are studies towards multipollutant approaches instead of single pollutants (12). However they all show, that polluted air is dangerous for humans and that effect is only increased in cities where the pollution is generally higher compared to rural areas (13). Whereas most studies up until now are focused on health risks as a result of pollution on a city or state scale more recent studies claim that the pollution and therefore health inequality is differing in cities as well down to neighborhood level revealing large and inequal distribution of air quality (14). The suggested increased grid density enhances the possibility to detect pollution sources and pollution heat maps. Whereas of now many areas are not covered my constant measurement, the future could hold more measurement devices around possible high pollution areas as factories, busy streets, airports, and harbors. This in turn would empower the people to undermine their knowledge of polluted air in their

area of residence with facts to prove it and allow them to introduce policies to decrease pollution by prohibiting factories, shipping routes, and highways to pass close to their homes. Therefore, the more high-resolution data available for the public, the better the air quality in urban areas becomes and less people are endangered from avoidable risks. This increase in more localized, sub-city determination of air pollutants would benefit people living in generally more polluted parts of cities the most due to the fact of inequal air quality in cities (15).

Many technologies for active gas detection are currently on the market and each has their own advantages and disadvantages based on their inherent sensing principle. There is a summary of selected technologies that are currently in use below in Table 5.2.

Table 5.2. Comparison of different sensing technology for gas detection.

Technology	Metal Oxide Sensors	Nanomaterials	Non-dispersive Infrared	Pellistor	Gas Chromatography
Advantages	below ppm sensitivity many target gases low cost fast response	ultra high sensitivity many analytes possible low-cost fast response simple fabrication low energy	ppm range sensitivity good selectivity stable long term no poisoning	high analyte concentrations possible	highly sensitive
Disadvantages	poor selectivity high energy consumption cross sensitivity drift behaviour	poor selectivity not ready for big scale drift behaviour	high power consumption possible overlap of analytes sophisticated fabrication expensive large	low selectivity low sensititivity high power consumption	very large size very high cost very complex

Pellistor devices exploit either the heat loss in presence of analyte gas (Thermal conductivity type) or the change of resistance that is induced by burning the analyte gas on their catalytic surface (catalytic type). Therefore, catalytic type can only be used to detect flammable gases (16). This principle allows for the detection of a wide range of flammable gases, therefore inherently bearing the risk of cross influences from non-target analytes in the environment. They also require elevated surface temperatures and therefore bear a risk of explosion in use (17). Their use is mostly limited to areas where high concentrations (percent range) of flammable gases need to be detected. Gas chromatography is the principle of selectively separating gaseous components in the sample along a

mobile phase in the device according to their properties. In this list gas chromatography is the principle that can achieve the highest selectivity as well as the highest sensitivity, however coming with the downside of the highest price, size and complexity. Hence, making them useless for their widespread application (18). The sensing principle of non-dispersive infrared sensors (NDIR) is based on the absorption of light of a given wavelength or spectrum in interaction with the target analyte molecule. A typical device incorporates multiple parts. Firstly, either a broadband light source in combination with an optical filter to select the correct wavelength or a narrow bandwidth emitter such as a light emitting diode or a laser diode. Secondly a tube where the analyte passes through and lastly a detector to capture the absorbed light. Many devices incorporate a reference channel without analyte gas to enable differential measurement (19,20).

$$I = I_0 * e^{\varepsilon * c * d}$$

Following the Lambert-Beer law with I_0 and I being the light intensity at input and output, ε as the wavelength dependent absorption coefficient of the analyte, concentration of analyte c and d the optical way length the light passes through. With the absorbance data of selected analytes over a part of the mid IR range in Figure 5.2 it becomes obvious that each gas absorbs infrared radiation at another wavelength. This technology is therefore a fitting tool to separately detect a certain gas species without the interference of another gas species at certain wavelengths but also brings out the disadvantage of this technology. For each analyte a separate detector at the given wavelength is required to receive a signal response. While there is work towards Micro-Electro-Mechanical Systems (MEMS) based miniaturized sensors (21) a main problem is the miniaturization of the optical wavelength the analyte passes through in truly miniaturized devices (22). This increases complexity, size and thus the cost of the IR based

sensor devices rendering them unfit for truly miniaturized systems right now while still maintaining their benefit for sensitive detection of single molecules at a bigger scale.

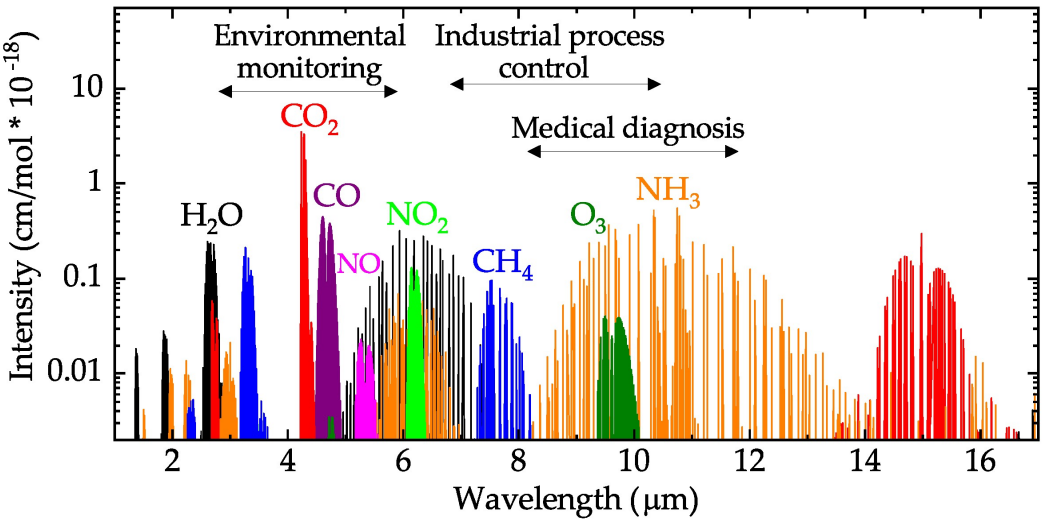

Figure 5.2. Wavelength dependent absorbance in the mid infrared regime for selected environmental pollutants. Taken from (20).

The detection principle of metal oxide (MOX) sensors is based on the resistance change of an active material on the sensor surface following an analyte interaction. After an increase in the sensor surface temperature to 150-400 °C oxygen atoms from the surrounding air interact with the active material such as SnO_2 and form ions which can in turn react with the analyte gas. Through electron interactions in the device and on the surface with the analyte an equilibrium is formed depending on the analyte gas concentration. Reducing gases such as H_2 increase the resistance in an n-type MOX sensor while oxidizing gases such as NO_2 reduce the resistance and vice versa for p-type sensors. The sensing properties of MOX sensors depend on the active material as well as the readout techniques. Common techniques are the measurement of the change in DC resistance in presence of gas as the most common method (23), Hall-effect measurements in combination with resistance measurements granting additional insight towards the charge carrier concentration and sign of the majority charge

carriers (24) or electrical impedance measurements to investigate the surface charge layer and electrode-metal oxide contacts (14, 15). MOX sensors are commonly applied in car exhausts and also indoor applications as the technology is mature already with the most commonly known example of the Figaro Gas-Sensor TGS-813 that is used for detection of combustible gases since many decades (16). MOX sensors are relatively simple to fabricate, can target many gases and exhibit a quick response time of seconds, however, they require a lot of energy to properly elevate the sensor temperature to achieve selectivity as well as sensitivity in the sub-ppm range. Meanwhile investigations towards irradiation with a fitting light source (27) are ongoing and deliver promising results that could pave the way for low-power MOX sensors.

All of the aforementioned sensing technologies are already established and offer little room for innovation whereas the potential of nanomaterials is not yet at its limit due to their more recent discovery with the most renowned representative, graphene, discovered in 2004 by Novoselov and Geim (28). Nanomaterial based sensors also have their own benefits and downsides. They consist of materials with at least one dimension on the nanoscale and the other dimensions possibly exceeding that scale. They offer unique properties not found in bulk material such as ultrahigh electron mobility (29) and high reactivity (30). Due to their properties they can be applied in numerous scenarios from drug delivery (31) to surface plasmon resonance (32) and chemiresistive gas sensing (33) as well as many more. Nanomaterials can be produced either bottom-up, where the nanomaterials are grown from the educts as well as top-down, where the nanomaterial is derived from a larger scale material down to nanoscale. During these processes the nanomaterials properties can be tuned to fit certain application scenarios by changing parameters in the process. They can be functionalized through a combination with other nanomaterials into compounds

to increase sensitivity or response time or to achieve higher selectivity (34) by addition of functional groups which react with specific analytes (35). Here, the reaction needs to be reversible to receive a proper sensing device. These sensors furthermore provide ultrahigh sensitivity down to ppb-level at low energy consumption with a fast response (seconds) and can be fabricated easily and at low-cost. However, they come with the downside that they can, also exhibit low selectivity, just as MOX sensors, and often come with a drift in the sensing signal over a long period of time. With the ever-growing research towards algorithms and artificial intelligence this will also become a much more prevalent method to strengthen the field of nanomaterial-based sensors. As visualized in Figure 5.3 a measurement device, in this case a nanomaterial-based gas sensor has several crucial points that need to be validated to make use of them on a big scale. The fitting material must be selected to achieve longevity, sensitivity, selectivity, and response time. On the method side one can choose from simple DC measurements with the lowest effort up to more sophisticated methods such as using alternating current or Hall-effect measurements to further increase the sensors performance as already known from MOX sensors. Another crucial aspect is the proper analysis of the resulting data to receive meaningful information about the analyte in question. This can enhance the sensors performance even further through the application of artificial intelligence and algorithm based data processing (36). Afterwards the data needs to be transferred to a format that can be understood by the end user such as different colors indicating different levels of threat to the users' health. Combining this effort with a proper choice of material as well as fitting data processing methods such as principal component analysis can lead the way to enable nanomaterials on their way towards wider application and help increase the mesh density of the current environmental measurement grid.

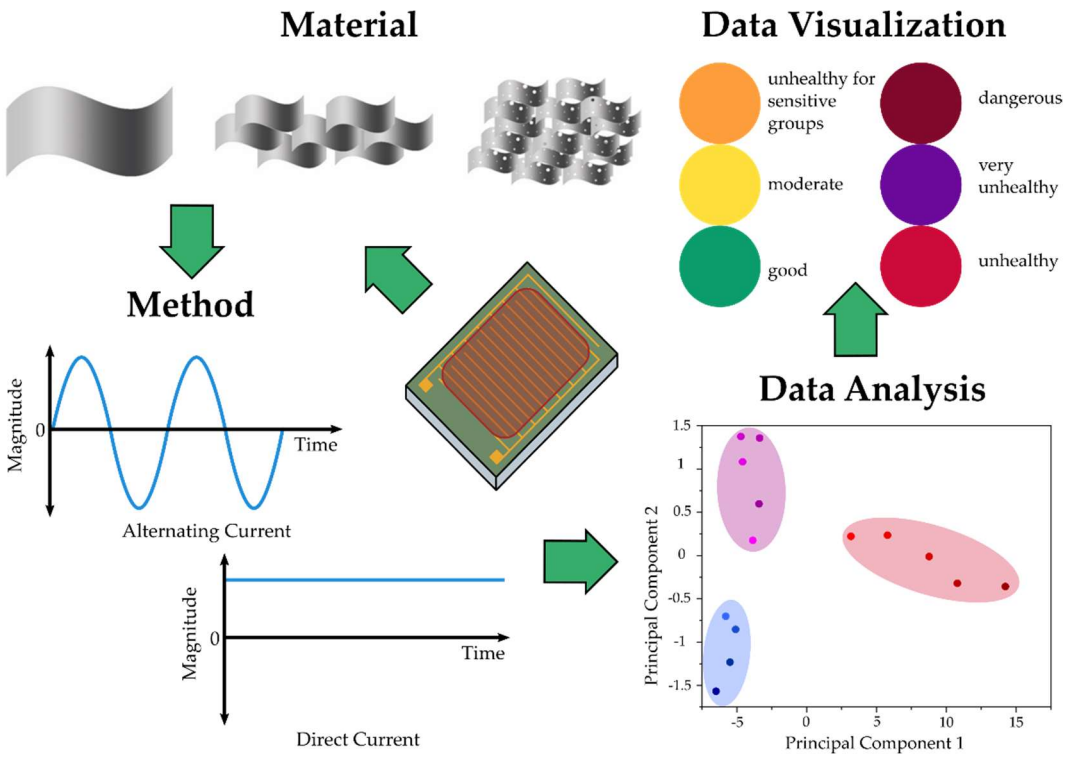

Figure 5.3. Schematic shows the approach to achieve useful data on the example of a chemiresistive gas sensor.

The energy efficiency of sensor devices surely is a point which takes priority in the list of things to be enhanced furthermore in easily deployable sensor devices. However, this could be not as crucial as thought of before. While the sensor devices still need to have a low-power consumption, the difference between ultra-low and low enough might not be as staggering. The material which would lead to lower power, being the cleanest and defect free material, might bear other problems. As discussed previously in this work in chapter 3 the graphene flakes consisting of a generally higher average size interact differently with the analyte compared to the graphene flakes of an inherently lower average area. From a theoretical point of view a large and sp^2-hybridized carbon lattice might be considered the optimum graphene sheet due to the long free path the electrons in the material can travel upon. Whereas more defects lead to a lower free path length, decreasing its conductance tremendously. However, in real life sensing applications the material with less defects shows remarkably less sensitivity

towards the analyte where the signal is lost in the noise from the electronics around it. However, the more defective material shows a higher signal response to identical analyte concentration leading us to the conclusion that there seems to be a sweet spot of defects in the material that creates the best signal response. Considering miniaturization of sensing devices nanomaterials are a valid choice as the go-to active material because they are inherently miniaturized and therefore strive in this part. Therefore, it is important to also have miniaturized electronics such as developing suitable hardware as described in Chapter 4 which allow the application of truly miniaturized devices. However, the selectivity of the materials towards the analytes is still an issue and other gases present in the sample may introduce perturbing cross influences on the signal response as is also the case with other sensing technologies. Through the introduction of advanced sensor stimulus such as electrical impedance spectroscopy as shown in Chapter 5 the cross influence towards humidity and possibly other gases can be reduced. Through the combination with additional signal processing including principal component analysis this can be achieved. As a PCA is only one of the simplest techniques in dimensionality reduction there is certainly a lot more research towards that area in the future. The possibility to apply even more advanced strategies such as non-linear processing techniques can certainly help shape the future of miniaturized sensor devices that can be on par with their huge currently existing counterparts. Additionally, another possible way to reduce the cross-influence of non-target analytes on the final signal response is the implementation of multiple sensor fields into a sensor array containing different materials, functionalization, or even composite materials. By allowing each material to be tailored towards a certain analyte or cross-influencing gas the selectivity of the sensing device might be drastically increased. In theory a portable gas sensor device could incorporate multiple sensor fields in an array

that allows for the selective detection of each analyte that influences the overall air quality in the devices surrounding making it a perfect match for the scenarios where detection of multiple analytes at once could increase the well-being of users. Here, the possibility of combination with advanced signal processing also is a key technology to achieve this goal and much research and breakthroughs in this area are to be expected. On a more low-level point of view many key aspects are still subject to investigation. Among them, but not limited to, the interdigitated electrode setup used in this work as well as the active materials thickness. For the geometry of the sensor device other configurations should be evaluated to find the optimum electrode setup that is easily mass-producible while also delivering the highest possible sensor response. Key parameters are the electrode width, length, and overall number of electrodes. As also explained in detail in Chapter 5 the active materials thickness plays an important role in the sensor characteristics. We could prove that the sensor response is inversely correlated to the active materials thickness. Therefore, decreasing the thickness of the active material will lead to an increase in sensitivity towards the analyte. However, we were limited in the material application on the sensor surface by the given tools and could only provide proof from the opposite approach by applying additional material on the devices resulting in a decrease in the signal response. The optimum possible case here would be a single atomic layer with defective material to achieve the highest possible sensor response. This might be achieved by a large-scale manufacturing of monolayer materials such as monolayer graphene grown by chemical vapor deposition or other processes used commonly used in the semiconductor business. The monolayer can afterwards be treated with either an oxygen plasma to introduce defects or be treated with wet processes to alter the overall surface composition by breaking the sp^2 hybridized bonds. While nanomaterials can decrease the need for heating

completely, they are still not applied in technical products and are more used as a gimmick in marketing with a graphene tennis racket being the most prominent example (37). Researchers evaluated the properties of the so-called graphene in the racket and found that the material is in terms of nomenclature graphite. These results raise awareness for a fundamental problem in nanomaterials, the lack of proper characterization of materials being synthesized. Mulvaney et al. tackled this issue already back in 2016 (38). When comparing nanomaterial fabrication to synthesis of organic compounds (39) the differences are staggering. In organic chemistry the characterization of novel compounds is standardized including methods and tools that need to be employed for each chemical. Purity, physical properties, and functional groups are determined by validated and standardized methods. This allows for reproducible fabrication of materials. The nanomaterial community lacks this kind of standardization and materials can be synthesized in many forms such as dispersed in solvents, powder form or as thin films grown on a carrier substrate. This will result in vastly different properties of the resulting substance which need to be characterized in a unified way. For future research it is of paramount importance to follow strict characterization standards. No new method or material can enter the mass fabrication without compatibility or at least overlap with past or present technologies and without proper characterization an industrial scale application is unthinkable for the near future. But with constant and further work in this direction, the progression towards nanomaterial based environmental sensors that can help create more awareness about pollution and help solve this issue will be achieved.

5.1 References

1. WHO Staff W team air quality and health. Air pollution. *World Health Organization*; [cited **2021** May 26]. Available from: https://www.who.int/health-topics/air-pollution#tab=tab_1

2. Meunier, C.; Ittershagen, M. Aktuelle Luftdaten. *Umweltbundesamt, Fachgebiet II 4.2 Beurteilung der Luftqualität* [cited May 13, **2021**. Available from: https://www.umweltbundesamt.de/daten/luft/luftdaten/stationen/eJzrXpScv9B4UXEykEhJXGVkYGipa2Cha2S0qCRzocWivNQFi4pLFixJSXQrgksamgL5IfnIipMTJyzKrWJblJvctDgnseS0g-eqea8a5Y4vzslLP-2gwpni8MliNgD2gCsO

3. Jahresbilanz - Bestand Fahrzeuge in Deutschland. *Kraftfahrtbundesamt*; **2021** Jan [cited 2021 May 27]. Available from: https://www.kba.de/DE/Statistik/Fahrzeuge/Bestand/Jahresbilanz/bestand_jahresbilanz_node.html

4. Weltweites Flugtracking in Echtzeit. [cited **2021** May 25]. Available from: https://de.flightaware.com/

5. Statista Research Department. Number of ships in the world merchant fleet as of January 1, 2020. [cited 2021 May 25] *Statista*; **2020** Jan. Available from: https://www.statista.com/statistics/264024/number-of-merchant-ships-worldwide-by-type/

6. Clark, L. P.; Millet, D. B.; Marshall, J. D. Changes in Transportation-Related Air Pollution Exposures by Race-Ethnicity and Socioeconomic Status: Outdoor Nitrogen Dioxide in the United States in 2000 and 2010. *Environ Health Perspect* **2017**, 125 (9), 097012.

7. Burnett, R.; Chen, H.; Szyszkowicz, M.; Fann, N.; Hubbell, B.; Pope, C. A.; Apte, J. S.; Brauer, M.; Cohen, A.; Weichenthal, S.; Coggins, J.; Di, Q.; Brunekreef, B.; Frostad, J.; Lim, S. S.; Kan, H.; Walker, K. D.; Thurston, G. D.; Hayes, R. B.; Lim, C. C.; Turner, M. C.; Jerrett, M.; Krewski, D.; Gapstur, S. M.; Diver, W. R.; Ostro, B.; Goldberg, D.; Crouse, D. L.; Martin, R. V.; Peters, P.; Pinault, L.; Tjepkema, M.; van Donkelaar, A.; Villeneuve, P. J.; Miller, A. B.; Yin, P.; Zhou, M.; Wang, L.; Janssen, N. A. H.; Marra, M.; Atkinson, R. W.; Tsang, H.; Quoc Thach, T.; Cannon, J. B.; Allen, R. T.; Hart, J. E.; Laden, F.; Cesaroni, G.; Forastiere, F.; Weinmayr, G.; Jaensch, A.; Nagel, G.; Concin, H.; Spadaro, J. V. Global Estimates of Mortality Associated with Long-Term Exposure to Outdoor Fine Particulate Matter. *Proc Natl Acad Sci USA* **2018**, 115 (38), 9592–9597.

8. Tessum CW, Paolella DA, Chambliss SE, Apte JS, Hill JD, Marshall JD. $PM_{2.5}$ polluters disproportionately and systemically affect people of color in the United States. *Sci Adv.* **2021** Apr;7(18):eabf4491.

9. Achakulwisut P, Brauer M, Hystad P, Anenberg SC. Global, national, and urban burdens of paediatric asthma incidence attributable to ambient NO_2 pollution: estimates from global datasets. *Lancet Planet Health*. **2019** Apr;3(4):e166–78.

10. Eum K-D, Kazemiparkouhi F, Wang B, Manjourides J, Pun V, Pavlu V, et al. Long-term NO_2 exposures and cause-specific mortality in American older adults. *Environ Int*. **2019** Mar;124:10–5.

11. Anenberg SC, Achakulwisut P, Brauer M, Moran D, Apte JS, Henze DK. Particulate matter-attributable mortality and relationships with carbon dioxide in 250 urban areas worldwide. *Sci Rep.* **2019** Dec;9(1):11552.

12. Dominici F, Peng RD, Barr CD, Bell ML. Protecting Human Health From Air Pollution: Shifting From a Single-pollutant to a Multipollutant Approach. *Epidemiology*. **2010** Mar;21(2):187–94.

13. Brønnum-Hansen, H.; Bender, A. M.; Andersen, Z. J.; Sørensen, J.; Bønløkke, J. H.; Boshuizen, H.; Becker, T.; Diderichsen, F.; Loft, S. Assessment of Impact of Traffic-Related Air Pollution on Morbidity and Mortality in Copenhagen Municipality and the Health Gain of Reduced Exposure. *Environ. Internat.* **2018**, 121, 973–980..

14. Southerland, V. A.; Anenberg, S. C.; Harris, M.; Apte, J.; Hystad, P.; van Donkelaar, A.; Martin, R. V.; Beyers, M.; Roy, A. Assessing the Distribution of Air Pollution Health Risks within Cities: A Neighborhood-Scale Analysis Leveraging High-Resolution Data Sets in the Bay Area, California. *Environ Health Perspect.* **2021**, 129 (3), EHP7679, 037006.

15. Demetillo, M. A. G.; Navarro, A.; Knowles, K. K.; Fields, K. P.; Geddes, J. A.; Nowlan, C. R.; Janz, S. J.; Judd, L. M.; Al-Saadi, J.; Sun, K.; McDonald, B. C.; Diskin, G. S.; Pusede, S. E. Observing Nitrogen Dioxide Air Pollution Inequality Using High-Spatial-Resolution Remote Sensing Measurements in Houston, Texas. *Environ. Sci. Technol.* **2020**, 54 (16), 9882–9895.

16. Tränkler H-R, Reindl L, editors. Sensortechnik [p1076-1080]: Handbuch für Praxis und Wissenschaft. Berlin, Heidelberg: *Springer Berlin Heidelberg*; **2014** [cited 2021 Jul 8]. (VDI-Buch). Available from: http://link.springer.com/10.1007/978-3-642-29942-1

17. Personal and Lightweight Flammable Gas Monitors. *Proc. Anal Div. Chem.Soc* **1976**, 13 (4), 108.

18. Harvey D. Modern analytical chemistry. Boston: *McGraw-Hill;* **2000**. 798 p.

19. Wong JY, Anderson RL. Non-dispersive infrared gas measurement. *S.l.: IFSA;* **2012**. 117 p.

20. Popa D, Udrea F. Towards Integrated Mid-Infrared Gas Sensors. *Sensors*. **2019** May 4;19(9):2076.

21. Vincent TA, Gardner JW. A low cost MEMS based NDIR system for the monitoring of carbon dioxide in breath analysis at ppm levels. *Sens Actuators B Chem.* **2016** Nov;236:954–64.

22. Hodgkinson J, Smith R, Ho WO, Saffell JR, Tatam RP. Non-dispersive infra-red (NDIR) measurement of carbon dioxide at 4.2μm in a compact and optically efficient sensor. *Sens. Act. B*. **2013** Sep;186:580–8.

23. Barsan N, Weimar U. 7.3.3 Fundamentals of Metal Oxide Gas Sensors. In: Proceedings IMCS 2012. Nürnberg/Nuremberg, Germany: *AMA Service GmbH*, Von-Münchhausen-Str. 49, 31515 Wunstorf, Germany; **2012** [cited 2021 May 26]. p. 618–21. Available from: http://www.ama-science.org/doi/10.5162/IMCS2012/7.3.3

24. Oprea A, Moretton E, Bârsan N, Becker WJ, Wöllenstein J, Weimar U. Conduction model of SnO_2 thin films based on conductance and Hall effect measurements. *J Appl Phys.* **2006** Aug;100(3):033716.

25. Barsan N, Weimar U. Understanding the fundamental principles of metal oxide based gas sensors; the example of CO sensing with SnO_2 sensors in the presence of humidity. *J Phys Condens Matter*. **2003** May 28;15(20):R813–39.

26. Pokhrel S, Simion CE, Quemener V, Bârsan N, Weimar U. Investigations of conduction mechanism in Cr_2O_3 gas sensing thick films by ac impedance spectroscopy and work function changes measurements. *Sens Act. B*. **2008** Jul;133(1):78–83.

27. Casals O, Markiewicz N, Fabrega C, Gràcia I, Cané C, Wasisto HS, et al. A Parts Per Billion (ppb) Sensor for NO_2 with Microwatt (μW) Power Requirements Based on Micro Light Plates. *ACS Sens*. **2019** Apr 26;4(4):822–6.

28. Novoselov KS. Electric Field Effect in Atomically Thin Carbon Films. *Science*. **2004** Oct 22;306(5696):666–9.

29. Bolotin, K. I.; Sikes, K. J.; Jiang, Z.; Klima, M.; Fudenberg, G.; Hone, J.; Kim, P.; Stormer, H. L. Ultrahigh Electron Mobility in Suspended Graphene. *Solid State Comm.* 2008, 146 (9–10), 351–355.

30. Xu L, Liang H-W, Yang Y, Yu S-H. Stability and Reactivity: Positive and Negative Aspects for Nanoparticle Processing. *Chem Rev.* **2018** Apr 11;118(7):3209–50.

31. Alexis F, Pridgen E, Molnar LK, Farokhzad OC. Factors Affecting the Clearance and Biodistribution of Polymeric Nanoparticles. *Mol Pharm*. **2008** Aug 1;5(4):505–15.

32. Huang X, El-Sayed MA. Gold nanoparticles: Optical properties and implementations in cancer diagnosis and photothermal therapy. *J Adv Res.* **2010** Jan;1(1):13–28.

33. Malik R, Tomer VK, Mishra YK, Lin L. Functional gas sensing nanomaterials: A panoramic view. *Appl Phys Rev.* **2020** Jun;7(2):021301.

34. Dhall S, Kumar M, Bhatnagar M, Mehta BR. Dual gas sensing properties of graphene-Pd/SnO_2 composites for H_2 and ethanol: Role of nanoparticles-graphene interface. *Int J Hydrog Energy*. **2018** Sep;43(37):17921–7.

35. Tian M, Miao J, Cheng P, Mu H, Tu J, Sun J. Layer-by-layer nanocomposites consisting of Co_3O_4 and reduced graphene (rGO) nanosheets for high selectivity ethanol gas sensors. *Appl Surf Sci.* **2019** Jun;479:601–7.

36. Freddi S, Drera G, Pagliara S, Goldoni A, Sangaletti L. Enhanced selectivity of target gas molecules through a minimal array of gas sensors based on nanoparticle-decorated SWCNTs. *The Analyst*. **2019**;144(13):4100–10.

37. Young RJ, Liu M. The microstructure of a graphene-reinforced tennis racquet. J *Mater Sci.* **2016** Apr;51(8):3861–7.

38. Mulvaney P, Parak WJ, Caruso F, Weiss PS. Standardizing Nanomaterials. *ACS Nano.* **2016** Nov 22;10(11):9763–4.

39. Peck RL. Characterization of Organic Compounds. *Anal Chem*. **1951** Jan 17;23(1):97–101.

6 Curriculum Vitae

Persönliche Daten

Name	Fabian Johannes Raphael Aumer
Addresse	Bjerrevej 16, 8700 Horsens Denmark
Geburtsdatum	30.03.1994
Geburtsort	Regensburg
Staatsangehörigkeit	deutsch

Hochschulausbildung

Juni 2018 - Juli 2021

Promotionsstudium Chemie an der Universität Regensburg Institut für Analytische Chemie, Chemo- und Biosensorik (Prof. Antje J. Bäumner, Dr. Thomas Hirsch)

„*Development of a Miniaturized Chemiresistive Gas Sensor Based on Carbon Nanomaterials for the Detection of Nitrogen Dioxide in Air*“

März 2016 - Mai 2018

Masterstudium Electrical and Microsystems Engineering an der OTH Regensburg (Note 1.8)

Abschlussthema: “*Process Integration of Graphene Sensors Using the Example of a Graphene Hall Device*”

Okt. 2012 – März 2016

Bachelorstudium Sensorik und Analytik an der OTH Regensburg (Note 2.5)

Abschlussthema: *"Examination of electrochemical copper deposition on carbon substrates"*

Sept 2000 – Mai 2012 **Allgemeine Hochschulreife** Regentalgymnasium Nittenau

Auszeichnungen

Mai 2019 Finalist des Studentpreises der Wirtschaftszeitung Regensburg

Arbeitserfahrung

März 2014-Mai 2018 Werkstudent bei Infineon Technologies AG Regensburg

Poster Präsentationen

2019 - Mikrosystemtechnik Kongress, Berlin, Deutschland

Carbon Nanomaterials for Miniaturized Gas Sensors

2019 - Innovation Week, München, Deutschland

Nanomaterials for Environmental Sensing

2019 - Innovation Week, Regensburg, Deutschland

New Nanomaterials for Chemiresistive Gas Sensing

Wissenschaftliche Vorträge

2021 - Smart Systems Integration, Grenoble, Frankreich

Electrical Impedance Spectroscopy on 8-channel PSoC-Based Miniaturized Board to Enable Data-rich Environmental Sensing

2021 - Group Seminar University of Regensburg

Impedimetric Sensing of NO_2 with Carbon Nanomaterials at Ambient Temperatures and in Presence of Humidity

2021 - Group Seminar University of Regensburg

Aerosol-Jet-Printed Graphene Electrochemical Histamine Sensors for Food Safety Monitoring

2020 - Institute Seminar University of Regensburg

Simultaneous Determination of NO_2 and Humidity

2020 - Group Seminar University of Regensburg

Low-Power Gas Sensing with Carbon Materials

2019 - Group Seminar University of Regensburg

A Handwriting Method for Low-Cost Gas Sensors

2019 - Group Seminar University of Regensburg

Chemiresistive Sensor Array and Machine Learning Classification of Food

2019 - Group Seminar University of Regensburg

A Parts Per Billion (ppb) Sensor with Microwatt (μW) Power Requirements based on Micro Light Plates

Wissenschaftliche Veröffentlichungen

---

4. **Fabian Aumer**, Thomas Hirsch 'Perspectives on Chemiresistive Gas Sensors Based on Nanomaterials, *submitted to Chemosensors*, **July 2021**.

3. **Fabian Aumer**, Eva-Maria Kirchner, Sebastian A. Schober, Thomas Hirsch 'Impedimetric Sensing of NO_2 with Carbon Nanomaterials at Ambient Temperatures and in Presence of Humidity', *prepared for submission to Sensors and Actuators B* **2021**.

2. **Fabian Aumer**, Torsten Hinz, 'Impedimetric Sensing of NO_2 with Carbon Nanomaterials at Ambient Temperatures and in Presence of Humidity', *submitted to Smart Systems Integration*, **January 30th 2021.**

1. **Fabian Aumer**, Fabian Hecht, Anton Kroener, Patrick Recum, Dr. Thomas Hirsch, 'Carbon Nanomaterials for Miniaturized Gas Sensors', *published at Mikrosystemtechnikkongress*, **October 30th 2019.**

7 Summary

This thesis addresses the development of a miniaturized chemiresistive gas sensor based on carbon nanomaterials for the detection of nitrogen dioxide in air.

Chapter 1 reviews the state of the art approaches towards chemiresistive gas sensing in air. The following section describes sensing mechanisms of metal oxide based gas sensors as well as in chemiresistive gas sensors. Furthermore sensors for different gases as NO_2, CO_2 and other toxic gases are examined. Materials used in chemiresistive gas detection in air, their sensitivity, target gases, detection limits as well as response/ recovery times and their operating temperatures are listed and compared. Approaches towards multigas sensing are shown and the importance of data evaluation using data processing and algorithms with focus on principal component analysis is explained. Key points in gas sensor development are sensitivity, elimination of cross sensitivity via selectivity, low-temperature operation and small size.

Chapter 2 explains two different preparation methods for reduced graphene oxide as a sensing layer and compares them for the applicability in gas sensing. The materials are characterized by Raman spectroscopy for defect density, scanning electron microscope for flake size and electrical characterization in a gas measurement setup. The materials differ in their defect density, flake size, resistance and sensitivity towards NO_2. The material with less defects and higher flake size exhibits a lower resistance and also a lower sensitivity towards NO_2 compared with the material with more defects and overall smaller flake size distribution that has a higher resistance. Therefore implying that the material choice is of utmost importance in the process of gas sensor development.

Chapter 3 explains the basics of electrical impedance spectroscopy (EIS) and its advantages in gas sensing compared to DC resistance measurements as low-

power method as no heating is required to achieve sensitivity and selectivity. To show the applicability an electrical read-out board capable of EIS measurement in the range from 100 Hz up to 62.5 kHz was designed and built. The validation of the board is done with a equivalent Randles test circuit that is commonly used to model electrochemical sensors. The results show that EIS is a fitting measurement method to use in gas sensing as the increased amount of data received from it can be used for further in-depth data evaluation such as principal component analysis which was shown to be a valuable tool in **Chapter 1**.

Chapter 4 shows the combination of material choice suited to the detection of NO_2 as well as application of EIS to further enhance the measurement data including the separate detection of relative humidity from NO_2, therefore increasing the selectivity of the sensor device to the target analyte in presence of another analyte. Two different material preparation methods are used to fabricate mechanically exfoliated graphene (meG) with high hydrophobicity and reduced graphene oxide (rGO) with lower hydrophobicity. Both materials are applied to the sensor device surface and examined via Raman spectroscopy as well as electrical characterization using EIS and DC resistance measurements in a gas chamber with varying content of NO_2 on ppb-level, relative humidity and a mixture of both analytes. The resulting data from EIS is then evaluated using PCA and a distinction between the analytes using pattern analysis. This demonstrates the possibility to build a miniaturized, low-operating-temperature, carbon nanomaterial based chemiresistive gas sensor in combation with proper data processing techniques for the detection of nitrogen dioxide in air.

8 Zusammenfassung

Die vorliegende Arbeit befasst sich mit der Entwicklung eines miniaturisierten chemiresistiven Gassensors auf der Basis von Kohlenstoff-Nanomaterialien zur Detektion von Kohlenstoffdioxid in Luft.

Kapitel 1 gibt einen Überblick über den Stand der Technik bei der chemiresistiven Gassensorik in Luft. Der folgende Abschnitt beschreibt die Sensormechanismen von Gassensoren auf Metalloxidbasis sowie in chemiresistiven Gassensoren. Weiterhin werden Sensoren für verschiedene Gase wie NO_2, CO_2 und andere toxische Gase untersucht. Die bei der chemiresistiven Gasdetektion in Luft verwendeten Materialien, ihre Empfindlichkeit, Zielgase, Nachweisgrenzen sowie Ansprech- und Erholungszeiten und ihre Betriebstemperaturen werden aufgeführt und verglichen. Ansätze zur Multigas-Sensorik werden aufgezeigt und die Bedeutung der Datenauswertung mittels Datenverarbeitung und Algorithmen mit Schwerpunkt Hauptkomponentenanalyse erläutert. Wichtige Punkte bei der Entwicklung von Gassensoren sind Empfindlichkeit, Eliminierung von Querempfindlichkeit durch Selektivität, Tieftemperaturbetrieb und Miniaturisierung.

In **Kapitel 2** werden zwei verschiedene Herstellungsmethoden für reduziertes Graphenoxid als Sensorschicht erläutert und hinsichtlich ihrer Anwendbarkeit in der Gassensorik verglichen. Die Materialien werden mittels Raman-Spektroskopie für die Defektdichte, Rasterelektronenmikroskop für die Flockengröße und elektrischer Charakterisierung in einem Gasmessaufbau charakterisiert. Die Materialien unterscheiden sich in ihrer Defektdichte, Flockengröße, Widerstand und Empfindlichkeit gegenüber NO_2. Das Material mit weniger Defekten und höherer Flockengröße weist einen geringeren Widerstand und auch eine geringere Empfindlichkeit gegenüber NO_2 auf,

verglichen mit dem Material mit mehr Defekten und insgesamt kleinerer Flockengrößenverteilung, das einen höheren Widerstand aufweist. Daraus ergibt sich, dass die Materialauswahl bei der Entwicklung eines Gassensors von größter Bedeutung ist.

Kapitel 3 erklärt die Grundlagen der elektrischen Impedanzspektroskopie (EIS) und ihre Vorteile bei der Gassensorik im Vergleich zu Gleichstromwiderstandsmessungen als stromsparende Methode, da kein Heizen des Sensors erforderlich ist, um Empfindlichkeit und Selektivität zu erreichen. Um die Anwendbarkeit zu zeigen, wurde eine elektrische Ausleseplatine entworfen und gebaut, die EIS-Messungen im Bereich von 100 Hz bis 62,5 kHz ermöglicht. Die Validierung der Platine erfolgt mit einem Ersatzschaltbild einer Randles-Testschaltung, die üblicherweise zur Modellierung elektrochemischer Sensoren verwendet wird. Die Ergebnisse zeigen, dass die EIS eine geeignete Messmethode für die Gassensorik ist, da die größere Menge an Daten, die sie liefert, für eine weitergehende Datenauswertung verwendet werden kann, wie z. B. die Hauptkomponentenanalyse, die sich in Kapitel 1 als wertvolles Werkzeug erwiesen hat.

Kapitel 4 zeigt die Kombination von Materialauswahl, die für die Detektion von NO_2 geeignet ist, sowie die Anwendung von EIS zur weiteren Verbesserung der Messdaten, einschließlich der separaten Detektion der relativen Feuchte von NO_2, wodurch die Selektivität des Sensors für den Zielanalyten in Gegenwart eines anderen Analyten erhöht wird. Zwei verschiedene Materialherstellungsmethoden werden verwendet, um mechanisch exfoliertes Graphen (meG) mit hoher Hydrophobizität und reduziertes Graphenoxid (rGO) mit geringerer Hydrophobizität herzustellen. Beide Materialien werden auf die Oberfläche des Sensorbauteils aufgebracht und mittels Raman-Spektroskopie sowie elektrischer Charakterisierung durch EIS- und

Gleichstromwiderstandsmessungen in einer Gaskammer mit variierendem NO_2-Gehalt im ppb-Level, relativer Luftfeuchtigkeit und einer Mischung beider Analyten untersucht. Die resultierenden Daten aus der EIS werden anschließend mittels PCA ausgewertet und eine Unterscheidung zwischen den Analyten mittels Musteranalyse vorgenommen. Dies demonstriert die Möglichkeit, einen miniaturisierten, auf Kohlenstoffnanomaterialien basierenden chemiresistiven Gassensor der bei niedriger Betriebstemperatur arbeitet in Kombination mit geeigneten Datenverarbeitungstechniken für den Nachweis von Stickoxid in Luft herzustellen.

9 Eidesstattliche Erklärung

Ich erkläre hiermit an Eides statt, dass ich die vorliegende Arbeit ohne unzulässige Hilfe Dritterund ohne Benutzung anderer als der angegebenen Hilfsmittel angefertigt habe; die aus anderen Quellen direkt oder indirekt übernommenen Daten und Konzepte sind unter Angabe des Literaturzitats gekennzeichnet.

Weitere Personen waren an der inhaltlich-materiellen Herstellung der vorliegenden Arbeit nicht beteiligt. Insbesondere habe ich hierfür nicht die entgeltliche Hilfe eines Promotionsberaters oder anderer Personen in Anspruch genommen. Niemand hat von mir weder unmittelbar noch mittelbar geldwerte Leistungen für Arbeiten erhalten, die im Zusammenhang mit dem Inhalt der vorgelegten Dissertation stehen.

Die Arbeit wurde bisher weder im In- noch im Ausland in gleicher oder ähnlicher Form einer anderen Prüfungsbehörde vorgelegt.

_____

Ort, Datum Unterschrift